UNIVERSIDAD DE GRANADA

FACULTAD DE CIENCIAS

DEPARTAMENTO DE ÓPTICA

PROGRAMA DE DOCTORADO EN FÍSICA Y CIENCIAS DEL ESPACIO

REFLECTANCE AND COLORIMETRIC MODELLING OF MULTILAYER BODIES OF TRANSLUCENT DENTAL MATERIALS

Tesis Doctoral

María de la Natividad Tejada Casado

Directores

Razvan Ionut Ghinea

Luis Javier Herrera Maldonado

Granada, 2022

Editor: Universidad de Granada. Tesis Doctorales
Autor: María de la Natividad Tejada Casado
ISBN: 978-84-1117-660-6
URI: https://hdl.handle.net/10481/79662

Reflectance and Colorimetric Modelling of Multilayer Bodies of Translucent Dental Materials

Memoria presentada por la Graduada en Óptica y Optometría y Máster Erasmus Mundus en Ciencia y Tecnología del Color

María de la Natividad Tejada Casado

para optar al Grado de Doctora por la Universidad de Granada con Mención de Doctorado Internacional

Fdo: María de la Natividad Tejada Casado

Granada, 2022

A mi madre, mi padre, mi hermana y Carlos.

"Lo importante es no dejar de hacerse preguntas"

- Albert Einstein

AGRADECIMIENTOS

Desde que tomé la decisión de embarcarme en el desarrollo de una Tesis Doctoral hasta que por fin ha visto la luz han pasado muchas cosas. Este texto es solo el resultado final de lo que, sin duda, ha sido un camino lleno de aprendizaje en el que he tenido la suerte de estar acompañada de personas que han disfrutado y padecido conmigo este proceso. Por eso quiero expresar en estas líneas mi más sincero agradecimiento a todas ellas.

En primer lugar, quiero agradecer a los directores de esta Tesis Doctoral, los profesores Luis Javier Herrera y Razvan Ghinea. Gracias Luis, por guiarme y orientarme siempre con esa buena energía que te envuelve, por tu disponibilidad y por esas llamadas en las que he aprendido y nos hemos divertido tanto, has sido y eres un apoyo imprescindible para mí. Gracias Razvan, por todo lo que me has enseñado directa e indirectamente y por hacerme ver que no importan las cuestas arriba si se caminan con la persona adecuada. A ambos, gracias por vuestra confianza en todo momento, espero que esta Tesis sea solo el principio de un largo camino que recorrer juntos.

Por supuesto, quiero agradecer también a una de las personas más importantes durante estos años, la profesora María del Mar Pérez. Gracias por ser el motor que hace que todo siga adelante, por arrimar el hombro incluso cuando no te correspondía y por todo lo que me has enseñado y ayudado.

También al resto de integrantes del Laboratory of Biomaterials Optics, mi grupo de investigación y segunda familia. Gracias Javi, por estar al pie del cañón desde el principio, por todo lo que me has ayudado y por todo lo que hemos compartido, tú mejor que nadie sabes lo duro que es este mundo a veces, y tener tu apoyo ha sido imprescindible, vales muchísimo y nos queda mucho por vivir juntos. A Juancho, gracias por ser pura disposición, por enseñarme a amar el laboratorio y por cuidarme como lo has hecho. A Ana, por todo lo que indirectamente ha implicado para ti este proyecto, gracias por tu serenidad y buenos consejos, y por supuesto por todas esas comidas en las que tanto hemos disfrutado juntos. Mención especial para Radu, gracias porque a pesar de ser el más pequeño tienes el corazón más grande, eres un ejemplo a seguir. Gracias Paco, por tu disponibilidad en todo momento. Y, gracias Cristina, por el apoyo que has sido para mí durante los tres meses que hemos vivido juntas. Gracias a todos por acogerme con los brazos abiertos desde el primer día.

I would also like to thank Vita Zahnfabrik H. Rauter GmbH & Co. KG for funding this project, which has made possible to complete this doctoral period with a scholarship. Also, thanks to Dr. Wolfgang Rauh and Dr. Henning Lübbe, who led this collaboration with VITA. Dr. Rauh, thank you for trusting me from the beginning. Henning, thank you for all the time and effort invested in this project, for your support and for taking care of me, not only during my internship at VITA but also during these almost three years.

Thanks to Professor Alvaro Della Bona, from the University of Passo Fundo, for making me feel at home during my research stay in Brazil, offering me all the

unimaginable attentions and dedicating your time and effort. And also, thanks to all the colleagues at the research center and all the people who participated in my experiments, who made everything very easy.

Gracias Oscar y Andressa, por hacer de los tres meses en Brasil la mejor experiencia posible. Habéis conseguido que estar lejos de casa sea mucho más fácil. Muchas gracias por toda vuestra ayuda y por todos los momentos y viajes compartidos. Ha sido poco tiempo, pero el suficiente para llevarme a dos buenos amigos.

Gracias a las profesoras Cristina Lucena, Cristina Benavides y Rosa Pulgar, de la Facultad de Odontología, por toda vuestra ayuda y por todos los trabajos en equipo en los que tanto he aprendido. Ojalá esto solo haya sido el principio.

Quiero agradecer también a todos los miembros del Departamento de Óptica de la Universidad de Granada, por acogerme y hacerme sentir muy cómoda desde el primer día. Gracias a los que durante estos años han sido los directores, los profesores Antonio Pozo y Rafa Huertas, que desde esa posición habéis hecho todo lo posible por ayudarme, proporcionándome un espacio de trabajo y permitiéndome usar todas las instalaciones y laboratorios que han posibilitado el desarrollo de esta Tesis.

En especial, quiero agradecer a los profesores Manuel Melgosa, Javier Hernández, Eva Valero, Luis Gómez y Miguel Ángel Martínez, porque durante mi trayectoria académica de alguna forma y sin saberlo plantasteis en mi la semilla de la curiosidad por este mundo académico. Sin vosotros no estaría hoy aquí.

También a mis compañeros-amigos, poca gente tiene la suerte de poder trabajar en un entorno como el que tenemos nosotros. Muchas gracias por acogerme desde el primer día y por quererme tanto, por haber sido un apoyo constante y un hombro en el que llorar. Gracias por todos los ratos compartidos en desayunos, almuerzos, meriendas, cenas, caminatas por la sierra, salidas por Ganivet y tardes de compras. Ojalá no paren nunca los ataques de risa. Gracias a Ana Belén, Sonia, Pilar, Miriam y

Rubén, y a todos los demás, que ya os he mencionado antes.

A mis amigas de toda la vida, Espe, María, Elena, Carmen y Clara, cada una de vosotras ha tenido una participación especial en esta etapa de mi vida, gracias por ser mi paz y sacar lo mejor de mí desde pequeñas, aunque a veces tenga ganas de que os vayáis de mi casa. A Paco, mi mejor amigo, por todos los años que hemos compartido juntos. Luvin, thank you for everything you taught me, you are very special. Gracias Yoko, por reírte de tus desgracias y de las mías, eres de esas personas con las que la distancia no existe. Marina, gracias porque a pesar de estar lejos te siento muy cerca. Gracias Amaia, por el apoyo que has sido desde que te conocí y por todas las risas que hemos compartido juntas. Y gracias a todas mis compañeras de rugby, por hacerme olvidarme de todo cuando más lo necesitaba.

Gracias a mi familia. Muchas gracias Mamá y Papá, por hacer que no me rindiera nunca, por escucharme siempre con paciencia y por demostrarme que se puede con todo. Carmen, eres un pilar imprescindible en mi vida, tenemos la suerte de estar cerca y de poder compartir muchos momentos juntas. Gracias por todos tus consejos y por tu disponibilidad para cualquier cosa, sé que siempre podré contar contigo.

Y, por último, gracias Carlos, porque apareciste en mi vida cuando más lo necesitaba. Muchas gracias por escucharme con paciencia, por cuidarme, ayudarme y por hacer las cosas muy fáciles. Gracias por todo lo que has sacrificado para seguir estando a mi lado. Aprendo de ti cada día que estamos juntos. Te quiero muchísimo.

A todos, mi más sincero agradecimiento.

CONTENTS

LIST OF FIGURES

LIST OF TABLES

ABBREVIATIONS AND ACRONYMS

λ: Wavelength

$\Delta C'$: Chroma Difference

ΔE: Color Difference

ΔE_{00}: CIEDE2000 Color Difference

ΔE^*_{ab}: CIELAB Color Difference

$\Delta H'$: Hue Difference

$\Delta H'$: Lightness Difference

-00: Relative to CIEDE2000 formula

-ab: Relative to CIELAB formula

ACP: Análisis de Componentes Principales

AT: Acceptability Threshold

BFD: Bradford University Color Difference Formula

Bis-GMA: Bisfenol-A-glicidil-metacrilato

CAD/CAM: Computer Aided Design / Computer Aided Manufacturing

CCT: Correlated Color Temperature

CIE: International Commission on Illumination

CIE94: ΔE(1994) Color Difference Formula

CMC: Colour Measurement Committee

CMF: Color Matching Functions

DRC: Dental Resin Composite

EN: Enamel

GFC: Goodness of Fit Coefficient

HCBB: Houston Center for Biomaterials and Biomimetics

HEMA: hydroxyethylmethacrylate

I: Intensity

ISO: International Organization for Standardization

JND: Just-Noticeable Difference

K-M: Kubelka-Munk

LDGC: Lithium-Disilicate Glass-Ceramics

LED: Light-Emitting Diode

MDP: Methacryloyloxydecyl Dihydrogen Phosphate

MLR: Multiple Linear Regression

PCA: Principal Component Analysis

PMMA: Poly(Methyl Methacrylate)

PT: Perceptibility Threshold

R: Reflectance

RMSE: Root Mean Square Error

S: Sample

SD: Standard Deviation

SLR: Simple Linear Regression

SPD: Spectral Power Distribution

TEGDMA: Triethylene Glycol Dimethacrylate

TSK Fuzzy: Takagi-Sugeno-Kang Fuzzy Approximation

UDMA: Urethane Dimethacrylate

UV: Ultraviolet

VD: VITAPAN Dentine

VE: VITAPAN Excell

VS-PC: VITA Suprinity

vol%: filling volume percentage

VP: VITA Physiodens

wt%: filling weight percentage

ZLS: Zirconia-containing Lithium-Silicate

ABSTRACT

Natural teeth represent one of the most complex biological structures, since they consist of at least three layers of different translucent tissues. In this sense, in order to be able to match all natural teeth, a wide variety of differently shaded materials is required. In the last decade, the development of biomaterials used in dental restorations has experienced an important breakthrough. New generations of dental biomaterials already outperform the mechanical properties of the biological tissues that are meant to replace, however this variety of shades and materials together with their complex optical properties, makes it difficult to design layered restorations that match the perception of the according natural tooth.

The appearance of a material may vary significantly depending on a wide range of properties such as surface topology, geometry, reflectance, transmittance and angle from which the material is viewed as well as the illumination parameters (angle of incident light, diffuse or directed illumination, etc.). In this sense, color and

appearance are still determining factors that must be well-managed both in clinical practices and dental industries. Therefore, the research studies in the field of esthetic dentistry have increased considerably.

In addition to knowing the optical and colorimetric properties of these biomaterials and dental structures, it is also interesting to be able to model and predict them. In the last 20 years, computational intelligence has been an indispensable and transversal tool in research in all areas of science including dentistry. The development of mathematical algorithms that are able to establish, or even predict, the final chromatic coordinates or reflectance spectra of these materials represents an important breakthrough with direct application in clinical practice and industry. In this context, many different predictive techniques such as fuzzy logic, neural networks, the Kubelka-Munk theory or linear and non-linear regression approaches have attempted to solve color prediction of these layered tooth structures and materials in the dental field. However, it remains an area not fully solved yet.

It is clear that color management in dentistry is not a trivial problem and there is no simple solution for it. Therefore, the main objective of this PhD Thesis is to measure, model and predict the colorimetric properties and final appearance of translucent layered biomaterials with application in dentistry, in order to provide new color prediction methods that could be applied in both clinical practice and industry, and that could contribute to the progress of knowledge in the field of esthetic dentistry and to the development of new dental materials and prosthetic teeth.

To meet this objective, several studies, based on different mathematical techniques, have been carried out in order to develop and test new color prediction algorithms.

From this point, this PhD Thesis is structured in 7 chapters. First, in Chapter 1, an extensive state of the art on the different topics related to this PhD Thesis is provided. Starting with some color basics concepts and their relation to color in dentistry. After

that, we dug into details on dental restorative materials, ending with an introduction to color prediction in dentistry and different mathematical concepts, highlighting principal components analysis (PCA) and linear regression Analysis. In Chapter 2, both general and specific objectives of this PhD Thesis are drawn.

In Chapters 3 and 4, PCA-based reflectance prediction algorithms are developed for monolithic and layered (stacked) dental materials, respectively. Chapter 5 presents a new linear regression-based color prediction algorithm for monolithic and layered (stacked) dental materials. Afterwards, in Chapter 6, the algorithms previously proposed for stacked layered samples are tested with more complex stratified layered samples.

Chapter 7 shows the final conclusions of our studies. Finally, all the references cited throughout this memory, as well as the scientific production and activities derived from the studies presented in this PhD Thesis and developed within the doctoral period, are listed.

RESUMEN

Los dientes naturales representan una de las estructuras biológicas más complejas, ya que están formados por al menos tres capas de diferentes tejidos translúcidos. En este sentido, para poder igualar colorimétricamente los dientes naturales, se requiere una gran variedad de materiales de diferentes colores. En la última década, el desarrollo de los biomateriales utilizados en las restauraciones dentales ha experimentado un importante avance. Las nuevas generaciones de biomateriales dentales ya superan las propiedades mecánicas de estos tejidos biológicos a los que pretenden sustituir, sin embargo la variedad de colores y materiales junto con sus complejas propiedades ópticas, dificultan el diseño de restauraciones por capas que se ajusten a la percepción del diente natural correspondiente.

La apariencia de cualquier material puede variar significativamente en función de una amplia gama de propiedades, como la topología de la superficie, la geometría, la reflectancia, la transmitancia y el ángulo desde el que se observa el material, así

como los parámetros de iluminación (ángulo de la luz incidente, iluminación difusa o dirigida, etc.). En este sentido, el color y la apariencia siguen siendo factores determinantes que deben ser bien gestionados tanto en las prácticas clínicas como en la industria odontológica. Por ello, los estudios de investigación en el campo de la odontología estética han aumentado considerablemente.

Además de conocer las propiedades ópticas y colorimétricas de estos biomateriales y estructuras dentales, también es interesante poder modelarlas y predecirlas. En los últimos 20 años, la inteligencia artificial ha sido una herramienta indispensable y transversal en la investigación en todas las áreas de la ciencia, incluida la odontología. El desarrollo de algoritmos matemáticos capaces de establecer o incluso predecir las coordenadas cromáticas o la reflectancia espectral de estos materiales representa un importante avance con aplicaciones directas en la práctica clínica y en la industria. En este contexto, diferentes técnicas de predicción como la lógica difusa, las redes neuronales, la teoría de Kubelka-Munk o las aproximaciones de regresión lineal y no lineal han intentado resolver el problema de la predicción del color de estas estructuras y materiales dentales en el ámbito odontológico. Sin embargo, sigue siendo una cuestión que no está del todo resuelta.

Está claro que la gestión del color en odontología no es un problema trivial y no existe una solución sencilla para ello. Por lo tanto, el objetivo principal de esta Tesis Doctoral es medir, modelar y predecir las propiedades colorimétricas y la apariencia final de biomateriales estratificados translúcidos con aplicación en odontología, con el fin de proporcionar nuevos métodos de predicción del color que puedan ser aplicados tanto en la práctica clínica como en la industria, y que puedan contribuir al progreso del conocimiento en el campo de la odontología estética y al desarrollo de nuevos materiales dentales y dientes protésicos.

Para cumplir con este objetivo se han realizado varios estudios, basados en difer-

entes técnicas matemáticas, con el fin de desarrollar y probar nuevos algoritmos de predicción del color.

A partir de aquí, esta Tesis Doctoral se estructura en 7 capítulos. En primer lugar, en el Capítulo 1, se ofrece una amplia revisión bibliográfica sobre los diferentes temas relacionados con esta Tesis Doctoral. Empezando por algunos conceptos básicos del color y su relación con el color en odontología. Después, profundizamos en los detalles de los materiales de restauración dental, y terminamos con una introducción a la predicción del color en odontología y diferentes conceptos matemáticos, destacando el análisis de componentes principales y el análisis de regresión lineal. En el Capítulo 2, se plantean los objetivos generales y específicos de esta Tesis Doctoral.

En los Capítulos 3 y 4, se desarrollan algoritmos de predicción de reflectancia basados en ACP para materiales dentales monolíticos y bicapa (apilados), respectivamente. El Capítulo 5 presenta un nuevo algoritmo de predicción del color basado en la regresión lineal para materiales dentales monolíticos y bicapa (apilados). Después, en el Capítulo 6, los algoritmos propuestos anteriormente para las muestras bicapa apiladas se prueban con muestras estratificadas polimerizadas más complejas.

El Capítulo 7 muestra las conclusiones finales de nuestros estudios. Por último, se enumeran todas las referencias citadas a lo largo de esta memoria, así como la producción científica y las actividades derivadas de los estudios presentados en esta Tesis Doctoral y otras actividades desarrolladas durante el periodo de doctorado.

CHAPTER

1

INTRODUCTION

1.1 Color basics

1.1.1 Color perception

From a physical point of view, the color of an object is associated with the electromagnetic radiation of a specific range of wavelengths visible to the human eye (the visible spectrum) that the object reflects or transmits. The visible light spectrum is the part of the wider electromagnetic spectrum that spans wavelengths from 380 to 780 nanometers. As mentioned before, these wavelengths mainly determine the colors that we see [6]. However, it is well established that color is not an intrinsic property of an object, but a psychophysical phenomenon produced as a consequence of light interaction with the human visual system [7]. When incident light reaches an object, part of it can be reflected, part absorbed, part transmitted and, in some cases, part of it can be scattered. Both reflected and transmitted light can, subsequently, interact with the human visual system and the resulting stimulation of the retina is recognized as the object's color by the brain [8]. Each object reflects, transmits, absorbs and scatters light differently, and these differences are producing different color stimuli and will result in different color perceptions. .

The sensitivity of the human eye varies from person to person, often causing color to appear differently to each individual [9]. This subjectivity often leads to inconsistencies when evaluating or communicating color.

Therefore, there are three main factors involved in the process of color perception: a light source, an object and the observer. However, the interaction of light with objects is not just a simple spectral phenomenon, since the reflectance or transmittance of a sample is not just a function of wavelength, but also a function of the illumination and viewing (measuring) geometry, as shown in Figure 1.1.

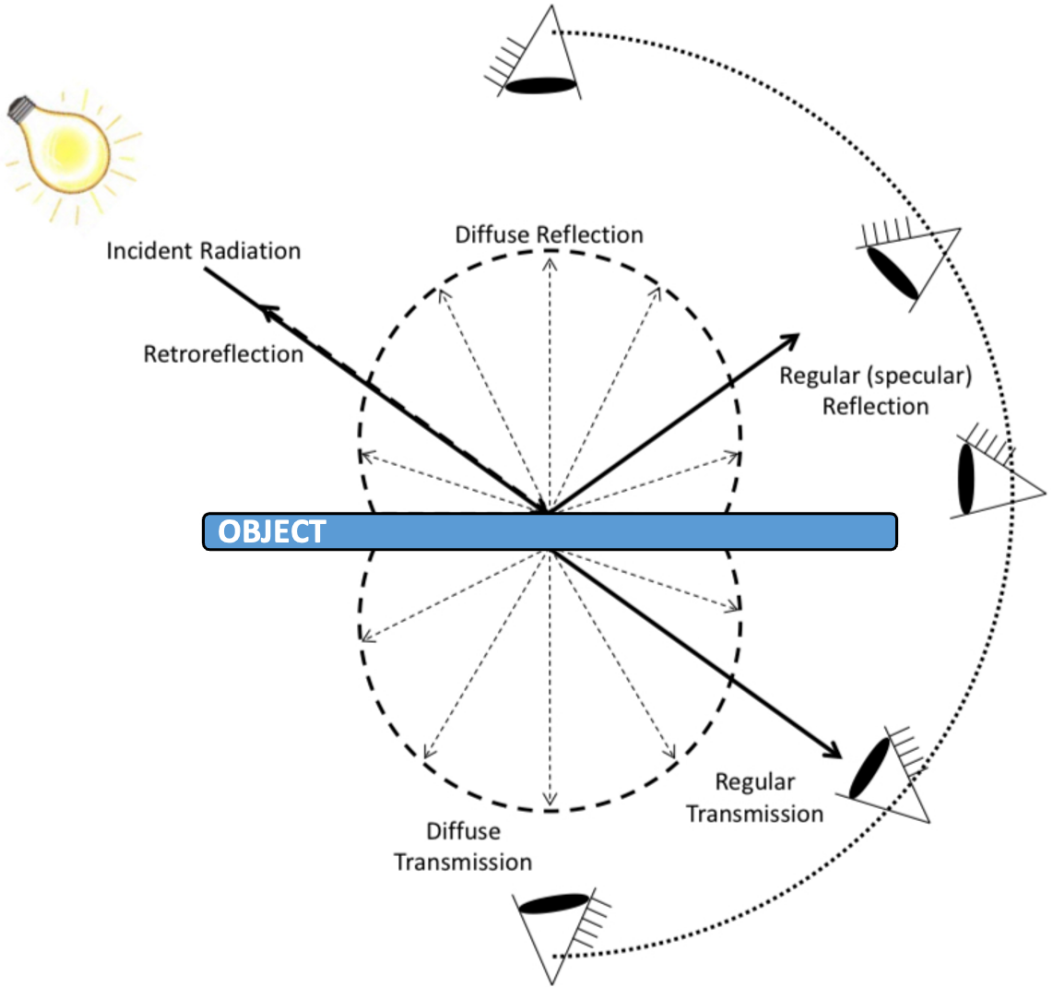

Figure 1.1: Schematic representation of the main factors that influence color perception.

In this sense, in order to produce a reliable color measurement system, all these factors need to be quantified and standardized. The illumination (light source) can be characterized by its spectral power distribution (SPD), which is the the relative intensity of the illumination for each wavelength of the visible spectrum. As described before, a given object can reflect (or transmit) a certain fraction of the incident light and this can be characterized by its reflectance (or transmittance) spectrum. If the object is observed in reflection, i.e. the observer and light source are in the same plane relative to the sample, then the product of these two terms (disregarding possible

light attenuation while propagating through the media) will result in the amount of light reaching the eye, which is characterized by the color matching functions (CMFs) of the standard observer. Finally, since the viewing geometry also affects the color perception, it needs to be also standardized, so different standard measuring geometries have been defined.

Thus in order to measure color, and be able to properly quantify it, it is necessary to specify each of these main components that affect color perception and color measuring [10].

First formalization of color science dates from 1931, when the International Commission on Illumination (CIE) recommended a set of standard illuminants for use in colorimetry, the color matching functions of a standard observer and a system of standard optical geometries for use in color-measuring instruments and set-ups. A short description of what they represent, as well as their current state of development, is given below.

- **Standard illuminants**

  A standard illuminant is a theoretical source of visible light with a given spectral power distribution [9]. Over the years, the CIE has proposed different illuminants in order to provide the basis for comparing colors. The first to be introduced were illuminants A, B, and C, which represent average incandescent light, direct sunlight, and average daylight, respectively. Later, the D series were introduced (D_{50}, D_{55}, D_{65} and D_{75}), representing the daylight in various phases. Illuminant E is the equal-energy radiator and was designed with a constant SPD inside the visible spectrum. A further series of fluorescent lights, illuminants F, were also defined. The last to be introduced, was as set of 9 LED illuminants for different LED types [11]. Currently, the CIE defines two standard illuminants: CIE Standard Illuminant A and CIE Standard Illuminant D65 [12].

In almost all applications in dentistry, except for research studies when the behavior of a material under different illuminants results of certain interest [13] or for metameric studies [14], the standard illuminant of primary choice is the CIE D65 Standard Illuminant, since the teeth and, if the case, the dental restorations, are often visually judged under daylight conditions.

- **Standard observer**

  As mentioned before, variations of the sensitivity of the human eye are present for different persons, leading to the necessity of establishing a so-called Standard Observer. The standardization of the observer was done by describing it's color matching functions, which define the chromatic response of a given observer to a light stimuli. Furthermore, due to the distribution of photo-receptors cells in the human retina (which varies from the fovea -maximum presence of cone-like cells- to the peripheral retina -maximum presence of rod-like cells), the response of the human visual system to the color stimuli also depends on the size of the projected image of the object on the retina, which is determined by the angle of the observer's field of view that the object sustains [15]. In order to eliminate this variable, in a first stage, the CIE defined a color-mapping function, the so-called CIE 1931 2° Standard Observer, to represent an average human's chromatic response within a 2° arc inside the fovea, because of the belief that our color-sensing cones were located in a 2-degree arc in the fovea (equivalent to a 1.7 cm diameter circle at 50 cm distance) [16]. However, although the fovea is the region most sensitive to color, the majority of everyday objects occupy a larger area of the retina. Therefore, as a recommendation when dealing with bigger objects (that sustain more than 4° field of view), the CIE 1964 10° Standard Observer (equivalent to a 8.8 cm circle diameter at 50 cm distance) was also

derived [17]. The CIE color matching functions: $\overline{x}(\lambda)$, $\overline{y}(\lambda)$ and $\overline{z}(\lambda)$ and $\overline{x}_{10}(\lambda)$, $\overline{y}_{10}(\lambda)$ and $\overline{z}_{10}(\lambda)$ are the numerical description of the chromatic response of the CIE 1931 2° and CIE 1964 10° Standard Observers, respectively.

In dentistry, when assessing color, the CIE 1931 2° Standard Observer is conventionally used, since the size of dental structures observed at a clinically relevant distance, correlates to the field of view of 2° [18,19].

- **Standard measuring geometries**

  Different illumination/viewing (or illumination/measuring in the case of a detector) geometries directly affect how light interacts with the sample, therefore affecting the amount of light that finally reaches the eyes (or detector, for color measuring instruments). Many materials will change their colorimetric properties depending on whether they are illuminated perpendicularly or from a certain angle and also whether they are illuminated with diffused or collimated light [9]. That is why, when evaluating the colorimetric characteristics of a material, in addition to the Standard Observer and the Standard Illuminant used, the measuring geometry must be also specified. Hence, achieving results that can be easily compared and reproduced implies standardization of the illuminating/measuring geometry. Accordingly, the CIE has specified several illuminating and viewing conditions [12,17] that can be used for standardized color measurements. To identify which geometry is ideal for evaluating and controlling the color of a given object, it should be understood how each of these illuminates and detects its color. For reflectance measurements, the CIE has defined four standard measuring geometries, which come as two pairs of optically reversible geometries (i.e. each pair produce the same measurement results), being indicated as illumination/measuring:

1. $45°$/normal (or $45°/0°$) and normal/$45°$;
2. Diffuse/normal and normal/diffuse.

The use of the $45°/0°$ and $0°/45°$ measurement geometries ensures that all components of gloss of the sample are excluded from the measurements [20]. Therefore, these geometries are ideal when it is necessary to compare colors of materials with various levels of gloss, as it is the case for almost all dental materials. In addition, as light intensity is well known to vary with distance from the source [21], for any illumination/measuring standard geometry, it is important to maintain a constant positioning of the specimen surface from the illuminant and the measuring systems.

1.1.2 CIE color spaces

Over time, various methods have been devised for quantifying color and express color numerically, thereby making it possible to communicate colors more accurately. Color spaces are mathematical models describing the way colors can be represented. The first attempt to standardize the representation of colors, was the Munsell color system, which introduced a method for expressing colors according to three properties: hue (basic color), value (lightness) and chroma (color intensity) [22]. In 1931, the CIE introduced the CIE XYZ color space, which is based on the XYZ tristimulus values [23]. This was the first color space that defined quantitative links between distributions of wavelengths in the electromagnetic visible spectrum and physiologically perceived colors by the human vision.

The CIE X, Y, Z tristimulus values are calculated using the CIE Standard Observer CMFs, $\overline{x}(\lambda)$, $\overline{y}(\lambda)$ and $\overline{z}(\lambda)$, a selected CIE Standard Illuminant SPD, $I(\lambda)$, and the spectral reflectance or transmittance of the sample, $S(\lambda)$, as follows:

$$X = k \int_{380}^{780} S(\lambda) I(\lambda) \bar{x}(\lambda) d(\lambda) \tag{1.1.1}$$

$$Y = k \int_{380}^{780} S(\lambda) I(\lambda) \bar{y}(\lambda) d(\lambda) \tag{1.1.2}$$

$$Z = k \int_{380}^{780} S(\lambda) I(\lambda) \bar{z}(\lambda) d(\lambda) \tag{1.1.3}$$

where the k constant for non-self luminous objects is calculated as:

$$k = \frac{100}{\int_{380}^{780} I(\lambda) \bar{y}(\lambda) d(\lambda)} \tag{1.1.4}$$

The color of any stimulus can be represented by these tristimulus values. Since the human retina is fitted with three different types of cone photo-receptor cells (sensitive to color), with different response to incoming visible light wavelengths [8], a full representation of all visible colors translates into a three-dimensional figure. However, the concept of color can be divided into two parts: brightness and chromaticity. Therefore, the CIE xyY color space was developed in order to be able to separate these two properties and use only two components (x and y) to encode the color's chromaticity and keep the Y value from the XYZ tristimulus values to encode the color's brightness or value [23]. This transformation of the tristimulus values to obtain the chromaticity coordinates xyz, allowed to establish a two-dimensional representation of color, the so-called chromaticity diagrams. Although this space is very suitable for describing color stimuli, it has the disadvantage that equal distances on the xy chromaticity diagram do not correspond to equal perceived color differences and, therefore, there are different perceptibility color thresholds depending on the area of the xy diagram (MacAdam ellipses) [24]. After several attempts to improve the diagram with the purpose to convert these ellipses into circles, no ideal transformation

was found.

To overcome this limitation, the CIE proposed the three-dimensional CIELAB and CIELUV color spaces, which replaced the two-dimensional chromaticity diagrams. These three dimensions correlate with the perceived brightness, chroma and hue for a given color stimulus, which is achieved by incorporating features to account for chromatic adaptation and nonlinear visual responses. The main aim in the development of these spaces was to provide standard practices for the measurement of color differences, which cannot be done in CIE XYZ and CIE xyY color spaces [20]. Apparently, there is no clear advantage of one over the other, however, over the years, the CIELAB color space has been more widely implemented in color applications than the CIELUV color space. In the specific case of dentistry, the CIELAB color space is almost exclusively used in dental color studies or color research [1, 21, 25–27].

1.1.2.1 CIE1976 L*a*b* color space

The CIE1976 L*a*b* color space (also known as CIELAB) expresses color as three values: L*, a* and b*, denominated chromaticity coordinates. This space was intended as a perceptually uniform space, where a given numerical change corresponds to a similar perceived change in color [17]. These CIE L*, a* and b* coordinates can be computed from the XYZ tristimulus values and for a reference white (X_n,Y_n,Z_n) as shown in the following equations:

$$L^* = 116\, f\left(\frac{Y}{Y_n}\right) - 16 \tag{1.1.5}$$

$$a^* = 500\left(f\left(\frac{X}{X_n}\right) - \left(\frac{Y}{Y_n}\right)\right) \tag{1.1.6}$$

$$b^* = 200\left(f\left(\frac{Y}{Y_n}\right) - \left(\frac{Z}{Z_n}\right)\right) \tag{1.1.7}$$

$$f(t) = \begin{cases} \sqrt[3]{t} & \text{if } t > \delta^3 \\ \frac{t}{3\delta^2} + \frac{4}{29} & \text{otherwise} \end{cases} \qquad \text{where } \delta = \frac{6}{29} \tag{1.1.8}$$

The CIE-L* chromaticity coordinate correlates to perceived lightness value, it ranges from 0 (black) to 100 (white). The CIE-a* and CIE-b* chromaticity coordinates are relative to the green–red and blue–yellow opponent colors, respectively, with negative values for green and blue and positive values for red and yellow. Values of 0 for CIE-a* and CIE-b* coordinates correspond with achromatic colors (black, gray, white) and as their values increase (or decrease), the saturation of the color increases. The range of these two coordinates is unbounded, and will be defined by the properties of the material, rather than the equations themselves. These CIE-L*a*b* coordinates are combined as cartesian coordinates in a three-dimensional color space as shown in Figure 1.2.

In some applications, representing color according to the perceived attributes of lightness, chroma and hue is of more practical interest [10]. In this case, the CIELAB color space is represented by cylindrical coordinates. In this color space, L* indicates lightness and it has the same interpretation as in the classical representation of the CIE-L*a*b* color space, C* relates to chroma, which is 0 at the center and increases according to the distance from the center; and h$^\circ$ relates to hue angle, is expressed in degrees, ranges from 0^o to 360^o and starts at CIE a* positive axis (Figure 1.2). The chroma and hue angle are computed from the a* and b* coordinates as indicated below:

$$C^* = \sqrt{a^{*2} + b^{*2}} \tag{1.1.9}$$

$$h^\circ = \arctan \frac{a^*}{b^*} \tag{1.1.10}$$

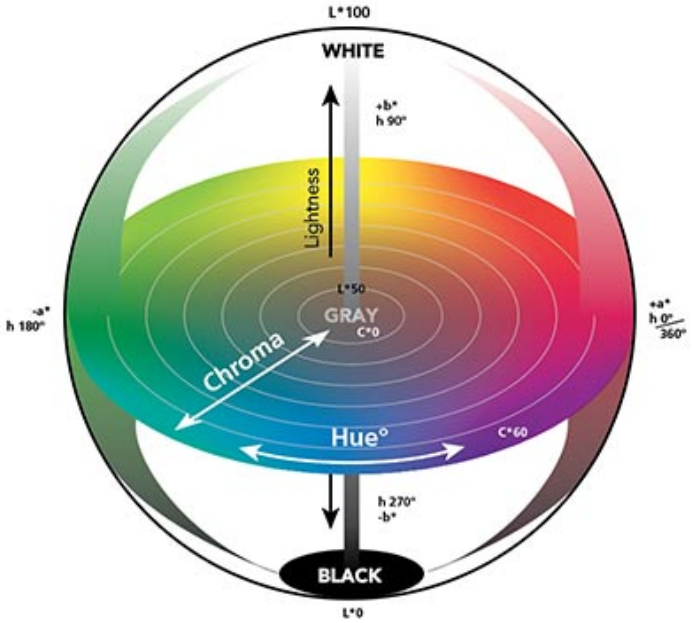

Figure 1.2: Schematic representation of the CIELAB color space (Reprinted from www.xrite.com).

1.1.3 CIE color difference equations

In the CIE L*a*b* color space, the color difference between two object color stimuli of the same size and shape, viewed in identical white to middle-gray surroundings, by an observer photopically adapted to a field of chromaticity not too different from that of average daylight, is quantified as the distance between the points representing their color in the color space [1]. These color differences can be expressed in terms of CIELAB color units as a single numerical value, ΔE, and this approach set the basis for the first total color difference formula introduced by the CIE in 1976, defined as the Euclidean distance between two points in the CIELAB color space, ΔE^*_{ab}:

$$\Delta E^*_{ab} = \sqrt{(L^*_1 - L^*_2)^2 + (a^*_1 - a^*_2)^2 + (b^*_1 - c^*_2)^2} \tag{1.1.11}$$

Although the CIELAB color space was designed aiming for perceptually uniform color differences throughout the whole space, this goal was not strictly achieved. As a consequence, soon after its implementation, the CIELAB ΔE^*_{ab} color difference formula was reported to present inhomogeneities [9, 28]. These perceptual non-uniformities pushed the CIE towards refining their definition over the years. After a long series of developments improving the CIELAB original total color difference formula, such as the CMC(l:c) [29], BFD(l:c) [30] and CIE94 [31] formulas, finally the CIEDE2000 total color difference formula was proposed [32]. This new metric clearly outperforms the before mentioned ones, and became the CIE recommendation for total color-difference computation in 2004 [17].

The CIEDE2000 color difference formula (ΔE_{00}), corrects the non-uniformity of the CIELAB color space for small color differences under reference conditions. Improvements in the color difference calculation were accounted by correcting for the effects of luminance, hue and chroma dependence, and chroma-hue interaction on the perceived color difference. Also, the scaling along the a* axis was modified to correct for the non-uniformity observed with gray colors [32]. After all these modifications, the resulting formula was defined as:

$$\Delta E_{00} = \left[\left(\frac{\Delta L'}{K_L S_L} \right)^2 + \left(\frac{\Delta C'}{K_C S_C} \right)^2 + \left(\frac{\Delta H'}{K_H S_H} \right)^2 + R_T \left(\frac{\Delta C'}{K_C S_C} \right) \left(\frac{\Delta H'}{K_H S_H} \right) \right]^{\frac{1}{2}} \tag{1.1.12}$$

where $\Delta L'$, $\Delta C'$ and $\Delta H'$ are the differences in luminance, chroma and hue for the two samples being compared. R_T is the rotation function, which is defined as the interaction between chroma and hue in the blue region. The weighting functions S_L, S_C and S_H adjust the total color difference for variation in the location of the color difference pair in L', a', b' coordinates. Finally, the parametric factors K_L, K_S, K_H are correction terms according to the experimental conditions of observation. Under

reference conditions, all these three parametric factors are set to 1.

The CIEDE2000 formula may not be the final word with respect to a color difference formula for small color differences for industry. However, at the present time the formula represents the most advanced development in this field and the best that can be achieved at this point.

1.2 Color in dentistry

In the last decades, esthetics has gained tremendous significance in dentistry. When performing a dental restoration, the reproduction of natural appearance of teeth represents nowadays a major concern, being appropriate tooth color determination one if its essential components [33]. Therefore, to guarantee the success of a dental restoration, this has to mimic not only the mechanical properties, but also the optical and esthetic properties of the dental tissues being replaced. In this sense, an exhaustive study of light interaction with these tissues is required to understand color in dental structures and, therefore, being able to develop appropriate dental restorative materials that could be used to replace them.

1.2.1 Color of dental structures

The permanent dentition consists of 32 teeth, which are divided into incisors, canines, premolars and molars. Each of them can be divided into two main parts, the root, which anchors the tooth to the alveolar bone, and the crown, which is the part that emerges from the maxillary bone, and the one of major concern in esthetic dentistry [34]. Teeth crowns consist of at least three layers of different materials:

- **Pulp**

  Dental pulp is composed of 25% organic matter and 75% water. It comprise the innermost layer of a tooth, and is a unique, specialized organ of the human body that serves four functions: formative, nutritive, sensory, and reparative [35]. It is composed of a central pulp chamber, which contains the large mass; pulp horns, and radicular canals [36]. Because of the continuous deposition of the dentine, the pulp chamber becomes smaller with age [37].

- **Dentine**

  Dentine is the middle layer of the tooth (between the enamel and the pulp), and makes up the bulk of the tooth's structure. It is made up of 70-72% inorganic materials (mainly hydroxyapatite and some non-crystalline amorphous calcium phosphate), 20% organic materials, and 8-10% water [38]. Dentine consists of microscopic channels, called dentinal tubules, which radiate outward through the dentine, from the pulp to the enamel border [39]. The different microanatomical structures and the tubular architecture, combined with the macroscopic anatomy of the dentine, produce a selective reflection/absorption of light. This effect may be responsible for the opacity of the primary dentine [40]. As the dental pulp ages, it reduces its size, leaving secondary dentine in its place and the surrounding dentine becomes harder and less permeable. At the same time, the chroma of the dentine becomes more saturated and opaque, and in general the brightness of the whole tooth decreases [41]. The color of dentine is typically a pale yellow. This yellow hue is generally what is seen penetrating through the enamel.

- **Enamel**

  Enamel is the hardest tissue in the human body. It is formed of 95% minerals

and 5% water and organic matter [42]. The primary mineral is hydroxyapatite, which is a crystalline calcium phosphate. In humans, enamel varies in thickness over the surface of the tooth, often thickest at the cusp (up to 2.5 mm) and thinner at its border with the cementum at the cementoenamel junction [43]. Enamel color varies from light yellow to grayish (bluish) white. Enamel is highly translucent and its translucency variations may be attributable to variations in the degree of calcification and homogeneity of the enamel [44].

It is largely accepted that the final color of a tooth is mainly determined by the scattering of the light within the internal tooth structures described above [25]. As with any other translucent sample, when light reaches a tooth surface, different phenomena associated with the interaction of light-tooth may occur: specular reflection at the tooth surface, diffuse reflectance, direct transmission through the tooth, absorption and scattering of light within the different tooth structures [1] (Figure 1.3).

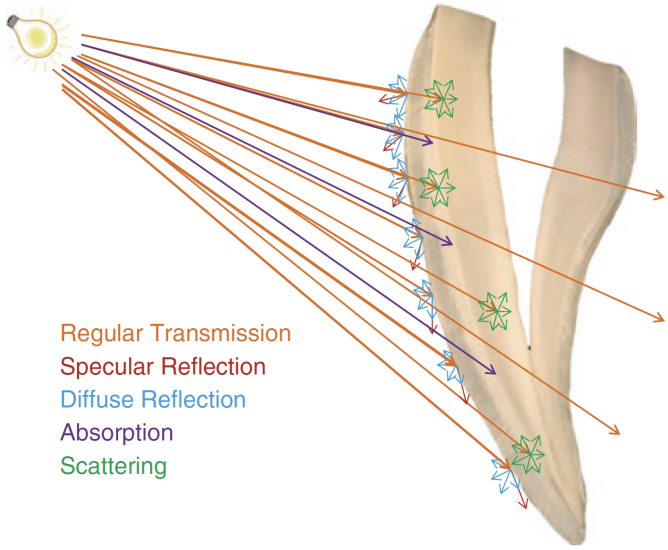

Figure 1.3: Schematic representation of the five phenomena (regular transmission, specular reflection, diffuse reflection, absorption and scattering) that may occur in the interaction of incident radiation and tooth [1].

However, not only these phenomena affect the appearance of dental structures. There are several other factors such as the translucency, opacity, surface gloss, surface roughness and fluorescence that may influence. Among them, translucency and opacity are the most important, since they modulate the quantity and quality of light interaction with the tooth. In this regard, due to the higher translucency of enamel layer, dentine shade will strongly affect the overall chromatic appearance of the tooth. It was also highlighted that yellowish teeth normally have a thin, translucent enamel through which the main color of the dentine is visible, while grayish teeth often have a more opaque, less translucent enamel [45,46]. Also, it has to be considered that the thickness of the different dental layers is not uniform throughout the dental structure, but vary with respect to different areas of the tooth [47,48]. These variations create a color change (gradient) along the different axes of the dental structures. For example, the dentine layer is thicker in the cervical area of the tooth, and significantly contributes to the tooth color in that specific region, while for the incisal area the dentine layer is thinner, and the enamel layer is thicker, therefore influencing the light transmission behavior in that region, and thus its color [49]. A very good example of all these factors can be observed in Figure 1.4, where the transillumination of natural teeth can be observed showing the major features of both dentine and enamel. Dentine gives the tooth its color, the perception of which is modulated by the enamel, a semitranslucent and highly opalescent tissue [2].

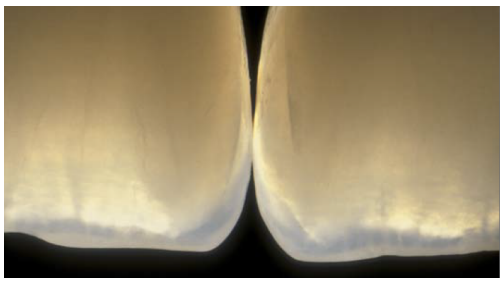

Figure 1.4: Transillumination of natural teeth (Reprinted form [2])

Different studies have shown an existing relationship between thickness, color and the optical properties of dental structures [50–53]. Moreover, tooth color is also affected by other factors such as as tooth type, gender, age, and ethnicity, as has been reported in many studies [54], in which the range and distribution of tooth color has been fully investigated. In general, the maxillary anterior teeth are slightly more yellowish than mandibular anterior teeth, and the maxillary central incisors have higher value than the lateral incisors and canines [55,56]. Also, teeth color shift with age was also reported, as they become darker and yellowish over the course of time [57]. While some studies have shown no differences in teeth color related to gender, other studies reported that females exhibit lighter and less yellowish incisors [55,58–61]. Studies investigating the relationship of skin color to tooth shade are contradictory. Most studies show no relationship, but some reported an inverse relationship where people with medium-dark skin tones were more likely to have higher value (lighter) teeth color than people with lighter skin tones, regardless of their age or gender [62].

So far, it is clear the fundamental role of color in the dental field. That is why many studies attempted to establish a reference chromatic space for dentistry, as a sub-space of the CIELAB color space. Ideally, this dental color space has to include the color of all natural dental structures as well as the color of all dental restorative materials [54,57]. A study carried out to better understand the VITA 3D-Master shade system, concluded that the average values of the CIE L*, a*, b*, C^* and h° chromaticity coordinates that more precisely define the dental color space were: L* = 62 - 78; a* = 1 - 6; b* = 12 - 31; C^* = 12 - 33 and h° = 78 - 86 [3]. More recently, another study established the color limits of the same set of samples, with slightly different outcome: L* = 51.5 - 85.5; a* = -1.5 - 12.6 and b* = 12.0 - 43.3 [63]. Another study, that compared the limits of the VITA 3D-Master shade system with a database of nine hundred and thirty-

three maxillary central incisors [64], established a dental color space defined by the following chromatic coordinates: L* = 65.1 - 83.2; a* = 1.7 – 8.9 and b* = 12.3 - 29.3, respectively.

It is clear that, for the moment, there is no wide agreement on the exact values of the chromaticity coordinates that set the boundaries of the dental color space, so slight variations from this coordinates are normally accepted. However, all aforementioned studies agree that the various tooth colors mainly differ in their lightness, and that is why the tooth color space is vertical to lightness axis and expands similar to a "banana" [3]. The lighter teeth are in the upper area and the darker ones in the lower area. The more chromatic tooth colors are situated at the outer curve of the "banana" which is further away from the achromatic central axis, as shown in Figure 1.5:

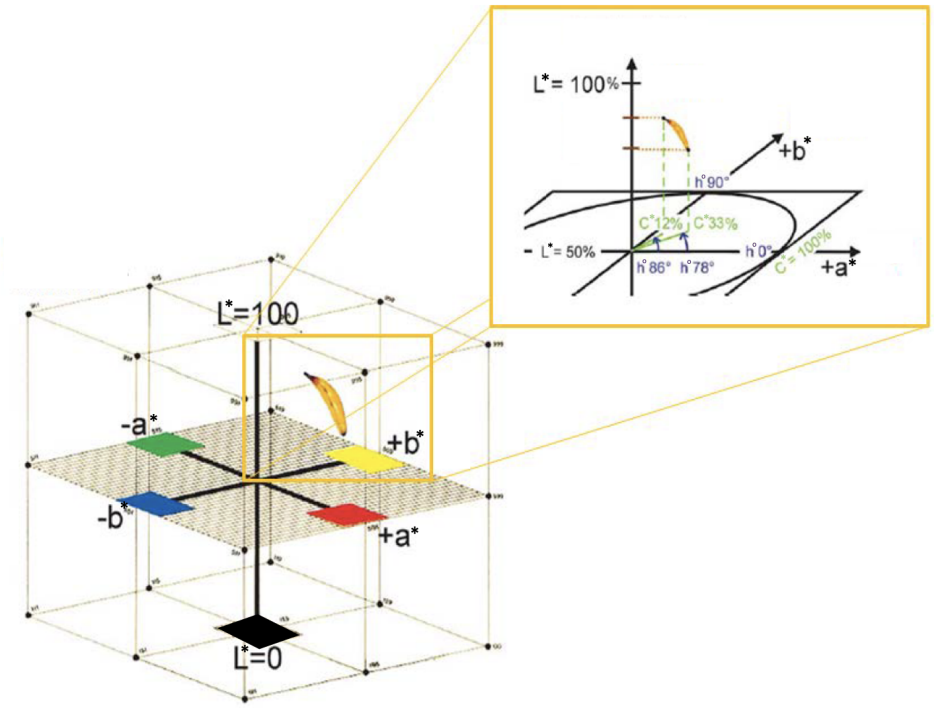

Figure 1.5: Schematic representation of the dental space within the CIELAB color space. (Reprinted from [3]).

1.2.2 Color measurement in dentistry

Considering the high clinical relevance of a precise tooth color determination, systems that aim for an objective and reproducible tooth color assessment are continuously being developed [65]. Yet, measuring color of dental structures is a challenging task, mostly because of the inherent characteristics of the human teeth, such as curved small surfaces, layered structure with complex optical properties and translucency, among others [66].

The current standard in dental practice remains the visual method using shade guide systems [65,67,68]. This method relies on the visual comparison of the elements of a shade guide (the shade tabs) with the dental structures to be color matched. The dental practitioner chooses the best match from the available shade tabs, in a highly subjective color matching task. There are several dental shade guides available (such as Ivoclar Vivadent Chromascop, Dentsply Esthet-X, Blue Line, etc.). However, the most widespread systems for visual tooth colour determination are the VITA Classical (VITA Zahnfabrik, Bad Säckingen, Germany) and the VITA 3D-MASTER (VITA Zahnfabrik, Bad Säckingen, Germany) shade guides (Figures 1.6a and 1.6b).

The VITA Classical shade guide system includes 16 shade tabs, and it has been the most popular dental shade matching system for many years. It consists of one-step shade matching by direct comparison between tooth and one of the A–D shade tabs. However, it presents some drawbacks, such as the empirical arrangement of shades and the uneven coverage of the available shades of the natural tooth color space, as shown in Figure 1.6d, where it can be seen that there is a better shade coverage for the central area of the tooth color space than for darker and lighter regions. This distribution of shade tabs complicates the visual shade matching and, therefore, might result in poor matches between natural tooth and the selected shade tab.

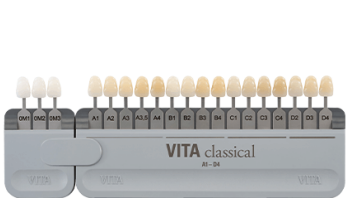

(a) VITA classical A1-D4®

(b) VITA Toothguide 3D-MASTER®

(c) VITA Linearguide 3D-MASTER

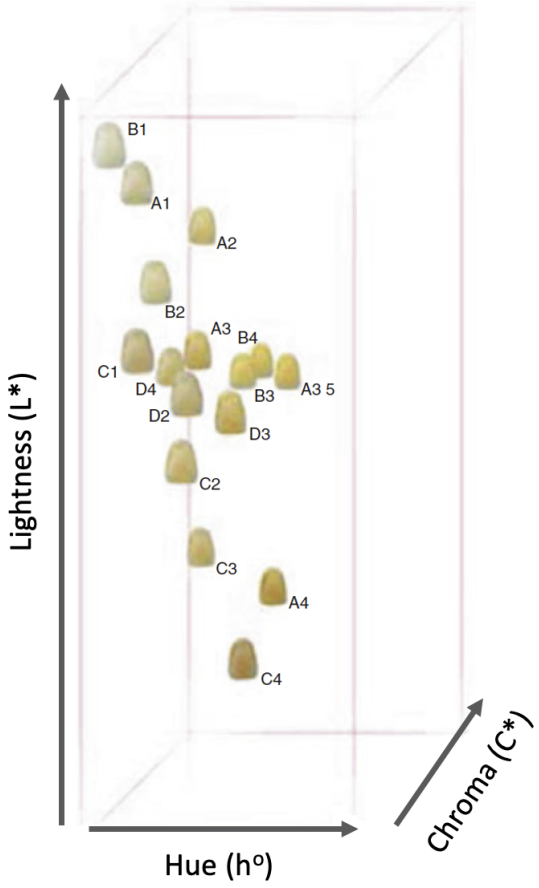

(d) VITA Classical shade distribution.

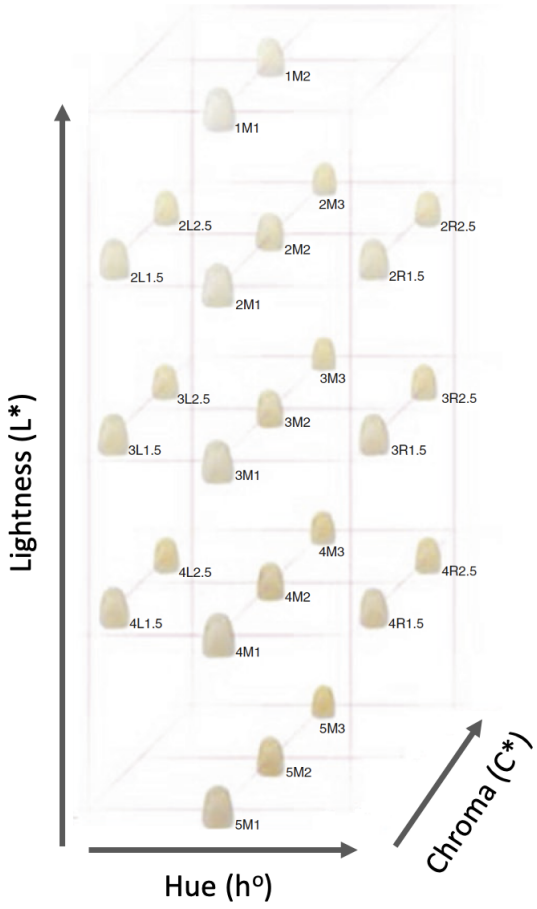

(e) VITA 3D-Master shade distribution.

Figure 1.6: Chromatic distribution of the VITA shade tabs. Lightness (L*) goes from darker (bottom) to brighter (top) shades. Hue (h°) goes from more yellow (left) to more red (right), and chroma (C*) goes from paler to more intensive shades. (Reprinted from Vita-Zahnfabrik and [4]).

Intending to overcome this adversity, the VITA 3D-MASTER shade guide system was developed. This is a shade guide system that includes 26 shade tabs and three

additional bleached shades. The main difference to VITA Classical is that the shade tabs are systematically arranged, to uniformly cover the dental chromatic color space (Figure 1.6e). In this system, tooth color is determined in three steps, corresponding to the three parameters of the three-dimensional CIE L*C*h° colour space: value, chroma and hue, and thus enables more accurate measurement [67]. However, the three-step shade matching procedure has been reported to be a more time consuming process [69]. To handle this issue, the VITA Linearguide 3D-Master (Figure 1.6c), which includes the same 29 shades from the 3D-Master system but in a linear design, was finally introduced.

Bearing in mind the numerous weaknesses of subjective tooth colour determination, which might be affected by a large variety of parameters, such as variability among different shade guides [70], the background [71] and surrounding area [72], lightning conditions [73], gender [74] or experience of the observer [75], instrumental shade matching was introduced in dentistry as an attempt to reduce the subjectivity of visual shade matching.

Colorimeters, spectrophotometers and digital imaging systems are the most popular instruments for objective color measurements in dentistry [68]. The colorimeter ShadeVision (X-Rite, Grandville, MI); the spectrophotometers Vita Easyshade (VITA Zahnfabrik, Bad Säckingen, Germany) and Shade-X (X-Rite, Grandville, MI); and the imaging systems SpectroShade Micro II (MHT, Niederhasli, Switzerland) and CrystalEye (Olympus,Tokyo, Japan), are currently among the most popular commercially available instruments for objective measurements of color in dentistry [1,68].

All these aforementioned instruments have their pros and cons. Colorimeters show good measurement repeatability but they are exposed to systematic errors caused by edge-loss effects from sample surface. Digital imaging systems represent the most basic approach to electronic shade taking, and still require a certain de-

gree of subjective shade selection with the human eye [76]. In this regard, due to their ability to measure the amount of light reflected throughout the visible spectral range, spectrophotometers can provide more systematic and precise measurements than colorimeters or digital imaging methods [77–80]. The recent incorporation of spectroradiometers for color measurements in dental research provided accurate and highly repeatable non-contact measurements. Spectroradiometers are recognized as the gold standard devices for objective accurate color measurements and have been widely used in many research studies for the evaluation of the colorimetric and optical properties of dental materials [13, 26, 81–84]. One of the main advantages of these devices is that they measure complete spectral data, which provides information on the consistency of the material and can detect potential problems of metamerism, allowing to calculate colorimetric data for the actual spectral power distribution of each source expected to illuminate the specimen [85]. However, their main constraint in the dental field is their impracticality in clinical scenarios. This adds up to other limitations, shared with other clinical commercial devices, such as single spot or large integrated area of measurement. So far in dentistry, spectroradiometric color measurements are used exclusively for research purposes [26].

In addition, it must be taken into account that instrumental color measurements of the same specimen do not necessarily produce identical results, even if repeated at the same site and using the same instrument [86, 87]. Differences may be caused by the quality of the instrument, operator ability, specimen handling and specimen condition, accidental or unknown causes [86–90]. In order to create a standardized protocol and quality control tool for color measurements in dentistry, a multi-center study was coordinated by the Houston Center for Biomaterials and Biomimetics (HCBB) at the University of Texas School of Dentistry, and it involved the University of Granada Faculty of Sciences, Vita Zahnfabrik and the Ohio State University College of

Dentistry [26]. The main purpose of this study was to propose a method of reflectance measurement harmonization for translucent dental specimens of clinically relevant thickness. The guidelines derived from this research have been indeed implemented for the development of the studies that will be later presented in this Thesis.

It is clear that, benefits and limitations exist among different shade determination methods, and the clinician must consider how the technology relates to his/hers expectations and needs. Therefore, whenever possible, instrumental and visual color matching methods should be used jointly for dental color assessment, as they complement each other and can lead towards better esthetic outcome.

1.2.3 Color difference thresholds in dentistry

To achieve the desired esthetic result in dental restorations, dental materials must efficiently match and reproduce the color appearance of natural teeth and other soft tissues. However, exact match of color is still a very rare event [91] and, thus, the quality of color match between a dental restoration and an adjacent natural tooth correlates, to large extent, with the magnitude and direction of the color difference between the above mentioned structures.

Since visual judgment is still the most frequent method for color evaluation in dentistry, a knowledge of the perceptual limits (visual thresholds) for color assessment is of vital importance in clinical dentistry and dental research. These thresholds can serve as a quality control tool and as a guide for the selection of dental materials, the evaluation of the clinical outcome and subsequent standardization [27, 92].

This limits can be only defined with psychophysical experimentation, which allows to correlate results of the observer evaluations with the instrument measurements. When assessing color difference thresholds, there are two relevant thresholds that have to be considered: perceptibility threshold (PT) and acceptability threshold

(AT). The perceptibility threshold relates to the smallest perceptible color difference, a just-noticeable difference (JND), that can be detected by an average human observer. In this context, the 50:50% perceptibility threshold refers to a situation in which 50% of the observers would notice a color difference between two objects while the other 50% notice no difference. Similarly, 50:50% acceptability threshold refers to a color difference that is considered acceptable for 50% of observers, meaning that the other 50% of observers would not consider the color difference as acceptable, which in a clinical situation, implies that the dental restoration requires color correction [93, 94]. The color differences between these two thresholds is the so-called industry tolerance. The interest on this tolerance range is clear, since maintaining the industrial production below the limits of the visual threshold would result very costly and time consuming, but there is still the need of maintaining the differences under an admissible limit.

As the standard for color research in dentistry, most studies trying to define color difference thresholds in this field used the CIELAB color space and its associated color difference formulas. Over the years, different color difference formulas have been used [31, 95], mostly ΔE^*_{ab} formula. However, recent studies have reported that the new CIEDE2000, ΔE_{00}, color difference formula provides a better fit than the CIELAB formula in the evaluation of visual tolerances [92, 96–98]. A variety of visual color threshold values have been reported in numerous studies related to teeth, gingiva and dental materials [27]. The first study that reported ΔE_{00}-based PT and AT for dentistry was published in 2010 [97]. They used the Takagi–Sugeno–Kang (TSK) fuzzy approximation, previously used in [99–101], and concluded that CIEDE2000 formula provided indeed a better fit than CIELAB formula for the evaluation of color difference thresholds of dental ceramics, and therefore recommended its use in dental research and in vivo instrumental color analysis. They also showed a significant difference between PT and AT for dental ceramics and validated that the TSK Fuzzy

Approximation is a reliable alternative approach for the color threshold calculation procedure.

Few years later, within the context of a multicenter study in which 7 research sites participated [92], the 50:50% PT and 50:50% AT values for dentistry under simulated clinical settings where determined. Visual color comparisons were performed at each site by a total of 25 observers, divided into five groups: dentists, dental students, dental auxiliaries, dental technicians, and laypersons. According to the results of this study, the overall CIELAB 50:50% PT and 50:50% AT were $\Delta E^*_{ab} = 1.2$ and $\Delta E^*_{ab} = 2.7$, respectively, while corresponding values computed with the CIEDE2000 color difference formula (ΔE_{00}) were $PT_{00} = 0.8$ and $AT_{00} = 1.8$. These results were included as reference values within ISO/TR 28642:2016 [94] and can be applied to all issues related to quality of tooth color matching in dentistry, such as color compatibility between dental materials and human tissues [102], color compatibility among dental materials [103], color stability during fabrication and at placement [104], coverage error evaluation of dental shade guides [105], color stability after aging [106], among many other applications.

Additionally, CIEDE2000 acceptability thresholds for individual axis of lightness ($\Delta L'$), chroma ($\Delta C'$), and hue ($\Delta H'$) were also reported [107] as 50:50% AT_{00} of 2.92, 2.52 and 1.90, respectively.

Therefore, as the current standard for color evaluation in dentistry and recommended by the ISO [94], together with other error metrics that will be later described, the CIEDE2000 color difference formula and its corresponding AT_{00} and TP_{00}, will be used as performance descriptors of the studies that will be further presented in this Thesis.

1.3 Dental restorative materials

When, in a clinical scenario, a dentist has to restore fully or partially a tooth, the success of the restoration depends not only on the ability to accurately interpret the characteristics of the natural dental structure to be restored or the skill and knowledge of the clinician, but also on the quality and properties of the restorative material used. There is currently a wide variety of dental restorative materials, including cement bases, amalgams, primers, bonding agents, liners, resin-based composites, hybrid ionomers, cast metals, metal-ceramics, ceramics, and denture polymers [108]. In this section, dental ceramics and resin-based composites will be introduced in detail, since they are the materials that will be used later in the Thesis.

Dental restorative materials can be divided into two categories: On one hand, direct restorative materials which are fabricated to be placed directly on the teeth structure, whereas indirect restorative materials are commonly used as prosthesis and are fabricated outside the oral environment [109]. To date, the ideal restorative material with favorable properties such as biocompatibility, long-term durability, high mechanical strength, appropriate fracture toughness, and tooth-like color and translucency has not been achieved. However, knowing the characteristics, properties and limitations of each restorative material helps chooseing the best material for each specific application in restorative dentistry.

1.3.1 Dental Ceramics

The development of new generation ceramics has been always a challenging issue in the dental field, requiring an extensive study on ceramic composition, microstructure, crystalline phase content, mechanical properties and biocompatibility.

Continuously, various types of ceramics and fabrication methods have been developed to satisfy the demands of dentists and patients in restorative dentistry, and dental ceramics have been widely used for dental applications due to their great clinical, physical, optical, and mechanical properties.

Over the years, there have been several attempts to manufacture suitable dental ceramics for use in restorative dentistry [110], from the introduction of traditional feldspathic porcelains to the development of modern ceramics with outstanding strength, toughness, and esthetics.

Originally, metal-ceramic materials, obtained by veneering feldspathic porcelains over metal substructures, were used. However, the use of these metal structures negatively impacts on the opacity of the restorative dental ceramic [111]. Therefore, as an answer to the increasing demand for restorations with better optical properties, metal-free materials (also known as all-ceramic) were developed. All-ceramic dental restorations present a high color match to the natural human teeth and outstanding mechanical properties, due to their large amount of crystalline phase (35–99 vol.%). The crystalline phase of the all-ceramics materials can be lithium disilicate glass-ceramics, alumina/zirconia, and zirconia. Alumina-reinforced leucite-based ceramic was the first product of all-ceramic restorations. Glass-infiltrated ceramics including VITA In-ceram Alumina, Spinell, and Zirconia (Vita Zahnfabrik, Bad Sächingen, Germany), which presented higher strength and better optical properties than feldspathic porcelains, were introduced afterward [109].

All-ceramic crowns offer increased potential for success in mimicking the appearance of natural teeth, especially when high degree of translucency is desired. After many attempts, modern glass-ceramics were developed in the 1990s, by introducing heat-pressed ceramics with easier fabrication procedures and better overall optical and mechanical properties. Leucite-reinforced (IPS Empress®; Ivoclar, Schaan,

Liechtenstein) and lithium disilicate-reinforced (IPS Empress® II, IPS e.max®; Ivoclar, Schaan, Liechtenstein) glass-ceramics are some examples [109].

1.3.1.1 Lithium-Disilicate Glass-Ceramics

Lithium-Disilicate Glass-Ceramics (LDGC) are fabricated using a combination of lost-wax and heat-pressed techniques by adding lithium oxide to the aluminosilicate glass. These are based on the system of $Li_2O : 2SiO_2$. Although LDGC are widely used with great success, the are still some remaining disadvantages. In this sense, the use of polycrystalline-reinforced zirconia-containing lithium-silicate ceramics (ZLS) was of great help [112].

ZLS is based on lithium-silicate glass with 10 wt% zirconia added as a nucleation agent. The microstructure of this kind of glass ceramics contains fine and round-shaped lithium metasilicate (Li_2SiO_3) crystals, rod-like lithium disilicate ($Li_2Si_2O_5$) crystals, and zirconia-containing glass matrix [112].

VITA Suprinity (Vita Zahnfabrik, Bad Sächingen, Germany) and CELTRA Duo (Dentisply-Sirona, Bensheim, Germany) are examples of these glass-ceramics applied in restorative dentistry. The main advantage of these materials is their effectiveness for the production of dental restorations, since, due to their improved composition, they can be already offered in their fully crystallized state or requiring a very short crystallization cycle, by the manufacturers.

However, there are still some common clinical complications associated with the use of all-ceramic restorations, mostly related to the fracture of the veneering porcelain or the substructure. Therefore, the success of the use of these materials depends, to a large extent, on the procedures utilized to prevent crack propagation as well as the capability of clinicians to properly select the materials, cements, procedures and thickness ratio [113–115].

1.3.2 Dental resin composites

Dental resin composites represent one of the many successes of modern biomaterials, due to their biocompatibility, esthetics, antibacterial, and nontoxic characteristics [116]. Although they still face some clinical drawbacks, such as lower durability than the ceramic-based materials, polymerization shrinkage, tooth sensitivity after application, marginal staining or secondary caries [117], the possibility of direct application (in-situ curing) has made them the most commonly used biomaterials for direct dental restorations.

1.3.2.1 Chemical composition of dental composites

Chemistry of a biomaterial is of critical importance since it provides information regarding its composition, the nature of its surface behavior, its potential for degradation in-vivo and so on, which are aspects that have an impact on the durability and lifetime of the material.

A dental composite includes a resin matrix, inorganic fillers, coupling agents and initiator-accelerator system [109].

The resin-based oligomer matrix is most commonly composed of bisfenol-A-glicidil-metacrilato (bis-GMA) and urethane dimethacrylate (UDMA). As these monomers are strongly viscous, it is essential to blend them with other monomers having lower molecular weights in order to facilitate blending and manipulation of the composite, such hydroxyethylmethacrylate (HEMA) or triethylene glycol dimethacrylate (TEGDMA), among others [118].

In order to enhance the hardness, wear resistance and translucency of the composite, as well as to reduce the curing shrinkage and thermal expansion coefficient [111,119], fillers are added in the structure of the resin matrix. Some examples

of filler particles used in dental composites are quartz, aluminum silicate, lithium aluminum silicate, ytterbium fluoride, and barium, strontium, zirconium and zinc glasses.

The coupling agent is a bonding agent, which is applied on the surface of filler particles to enhance their chemical bond to the matrix [109]. The coupling agent system usually consists of organic silane such as 3-methacryloxypropyltrimethoxysilane and 10-methacryloyloxydecyl dihydrogen phosphate (10-MDP) [120].

Finally, in order to obtain a hardened structure the initiator-accelerator system is used to polymerize and cross-link the polymeric matrix when external energy (light or heat) is applied.

1.3.2.2 Classification of dental composites

Dental composites can be classified according to different aspects such as their composition, performance characteristics, elastic modulus, surface roughness and compressing strength, among others [121–123]. There are two mainly used classifications of dental composites: based on the particle size of reinforcing fillers and based on their curing modes.

- **Filler particle size:**

  According to their filler particle size, composites can be classified into: macrofilled, microfilled, hybrids and nanofilled composites [117].

  Conventional dental composites, also known as macrofilled composites, contained large particles (10–50 μm) with spherical or irregular shapes. These were mechanically strong and difficult to polish, however they presented low wear resistance [124,125]. They were also almost opaque and difficult to retain a favorable color match. Due to the large filler particles in their structure, achieving

smooth surfaces was rather impossible [125].

Later, amorphous spherical silica of approximately (0.01 μm and 0.1 μm) and resin fillers inserted in a polymeric matrix (5 μm to 50 μm) were incorporated to formulate microfill composites [109]. These were more esthetically pleasing but, due to the low filler contents, their strength was rather poor and therefore they were more vulnerable to fractures and prone to lose their anatomical shape due to wear.

To attempt for long-term esthetics and improved mechanical properties, the particle size of conventional composites (macrofilled and microfilled) was reduced to produce the so-called hybrid composites, composed of microfine particles (0.01–0.1 μm) accompanied with fine particles (0.1–10 μm) and submicron particles (0.4–1.0 μm). Compared to macrofilled and microfilled, these type of resin-based composites present lower shrinkage, improved polishing performance and better esthetics [126], and they are produced in a variety of different shades with tailored opacity and translucency [127]. Therefore, they can be considered among the best materials for posterior restorations.

Finally, with the advent of nanotechnology, nanofilled composites (with particles ranging between 1–100 nm) were introduced. Most of the nanocomposites are composed of conventional particles accompanied with nanofillers, therefore they can be called hybrid nanocomposites. They present higher polishability and better optical properties than other types of composites. However, nanofilled and nanohybrid composites do not present any significant benefit over microhybrids regarding surface condition, marginal quality and wear or fatigue resistance [128]. Thus, it is up to the clinical dentist to choose between the proposed restorative materials for each particular case.

- **Curing modes:**

  Polymerization efficiency affects several properties of composites such as degree of conversion, degree of cross-linking, mechanical properties, shrinkage stress, curing depth, trapped free radicals, and biocompatibility [109]. In this regard, dental composites used for direct restorations can be divided into chemically activated (self-cured), photochemically activated (light-cured) or dual-cured composites [129].

  Chemical-cured composites polymerization is initiated by an oxidation-reduction initiator system when a base and a catalyst paste are mixed together at room temperature. The catalyst paste contains benzoyl peroxide initiator, while the base paste contains tertiary amine such as N, N-dimethyl-p-toluidine. When the two parts are mixed, the radicals formed by the reaction of the initiator and the amine are able to react with the monomers that would become polymerized later [130].

  Among the disadvantages of this type of composites it can be highlighted that pore formation is inevitable during the mixing process, which makes the structure weaker, and also that they need to be quickly manipulated after the mixing process, as there is still a lack of control of the working time of the mixed pastes. Therefore, these self-cure composites are mostly used as resin-based luting cements or core materials, rather than direct restorations [129].

  In order to overcome these drawbacks of chemically activated composites, light-cured resins contain photosensitizer and amine initiator, which initiate free radicals using a light source without the need of a mixing process. The first product of this type were UV-activated composites. However, these resin-based composites have been replaced by safer visible blue light-activated compos-

ites [131]. These contain CQ/amine complex initiation which provides superior curing depth and controllable working time. These composites present several benefits, such as low porosity, good strength, low staining, improved color stability, controlled working time by exposure to light and availability of multiple shades [109]. Noteworthy, these resins still present some drawbacks, such as limitations of expensive lamps, dependence of curing on light intensity, light angle, and curing depth thickness of up to 2 mm, forcing them to be applied in small thickness increments at a time, which results in more time-consuming clinical processes [117].

In this regard, the development of dual-cured resins has allowed the curing process of composites to be completed and to have increased curing depth by combining the advantages of light and chemical curing systems.

Most of the advances discussed herein remain in the research stage and there is much potential for further improvement. Therefore, it is clear that, research in the field of dental composites continues to propose and achieve significant advances in resin formulation, filler loading and modification, as well as curing methodologies and mechanisms.

1.4 Color prediction in dentistry

The importance of color in esthetic dentistry has become evident over the last decades. To meet this increasing demand, dental material manufacturers have introduced a wide variety of materials and shades, that has to match the appearance (optical properties and color) of the natural structures that they are meant to re-

place. Therefore, an adequate knowledge of the optical and colorimetric properties of these materials is of great interest, since it leads to a better esthetic result [132]. This requirement is difficult to fulfil as, from the optical point of view, these natural tissues are very complex, presenting very characteristic chromatic properties and translucency [133]. Yet, color matching of restorations is a very difficult step for most clinicians, and accurate shade determination is still a challenge.

In this regard, the use of artificial intelligence and color prediction methods can have an impact on the dental profession and also complement the development of digital technologies and tools [134].

Given this demand for esthetics, a specific treatment such as teeth bleaching is becoming increasingly popular among patients and dentists, as it is a relatively non-invasive method of whitening and lightening the teeth. The effectiveness of a tooth-bleaching treatment was usually judged by visual inspections and comparisons with shades guides. Therefore, different authors implemented fuzzy logic approaches [101] and multivariate linear regression models [135], which can be applied in clinical scenarios to predict the color change after bleaching.

In addition, in order to provide scientific information on shade selection for toothless patients, some authors implemented color prediction models based on some characteristics of the dentate subjects, such as age, gender and the color of the other craniofacial structures [59, 60]. They studied both linear and non-linear regression approaches and concluded that linear regression models were the most suitable for the prediction the CIE-L*a*b* color coordinates of the central incisors.

The Kubelka-Munk theory (K-M), which has been mainly used to determine the optical properties of non-homogeneous media [136, 137], was also proven to be valid for reflectance prediction of dental samples. This theory is able to provide simple mathematical expressions to determine the optical parameters from reflection and

diffuse transmission measurements of a sample. Already in early 1980s, some authors successfully predicted the color of different dental composites using this theory. More recently, different authors have proven this theory to be valid for reflectance, and therefore color prediction of single [138,139] and layered dental resin composites [138].

Furthermore, a recent study [140], confirmed the possibility of using a combination of Genetic Algorithms and Neural Networks for computational color matching in dental restorations, while other authors were able to predict reflectance data of experimental dental resin composites with added pigments by using a multiple nonlinear regression model [141].

Over the years, many mathematical techniques have been developed to reconstruct spectral reflectance data in different color research areas [142–146]. Among all of them, linear regression and principal component analysis (PCA) are worth to be highlighted for their simplicity and versatility [147–149].

It is clear that, color prediction in dentistry is a growing research area [134]. However, the prediction of the reflectance spectrum as well as the color coordinates of monolithic and layered dental materials as a function of their thickness is still an unsolved problem. These type of predictions have the potential to provide essential information of the final appearance of a dental restoration, which can be of vital importance to reduce the trial-and-error of manufacturing processes and to improve the esthetic outcome of a dental restoration.

1.4.1 Regression analysis

Regression problems are frequent in machine learning, and regression analysis is a commonly used technique to solve them. Regression attempts to determine the relationship between one dependent variable and a series of other variables. Regression analysis includes several variations, such as linear, multiple linear, which are the

most common, and non-linear, which is far more complicated, and is commonly used for data sets in which the dependent and independent variables show a nonlinear relationship [150].

Linear regression models:

The most well-known regression modelling technique is linear regression, which assumes a linear connection between a dependent variable and a single or a set of independent variables. The linear regression model is so-called simple (SLR) when only one independent variable is used, or complex, when several independent variables are used. The mathematical representation of a multiple linear regression (MLR) model is:

$$y = \beta_0 + \beta_1 x_1 + ... + \beta_m x_m + \epsilon \tag{1.4.1}$$

which determines the best-fit hyperplane that passes through all the data points with the smallest possible distance between the fit and each data point.

Polynomial regression [151, 152] is a type of MLR that allows for higher-order regression models of the relationship between independent and dependent variables. Although polynomial regression fits a nonlinear model to the data, as a statistical estimation problem it is linear, in the sense that the regression function is linear in the unknown parameters that are estimated from the data. In case of considering h^{th} degree polynomial and a single independent variable, the mathematical representation (now being be a curve rather than a straight line) would be:

$$y = \beta_0 + \beta_1 x + \beta_2 x^2 + ... + \beta_h x^h + \epsilon \tag{1.4.2}$$

where h is the polynomial degree [150].

To optimize a polynomial regression model, a simple data set can be used, consisting of n points (x_i, y_i), with $i = 1, \ldots, n$, where x_i is an independent variable and

y_i is a dependent variable. The model function can be defined as $f(x, \beta)$, being β a vector holding m parameters, β = ($\beta_1, \beta_2, ..., \beta_m$). The goal is to find the parameters β_j so that the model function best fit the data [150]:

$$\hat{\beta} = (X^T X)^{-1} X^T Y \tag{1.4.3}$$

The fit of a model to a data point is measured by its residual, defined as the difference between the observed value of the dependent variable and the value predicted by the model:

$$r_i = y_i - f(x_i, \beta) \tag{1.4.4}$$

The least-squares method finds the optimal parameter values by minimizing the sum of squared residuals, S:

$$S = \sum_{i=1}^{n} r_i^2 \tag{1.4.5}$$

Linear regression models have been widely used for color prediction in dentistry. Some authors, attempted to predict teeth color with respect to age and gender [60]. This technique has also been used to evaluate the role of enamel thickness and predict refractive index on human tooth color [153], while other authors implemented a MLR method to predict the CIE-L*a*b* values of dental ceramics with different pigment concentrations [154], and evaluated its performance versus the Kubelka-Munk theory approach [155]. These are just a few examples of the huge amount of studies that implemented regression modeling in dental research.

1.4.2 Principal Components Analysis basis

Principal component analysis is a mathematical algorithm that reduces the dimensionality of the data while retaining most of the variation in the data set [147–149]. It accomplishes this reduction by identifying directions, called principal components, along which the variation in the data is maximal. By using a few components, each sample can be represented by relatively few numbers instead of by values for thousands of variables [147]. In other words, any sample can be represented as a linear combination of a few principal components and weighting coefficients.

PCA Algorithm:

Although understanding the details underlying PCA requires knowledge of linear algebra [147–149], the basics can be explained with simple geometrical interpretations of the data. The steps involving the PCA Algorithm are:

1. Data standardization.

   The first step is to normalize the data so that each variable contributes equally to the analysis. This is done by subtracting the respective means from the numbers in the respective column:

   $$x_s^i = \frac{x^i - \mu_x}{\sigma_x} \tag{1.4.6}$$

2. Calculate covariance matrix of the data set.

   Covariance measures how two features vary with each other. For a given data set with n samples, the covariance ,σ_{jk}, between two feature vectors x_j and x_k can be calculated using the following equation:

   $$\sigma_{jk} = \frac{1}{n-1} \sum_{n}^{i=1} (x_j^i - \mu_j)(x_k^i - \mu_k) \tag{1.4.7}$$

Therefore for a standardized data set, covariance matrix can be computed as:

$$C = \frac{X^T X}{n-1} \tag{1.4.8}$$

were X is the data set and X^T is the transpose.

3. Compute Eigenvectors and corresponding Eigenvalues.

   In linear algebra, an eigenvector is a nonzero vector that changes at most by a scalar factor when a linear transformation is applied to it. It represents the principal components (the directions of maximum variance) of the covariance matrix. The eigenvalues are their corresponding magnitude. In this sense, the eigenvector that has the largest corresponding eigenvalue represents the direction of maximum variance.

   For a given covariance matrix, C, an eigenvector, $\vec{v}$ satisfies the following condition:

   $$C\vec{v} = \lambda\vec{v} \Rightarrow (C - \lambda I)\vec{v} = 0 \tag{1.4.9}$$

   where λ is the eigenvalue associated with eigenvector $\vec{v}$ of C, and I is the identity matrix.

4. Extract the principal components with the highest eigenvalues.

   To do so, the eigenvectors are sorted with respect to their decreasing order of eigenvalues. After choosing the more representative principal components, the new matrix of vectors is created and is known as feature vector matrix, Z.

5. Compute protection matrix.

   Finally, the projection matrix, which contains the transformed data of the original data set, can be computed by simply multiplying the feature vector matrix

with the data set matrix, as shown in:

$$W = ZX \tag{1.4.10}$$

Many applications beyond dimensional reduction, classification and clustering have taken advantage of the global representations of this decomposition. Applications, including patterns recognition and filtering [156], estimating missing data [157] or associating genes and expression patterns with activities [158], are some examples.

In dentistry, PCA was used to find appropriate axes for dental color evaluation by analyzing spectral data itself, rather than conventional 3-dimensional color spaces [159]. However, it may be further exploited, as it is a powerful tool for the characterization of multidimensional data, especially spectral data, whose reads present a high colinearity among the near wavelenghts. PCA operation as an approximator allows to manage spectral data by handling a few principal components, which consequently reduces the amount of data needed, with disposable information loss. The use of a reduced number of principal components acts further as a regularization technique to avoid noise and overfitting [160]. These advantages may be thus harnessed for spectral estimation in dentistry.

CHAPTER

2

MOTIVATION AND OBJECTIVES

This PhD Thesis is intended to contribute to the progress of knowledge in the field of esthetic dentistry and development of dental materials. Over the last decades, the area of esthetic dentistry has been improving exponentially. To meet the increasing demand for esthetics, dental material manufacturers are continuously introducing new dental materials that mimic the mechanical, optical and colorimetric properties of the natural dental tissues that they will replace. These tissues are very complex, presenting very specific optical and colorimetric properties. Moreover, since dental structures consist of several layers of different materials (pulp, dentine and enamel), dental restorations must be also reproduced through layering of different materials and shades, which makes the shade matching process even more complicated.

Accurate color determination of dental materials is a complex procedure that must be well managed both in clinical practice, to guarantee the success of a dental restoration, as well as in industry, to improve the development of new dental materials. Since the reflectance spectrum of any object is independent of illumination and viewing conditions, this is one of the best ways to describe its color. In this sense, known the reflectance spectrum of any kind of dental material of different thickness, or, even more interesting, being able to predict it, can provide essential information on its final appearance after application.

Nevertheless, there are specific situations where the access to reflectance measurement is not straightforward, as is the case of many clinical scenarios, where most of the devices currently available for dental color measurement and shade matching provide exclusively colorimetric values. Therefore, any proposed predictive method should account for these specificities and incorporate them in its development.

Over the years, many mathematical techniques have been developed to reconstruct spectral reflectance data in different color research areas, among which outstanding the linear regression and principal component analysis, due to their simplicity and

versatility. In the specific field of dentistry, color prediction is a fast growing research area. In this context, it is of great interest to have appropriate models and methods that can predict the reflectance spectrum as well as the chromatic coordinates of both monolithic and layered dental biomaterials, with direct applications in industry and clinical practice. These type of predictions have the potential to provide essential information of the final appearance of a dental restoration, which can be of vital importance to reduce the trial-and-error of manufacturing processes and to improve the esthetic outcome of a dental restoration.

Taking into account all the above mentioned, the following objectives were established for the present PhD Thesis:

1.1 Main objective

The main objective of the research presented in this PhD Thesis is to measure, model and predict the reflectance and colorimetric properties of a large variety of monolithic and layered (stacked -monolithic samples placed one on top of the other - and stratified - manufactured and polymerized layered samples) translucent biomaterials with direct application in dentistry.

1.2 Specific objectives

1. To develop PCA-based predictive algorithms that enable satisfactory estimation of the reflectance spectrum and color coordinates of flat monolithic samples of translucent dental materials (dental ceramics and resin composites) with different shades and thicknesses.

2. To develop PCA-based predictive algorithms that enable satisfactory estimation of the reflectance spectrum and color coordinates of stacked layered samples of dental resin composites with different shades and thicknesses and to optimize the training set - test set selection strategy.

3. To develop linear regression algorithms that enable satisfactory estimation of CIE-L*a*b* chromaticity coordinates of monolithic and stacked layered samples of dental resin composites with different shades and thicknesses and under different illuminants.

4. To evaluate and validate the use of the PCA-based reflectance prediction algorithm and linear regression-based CIE-L*a*b* chromaticity coordinates prediction algorithm in the case of stratified layered dental resin composites with different shades and thicknesses.

CHAPTER

2

MOTIVACIÓN Y OBJETIVOS

Con esta tesis doctoral se pretende contribuir al avance del conocimiento en el campo de la odontología estética y el desarrollo de materiales dentales. En las últimas décadas, el área de la estética dental ha ido mejorando exponencialmente. Por eso, para satisfacer la creciente demanda de estética, los fabricantes de materiales dentales continúan introduciendo nuevos materiales dentales que imitan las propiedades mecánicas, ópticas y colorimétricas de los tejidos dentales naturales a los que van a sustituir. Estos tejidos son muy complejos y presentan propiedades ópticas y colorimétricas muy específicas. Además, dado que las estructuras dentales están formadas por varias capas de diferentes tejidos (pulpa, dentina y esmalte), las restauraciones dentales deben reproducirse también mediante la estratificación de diferentes materiales y tonos, lo que complica aún más el proceso de determinación del color.

La determinación precisa del color de los materiales dentales es un procedimiento complejo que debe ser bien gestionado tanto en la práctica clínica, para garantizar el éxito de una restauración dental, como en la industria, para mejorar el desarrollo de nuevos materiales dentales. Dado que la reflectancia espectral de cualquier objeto es independiente de la iluminación y de las condiciones de observación, es una de las mejores formas de describir su color. En este sentido, conocer la reflectancia espectral de cualquier tipo de material dental de diferente espesor o, lo que es más interesante, poder predecirla, puede proporcionar información esencial sobre su apariencia final tras su aplicación.

No obstante, existen situaciones específicas en las que obtener medidas de reflectancia no es sencillo, como ocurre en muchos escenarios clínicos, ya que la mayoría de los dispositivos disponibles actualmente para la medición del color dental proporcionan exclusivamente valores colorimétricos. Por lo tanto, cualquier método predictivo que se proponga debe tener en cuenta estas particularidades e incorporar-

las en su desarrollo.

A lo largo de los años, se han desarrollado muchas técnicas matemáticas para reconstruir la reflectancia espectral en diferentes áreas de investigación del color, entre las que destacan la regresión lineal y el análisis de componentes principales (ACP), debido a su simplicidad y versatilidad. En el campo específico de la odontología, la predicción del color es un área de investigación en pleno crecimiento. En este contexto, es de gran interés disponer de modelos y métodos adecuados que puedan predecir la reflectancia espectral así como las coordenadas cromáticas de los biomateriales dentales, tanto monolíticos como por capas, con aplicaciones directas en la industria y en la práctica clínica. Este tipo de predicciones tienen el potencial de proporcionar información esencial sobre el aspecto final de una restauración dental, lo que puede ser de vital importancia para reducir el proceso de ensayo-error a nivel de fabricación y mejorar el resultado estético de una restauración dental.

Teniendo en cuenta todo lo anterior, se establecieron los siguientes objetivos para la presente Tesis Doctoral:

2.1 Objetivo principal

El objetivo principal de la investigación presentada en esta Tesis Doctoral es medir, modelar y predecir la reflectancia y las propiedades colorimétricas de una gran variedad de biomateriales translúcidos monolíticos y con capas (apilados -apilamiento de muestras monolíticas- y estratificados -muestras fabricadas y polimerizadas como bicapa) con aplicación directa en odontología.

2.2 Objetivos específicos

1. Desarrollar algoritmos predictivos basados en ACP que permitan estimar satisfactoriamente la reflectancia espectral y las coordenadas de color de muestras monolíticas planas de materiales dentales translúcidos (cerámicas y resinas de composite) con diferentes colores y espesores.

2. Desarrollar algoritmos de predicción basados en ACP que permitan estimar satisfactoriamente la reflectancia espectral y las coordenadas de color de muestras bicapa apiladas de resinas de composite de diferentes colores y espesores, y optimizar la estrategia de selección de los conjuntos de entrenamiento y test.

3. Desarrollar algoritmos de regresión lineal que permitan estimar satisfactoriamente las coordenadas de cromaticidad CIE-L*a*b* de muestras monolíticas y bicapa apiladas de resinas de composite de diferentes colores y espesores y bajo diferentes iluminantes.

4. Evaluar y validar el uso del algoritmo de predicción de reflectancia basado en ACP y el algoritmo de predicción de coordenadas CIE-L*a*b* basado en regresión lineal en el caso de resinas de composite bicapa estratificadas con diferentes colores y espesores.

CHAPTER

3

REFLECTANCE AND COLOR PREDICTION OF DENTAL MATERIAL MONOLITHIC SAMPLES WITH VARYING THICKNESS

In this Chapter, a PCA-based prediction algorithm is developed and proposed for reflectance and color prediction of different shades of monolithic dental ceramics and dental resin composite with clinically relevant different thickness.

It extends the study published as:

M. Tejada-Casado, R. Ghinea, M. M. Perez, H. Lübbe, I. Pop-Ciutrila, J. Ruiz-López, and L. Herrera, "Reflectance and color prediction of dental material monolithic samples with varying thickness," *Dental Materials*, vol. 38, no. 4, pp. 622–631, 2022.

3.1 Introduction

As previously mentioned in the first Chapter of this Thesis, accurate shade determination is a key aspect of aesthetically successful restorations and a challenge to both dentists and dental technicians. Therefore, an adequate knowledge of the optical properties of the restorative materials used is of great interest, since it would lead to a better overall aesthetic result. However, full comprehension of these properties might be difficult to achieve as, from the optical point of view, these tissues are very complex, presenting very characteristic chromatic and translucency properties [133].

Since the reflectance spectrum is independent of illumination and observer, it is one of the best ways to describe the color of any object. Therefore, knowing the reflectance spectrum of dental materials with a given thickness, or, even more interesting, being able to predict it, has the potential to provide essential information on the final appearance of a dental restoration. This can be of vital importance to reduce the trial-and-error of manufacturing processes and to improve the aesthetic outcome of a dental restoration, resulting in increased patient satisfaction.

In the past few years, different methods were used in dentistry for reflectance prediction of dental samples, such as the Kubelka-Munk theory [138, 139], genetic algorithms and neural networks [140] or multiple nonlinear regression models [141].

Although principal component analysis was originally a statistical technique used for reducing the dimensionality of data sets while minimizing information loss, in many different disciplines it has been adapted for other purposes [145, 149]. PCA operation as an approximator allows to manage spectral data by handling a few principal components and it is a powerful tool for the characterization of multidimensional data, especially spectral data, whose reads present a high colinearity among the nearby wavelengths. These advantages may be thus harnessed for spectral estimation in dentistry.

There are some studies that highlight an existing relationship between thickness and the color and optical properties of dental materials [45, 46, 50–53, 161]. However, the prediction of the reflectance spectrum and color coordinates of a dental material as a function of its thickness is still an unsolved problem.

Therefore, the main objective of the research presented in this Chapter is to predict the measured reflectance and color coordinates of different types of flat dental samples (both dental ceramics and resin composites) with varying thickness.

The following research hypotheses were tested in this study:

1. The reflectance spectrum within the visible range of dental samples can be satisfactory predicted as a function of thickness.

2. The color of dental material samples with varying thicknesses can be predicted within clinically acceptable color difference limits.

3. Performance of PCA-based models for reflectance estimation is material dependent.

3.2 Materials and method

3.2.1 Specimen preparation

Dental ceramic samples - VITA SUPRINITY® PC (VS-PC) (Vita Zahnfabrik, Bad Säckingen, Germany) - and dental resin-based composite (DRC) samples - VITAPAN DENTINE (VD) (Vita Zahnfabrik, Bad Säckingen, Germany) - with different shades were used in this study (Table 3.1).

Table 3.1: Evaluated materials with corresponding class, composition, selected shades and thickness.

Material	Classification	Composition	Shades	Thicknesses (mm)
VITA Suprinity (VS-PC)	ZrO2 lithium silicate glass ceramic	SiO_2 (56-64wt%), Li_2O (15-21wt%), ZrO_2 (8-12wt%), P_2O_5 (3-8wt%), K_2O (1-4wt%), Al_2O_3 (1-4wt%), CeO_2 (0-4wt%), La_2O_3P (0.1wt%) and pigments (0-6wt%)	A1, A2, A3, A3.5, B2, D2, D2	0.6 ± 1.0 0.9 ± 1.0* 1.2 ± 1.0* 1.5 ± 1.0* 2.0 ± 1.0
VITAPAN Dentine (VD)	Microfiller Reinforced Polymer Matrix (MRP composite)	PMMA (84-86%), SiO_2 (14-15%) and Pigments ($< 1\%$)	A1, A2, A3, A3.5, B2, D2, D2	0.5 ± 1.0 1.0 ± 1.0* 1.5 ± 1.0* 2.0 ± 1.0* 2.5 ± 1.0

* refers to the samples being used to test the algorithm.

The machinable VS-PC (14mm x 12mm x 18mm) ingots (Figure 3.1a) were sectioned with a diamond disk at low speed in a precision cutting machine (Isomet 1000, Buehler, Lake Bluff, IL, USA) (Figure 3.1b), sliced to the desired thickness in their precrystallized state and consequently submitted to the crystallization process, as indicated by the manufacturer in a Programat EP 3000 furnace (Ivoclar Vivadent, Schaan, Liechtenstein). Next, the specimens were polished with wet silicon carbide paper of increasing grit number (400-, 600-, 800-, and 1200-grit) until the desired thicknesses were achieved: 0.6 mm, 0.9 mm, 1.2 mm, 1.5 mm and 2 mm with a tolerance of $\pm$0.1 mm (Table 3.1). For each shade and thickness three samples were prepared (Figure 3.1c).

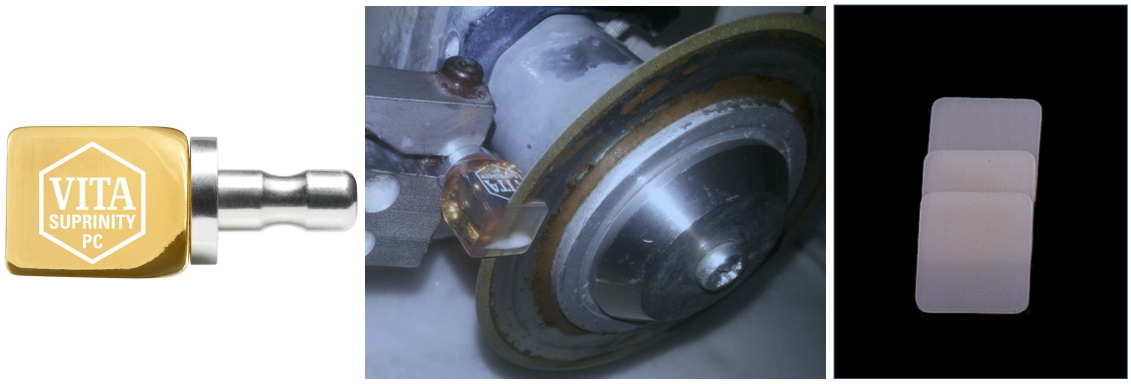

(a) **(b)** **(c)**

Figure 3.1: Fabrication process of VS-PC specimens. **a)** Precrystallized VS-PC block (Reproduced from www.vita-zahnfabrik.com). **b)** Isomet disc used for sectioning the blocks (Reproduced from [5]). **c)** Specimens after crystallization and polishing.

The fabrication of the VD samples was carried out at Vita Zahnfabrik facilities. These were based on the same organic masses that are used for the production of prosthesis teeth. These masses consist of an organic monomeric matrix, a microbead filling material, organic additives and inorganic pigments. First, the components were added and homogenized in fabrication-sized mixers and kneaders until a homogeneous mass of dough-like constitution and viscosity was achieved. Since the exposure of these masses to ambient temperature would drastically increase the polymerization speed of the monomeric organic matrix material, all masses were transferred to and stored in conventional deep-freezers to prevent their continuous polymerization. Prior to their use, they were taken out of the deep-freezers and exposed to ambient temperatures for a few minutes. The fabrication of the pellets started with slices of the produced masses, which were previously calendered in conventional twin-roll calenders to sheets of specific thicknesses. Then, a specific amount of material from these sheets was inserted into a 1.5 cm diameter metal molds and subsequently exposed to a combined heat-and-pressure treatment in a conventional transfer press to complete

the polymerization of the masses. There they were heated at 180 C° for 3 minutes. Next, the molds were cooled to 60 C° before the samples were extracted. All samples were ground on a JUNG surface grinder machine (United Grinding, Miamisburg, OH, USA) to the following specific thicknesses: 0.5 mm, 1.0 mm, 1.5 mm, 2.0 mm and 2.5 mm, with a tolerance of $\pm$0.1 mm. All samples were polished with 9μm diamond paste by the same trained operator. For each shade and thickness one sample was prepared (Figure 3.2).

Figure 3.2: Finished VD specimens after polymerization and polishing.

All specimens were cleaned from debris with distilled water in an ultrasonic bath (Elmasonic S30H, Elma Schmidbauer, Singen, Germany) for 10 minutes, and dried with gauze and compressed air.

3.2.2 Spectral reflectance and color coordinates

A spectroradiometer (SpectraScan PR 670, Photo Research, Syracuse, NY, USA), a fiber-coupled Xe-Arc light source (66485-300, Newport Corporation, Irvine, CA, USA) and a Spectrally Calibrated Reflectance Standard (SRS-3, Photo Research, Syracuse, NY, USA), were used to measure the spectral reflectance spectrum of the samples in the 380 nm – 780 nm range. The samples were measured over a black standardized background (Ceramic color standards CCSII, Lucideon, Staffordshire, UK; $L^* = 23.3$; $a^* = -0.3$; $b^* = -1.0$) inside a completely dark room. The spectroradiometer was placed 40 cm away from the samples, in a set-up corresponding to CIE $45°/0°$ illuminating/measuring geometry (Figure 3.3). Three short-term repeated reflectance

measurements were performed without replacement, and the results were averaged. Spectral reflectance values were converted into CIELAB color coordinates using the CIE 2° Standard Observer and the CIE D65 Standard Illuminant.

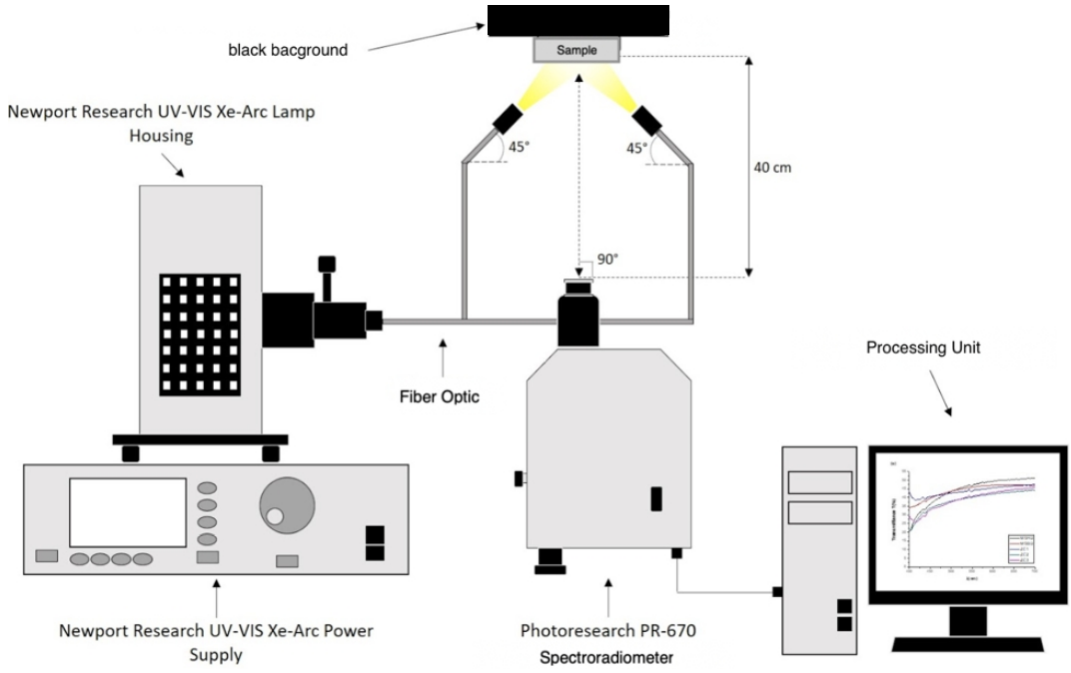

Figure 3.3: Schematic representation of the measurement set-up used to measure spectral reflectance of the samples.

3.2.3 Computational method

Reflectance spectrum $R(\lambda)$ prediction as a function of sample thickness was performed using a PCA-based algorithm.

In order to develop and assess the predictive models, samples were divided in different training and testing groups, using a single thicknesses at a time as test. That is, if the reflectance spectra of one of the dental samples was to be predicted, only the samples corresponding to the same material and shade but with different thickness were included as training data for the development of the predictive model. This separation into training and testing groups was repeated for all thicknesses of each

shade, so that all samples were part of each training-test groups, but only belonged to either training or test each time. A diagram of this division is shown in Figure 3.4.

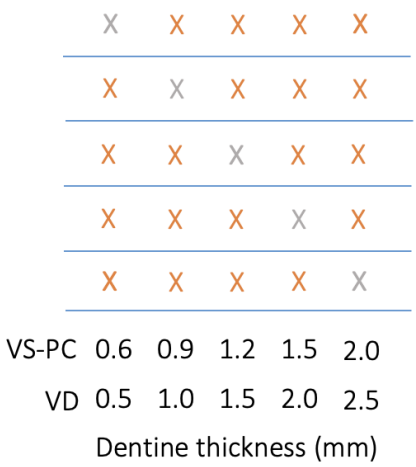

Figure 3.4: Schematic representation of samples being included in the training (orange) and testing (gray) sets.

The fundamentals of this predictive technique are described hereunder.

Given a reflectance training set (noted as X), any reflectance spectrum $R(\lambda)$ can be represented as a linear combination of a few spectral functions $a_i(\lambda)$, being those the eigenvectors of XX^T, as shown in equation 3.2.1:

$$R(\lambda) = \alpha_1 a_1(\lambda) + \alpha_2 a_2(\lambda) + ... + \alpha_n a_n(\lambda) \tag{3.2.1}$$

where α_i are the weighting coefficients, which correspond to the inner products of the original reflectance spectrum, $R(\lambda)$, and their respective eigenvectors according to:

$$\alpha_i = \sum R(\lambda) a_i(\lambda) \tag{3.2.2}$$

After extracting the eigenvectors from XX^T, the resultant matrix is sorted by coefficient value in descending order, establishing a priority ranking for the eigenvectors as a function of the amount of data that they are able to cover. Finally, we can choose

as many principal components as we want to reconstruct our data.

For a given dataset of N-samples and a certain number of M-PCs in the model, the weights are generated as shown in 3.2.2, obtaining:

$$W = \begin{bmatrix} \alpha_{(PC_1 1)} & \alpha_{(PC_1 2)} & \cdots & \alpha_{(PC_1 N)} \\ \alpha_{(PC_2 1)} & \alpha_{(PC_2 2)} & \cdots & \vdots \\ \vdots & \vdots & \ddots & \vdots \\ \alpha_{(PC_M 1)} & \cdots & \cdots & \alpha_{(PC_M N)} \end{bmatrix}_{M \times N} \tag{3.2.3}$$

Since the coefficients that would correspond to a certain thickness can be computed by linear-regression approaches, the reflectance of the new sample can be estimated by multiplying those computed coefficients with their corresponding eigenvectors, as shown in equation 3.2.1.

In order to find the best PC-number and polynomial-degree combination to be used in the proposed algorithm, different tests were carried out including from 1 PC to 4 PC, and polynomial degrees of 1^{st}, 2^{nd} and 3^{rd} order, for the modelling of the coefficient values according to the thicknesses of the samples. From the current database, it was found that 3 PC and second degree polynomial regression were the hyperparameters providing the best performance. More details are discussed in the next section.

Once these curves are determined, the coefficients corresponding to any different desired thickness can be extracted. An example of how these weighting coefficients are obtained is shown in Figure 3.5.

3.2.4 Performance metrics

In order to evaluate the matching quality between estimated and measured reflectances, different performance metrics have been used. These performance metrics

were divided into two analysis groups: spectral curve analysis and color difference analysis.

3.2.4.1 Spectral Curves Differences

The degree of similarity between the estimated and measured spectral reflectances was assessed using two spectral metrics: the Root Mean Square Error (RMSE) and the Goodness-of-fit coefficient (GFC) [162].

$RMSE$ focuses on the absolute differences between two spectral signals and, thus, it is not independent of scale factors. A perfect match between two spectral signals is described by $RMSE = 0$, while higher values of $RMSE$ correspond to increasing disagreement between the two analyzed spectral curves. $RMSE$ is calculated as shown in equation 3.2.4:

$$RMSE = \sqrt{\frac{1}{n}\sum_{j=380}^{780}(R_m(\lambda_j) - R_e(\lambda_j))^2} \tag{3.2.4}$$

where $R_m(\lambda_j)$ and $R_e(\lambda_j)$ are the measured and estimated spectral curves respectively at each wavelength.

GFC corresponds to the cosine of the angle formed by the two samples compared in the high-dimensional vector space of spectral signals. This metric is independent of scale factors. Values of $GFC \geq 0.999$ and $GFC \geq 0.9999$ correspond to good and excellent spectral matches, respectively [162]. It is calculated as shown in equation 3.2.5:

$$GFC = \frac{|\sum_{j=380}^{780} R_m(\lambda_j) \cdot R_e(\lambda_j)|}{|\sum_{j=380}^{780}[R_m(\lambda_j)]^2|^{\frac{1}{2}} \cdot \sum_{j=380}^{780}[R_e(\lambda_j)]^2|^{\frac{1}{2}}} \tag{3.2.5}$$

where $R_m(\lambda_j)$ and $R_e(\lambda_j)$ are the measured and estimated spectral curves being compared at each corresponding wavelength.

Finally, the correlation coefficient R^2 was computed for every pair of measured and estimated reflectance values. R^2 varies between 0 and 1, with higher values corresponding to a better match between the analyzed spectral curves (for a perfect fit, $R^2 = 1$).

3.2.4.2 Evaluation of color differences

Total color differences between CIE L*a*b* values corresponding to measured and predicted spectral curves were computed using the CIEDE2000(1:1:1) total color difference formula (Eq. 3.2.6), since it is the current recommendation of the International Commission on Illumination (CIE) [12] for color difference computation, and has shown to provide a better fit with human perception [95].

$$\Delta E_{00} = \left[\left(\frac{\Delta L'}{K_L S_L} \right)^2 + \left(\frac{\Delta C'}{K_C S_C} \right)^2 + \left(\frac{\Delta H'}{K_H S_H} \right)^2 + R_T \left(\frac{\Delta C'}{K_C S_C} \right) \left(\frac{\Delta H'}{K_H S_H} \right) \right]^{\frac{1}{2}} \tag{3.2.6}$$

ΔE_{00} values were benchmarked according to the 50:50% perceptibility (PT_{00}), $\Delta E_{00} = 0.8$, and acceptability (AT_{00}) thresholds, $\Delta E_{00} = 1.8$, for dentistry, as reported in literature [27,92] and recommended by the ISO/TR 28642:2016 [94].

3.3 Results and discussion

All the samples used in this study were translucent at clinically relevant thicknesses, therefore a black background was used in order to simulate the darkness in the oral cavity.

A spectroradiometer was used to measure all the specimens, since it is considered the gold standard device for the evaluation of the colorimetric and optical properties of dental materials [4,161,163–167], which ensures the precision of our measurements

when compared with other commercial dental devices used in clinical scenarios and other studies, such as colorimeters, spectrometers and spectrophotometers [67,68,140].

Complementary, for the evaluation of the color differences, the CIEDE2000 formula was used since it is widely implemented in dental color research [13,53,137] and it has proven to fit more accurately with visual perception [95].

To the best of our knowledge, there are no available studies that implement PCA-based algorithm for spectral reconstruction and color matching in dentistry. However, there is available research that use, for this specific application, algorithms based on other approaches, such as Kubelka-Munk theory, a combination of Genetics Algorithms with Neural Networks or regression approaches [138, 140, 141]. The novelty of our method is related with the evaluation of the results, as we used both spectral and colorimetric metrics. This metrics have been thoroughly researched and applied in other studies in the dental field [13,92,95,137], and allowed comparisons of results with standard (specific) color difference thresholds for dentistry, which enables precise analysis of the performance of our algorithm. Additionally, the use of a shade-specific (adaptive selected training samples) database of different material reflectances to derive the PCA basics, represents a key advantage of this method, since with just a 4-samples training set it allows reconstruction of complete reflectance spectra by estimating the corresponding weighting coefficients of a certain thickness.

As mentioned before, PCA models with 2 to 4 principal components, as well as first to third order degree polynomial regressions were tested for coefficient prediction of the samples used in this study. Statistics of ΔE_{00} color differences between measured and predicted CIE-L*a*b* values (including all specimens and both materials used in the study) for different polynomial degrees and when different numbers of principal components were used to estimate the weighting coefficients, are presented in Table 3.2.

Table 3.2: Statistics of ΔE_{00} color differences between measured and predicted CIE-L*a*b* values, including all specimens and both materials used in the study, for different polynomial degrees and when different numbers of principal components are used to estimate the weighting coefficients.

Polynomial Degree	ΔE_{00}	1 PC	2 PC	3 PC	4 PC
1^{st}	**Max**	7.89	5.98	5.97	5.97
	Mean	3.07	1.96	1.95	1.95
	SD	1.80	1.28	1.28	1.28
	<AT%	28.57	51.43	51.43	51.43
	<PT%	5.71	20.00	20.00	20.00
2^{nd}	**Max**	6.20	5.96	**5.90**	6.25
	Mean	2.79	1.62	**1.61**	1.63
	SD	1.80	1.24	1.25	1.27
	<AT%	35.71	**70.00**	**70.00**	**70.00**
	<PT%	15.71	31.43	31.43	**32.85**
3^{rd}	**Max**	16.30	17.76	17.64	16.88
	Mean	3.70	3.18	3.11	3.07
	SD	3.49	4.40	4.39	4.34
	<AT%	27.14	57.14	60.00	60.00
	<PT%	14.29	28.57	30.00	30.00

Regarding the polynomial degree, there is no doubt that second degree polynomial regression proved to be the best choice in terms of prediction capability. This can be explained by the curve-like shape of the data, so that using 1^{st} degree polynomial regressions was insufficient to find the fit-line (Figure 3.5a), while using 3^{rd} degree polynomial regressions led to an over-fit of the data points (Figure 3.5c). Therefore, the use of 2^{nd} degree polynomial regressions was the optimal approach to find the best-fit-curve to these data points, as can be observed in Figure 3.5b. Nonetheless, when it comes to the number of PC used to reconstruct the data, the analysis is more complicated. It is clear that using only 1 PC was insufficient to obtain optimal results, since the percentage of samples below PT_{00} and AT_{00} were very low. However, when analysing the results obtained when 2, 3 and 4 PCs were used, similar percentages of samples below PT_{00} and AT_{00} were registered for the three of them. The decision of using 3 PC was based on the total maximum and mean values, which were slightly

better when 3 PC were used, considering also that, computationally speaking, the difference between using 2 or 3 PC did not decrease the algorithm efficiency in a significant way.

Therefore, the predictive PCA algorithm used in this study correspond to 3 principal components with second degree polynomial regression for coefficient modelling.

(a) Best-fit-line obtained using 1^{st} degree polynomial.

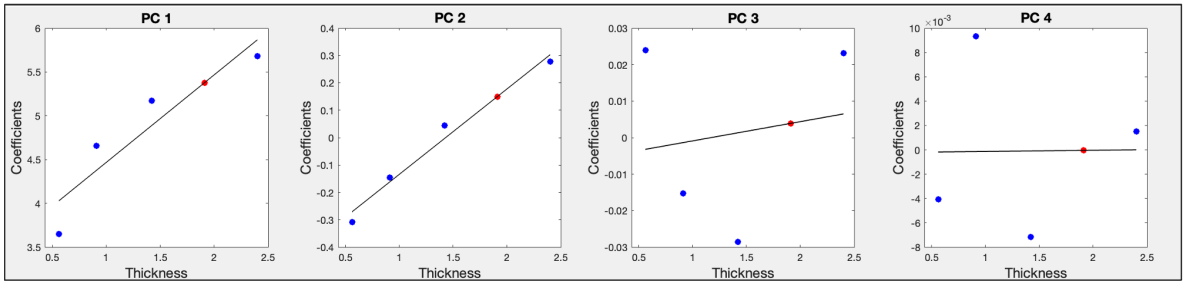

(b) Best-fit-curve obtained using 2^{nd} degree polynomial.

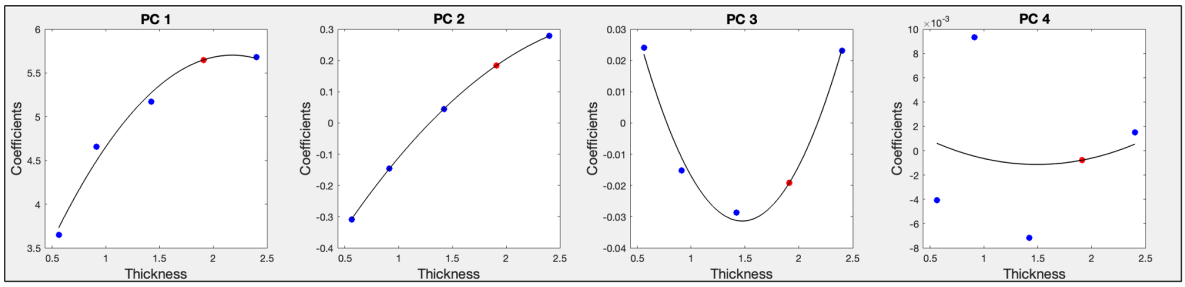

(c) Best-fit-curve obtained using 3^{rd} degree polynomial.

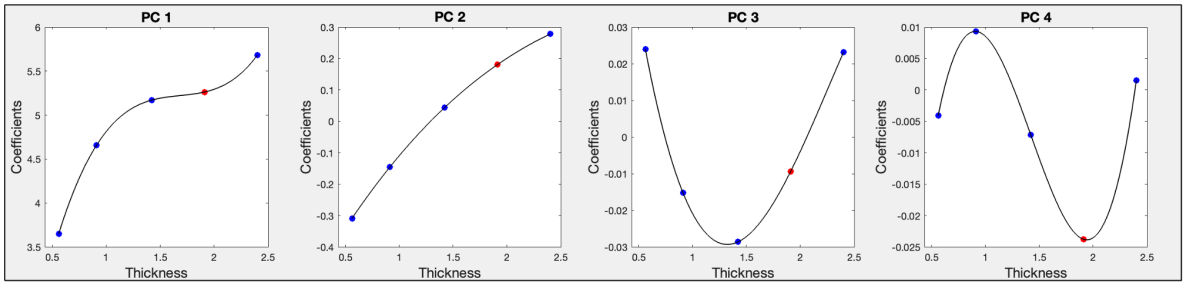

Figure 3.5: Examples of different degrees best-fit-polynomials for 4 Principal Components for weighting coefficients (blue) and estimated coefficient (red) of a 2.0 mm thickness sample when the other four samples are used to train the model.

The results of ΔE_{00}, RMSE and GFC metrics between measured and estimated reflectances for all the specimens tested in this study, are presented in Table 3.3, where the values for each sample of a certain thickness corresponds to the estimations when the other four samples of the same shade are used as the training set in the algorithm.

Table 3.3: ΔE_{00}, RMSE and GFC metrics between measured and estimated reflectances.

	Suprinity Translucent				**VITAPAN Dentine**			
	Thickness	ΔE_{00}	**RMSE**	**GFC**	**Thickness**	ΔE_{00}	**RMSE**	**GFC**
A1	**1.94**	2.86	0.0503	0.9999	**2.44**	2.93	0.0572	0.9999
	1.44	0.87	0.0168	0.9999	**1.95**	1.01	0.0203	0.9999
	1.15	0.80	0.0163	0.9999	**1.47**	0.46	0.0036	0.9999
	0.89	0.54	0.0037	0.9999	**0.97**	1.23	0.0193	0.9999
	0.53	2.21	0.0173	0.9996	**0.54**	3.68	0.0493	0.9999
A2	**1.95**	1.05	0.0135	0.9996	**2.43**	1.29	0.0171	0.9998
	1.45	0.31	0.0059	0.9999	**1.93**	0.45	0.0046	0.9999
	1.14	0.66	0.0138	0.9999	**1.43**	0.52	0.0064	0.9999
	0.83	0.78	0.0120	0.9998	**0.93**	0.79	0.0115	0.9999
	0.56	1.39	0.0178	0.9995	**0.56**	1.75	0.0218	0.9999
A3	**1.94**	5.90	0.0683	0.9922	**2.40**	2.01	0.0295	0.9999
	1.45	1.34	0.0150	0.9995	**1.91**	0.55	0.0073	0.9999
	1.14	0.45	0.0051	0.9999	**1.42**	0.63	0.0094	0.9999
	0.88	1.61	0.0201	0.9994	**0.91**	1.38	0.0193	0.9999
	0.58	4.30	0.0471	0.9956	**0.56**	3.15	0.0366	0.9998
A3.5	**1.95**	4.77	0.0683	0.9971	**2.43**	2.81	0.0395	0.9999
	1.45	1.04	0.0139	0.9998	**1.93**	0.83	0.0122	0.9999
	1.15	0.27	0.0042	0.9999	**1.44**	0.14	0.0015	0.9999
	0.90	1.59	0.0201	0.9996	**0.94**	1.21	0.0159	0.9999
	0.61	3.86	0.0456	0.9974	**0.60**	2.89	0.0331	0.9999
B2	**1.95**	4.15	0.0662	0.9985	**2.40**	1.54	0.0261	0.9999
	1.47	0.73	0.0129	0.9999	**1.90**	0.52	0.0090	0.9999
	1.17	1.05	0.0070	0.9998	**1.41**	0.16	0.0024	0.9999
	0.85	1.70	0.0221	0.9996	**0.90**	0.55	0.0074	0.9999
	0.62	2.96	0.0412	0.9991	**0.55**	1.55	0.0177	0.9998
C2	**1.94**	2.65	0.0227	0.9991	**2.45**	3.03	0.0450	0.9998
	1.45	0.51	0.0045	0.9999	**1.93**	0.93	0.0148	0.9999
	1.13	0.56	0.0040	0.9999	**1.44**	0.11	0.0020	0.9999
	0.89	1.12	0.0091	0.9998	**0.93**	1.12	0.0145	0.9999
	0.59	2.28	0.0195	0.9995	**0.56**	2.95	0.0332	0.9999
D2	**1.96**	3.16	0.0552	0.9989	**2.43**	2.87	0.0492	0.9999
	1.44	1.04	0.0189	0.9999	**1.93**	0.95	0.0171	0.9999
	1.17	1.28	0.0229	0.9999	**1.41**	0.30	0.0023	0.9999
	0.91	0.73	0.0083	0.9999	**0.94**	1.21	0.0172	0.9999
	0.61	1.28	0.0096	0.9995	**0.56**	3.32	0.0407	0.9999

The means and standard deviations of the performance metrics (ΔE_{00}, RMSE and GFC), as well as the percentage of samples below AT_{00} and PT_{00} values for both materials, all shades and all predicted thicknesses, are presented in Table 3.4.

Table 3.4: Statistics of error metrics for the extrapolation approach (70 specimens considered for prediction).

Samples	Variable	Mean	SD	$< AT_{00}(\%)$	$< PT_{00}(\%)$
	RMSE	0.0229	0.0229		
	GFC	0.9992	0.0015		
VS-PC	**ΔL***	1.43	1.22		
(n = 35)	**Δa***	0.24	0.29		
	Δb*	1.63	1.81		
	ΔE_{00}	1.77	1.41	68.57	28.57
	RMSE	0.0205	0.0154		
	GFC	1.0000	0.00001		
VD	**ΔL***	1.68	1.29		
(n = 35)	**Δa***	0.19	0.17		
	Δb*	0.48	0.40		
	ΔE_{00}	1.45	1.07	71.42	34.28
	RMSE	0.0217	0.0174		
	GFC	0.9996	0.0011		
VS-PC and VD	**ΔL***	1.56	1.26		
(n = 70)	**Δa***	0.22	0.24		
	Δb*	1.05	1.43		
	ΔE_{00}	1.61	1.26	70.00	31.42

The spectral error metrics values ($RMSE = 0,02$; $GFC > 0,999$) denote an excellent fit between predicted and measured spectral reflectances. In terms of color agreement between measured and predicted reflectance, overall mean total color difference was lower or equal to the corresponding acceptability thresholds in all cases (overall $\Delta E_{00} = 1.61$, VS-PC $\Delta E_{00} = 1.77$ and VD $\Delta E_{00} = 1.45$). Slightly better values were registered for the DRC material, although for both materials all the performance metrics between predicted and measured values showed very good agreement. Moreover, the color differences between predicted and measured color were not noticeable to an average human observer (lower than PT_{00}) in approximately one third of all cases ($< PT_{00}\%$ = 31.42%). Again, the number of predicted-measured pairs that exhibited color differences lower than the corresponding AT_{00} or PT_{00} is

slightly higher for VD than for VS-PC material.

It is important to note that under the presented experimentation context, different modelling behaviours can be expected when dealing with the reflectance estimation of samples with thicknesses outside of the range of available training samples (extrapolation approach, i.e. test theoretical thicknesses of 0.5 mm and 2.5 mm), than with thicknesses to be predicted within the range of available samples (interpolation approach, i.e., theoretical thicknesses of 1 mm, 1.5 mm and 2 mm). Thus, it is also interesting to assess and compare the prediction capability of the proposed models when prediction of extreme values is avoided, i.e. if we limit the prediction scheme to interpolation (values, which are adequately represented by the data included in the training set). Table 3.5 shows the means and standard deviations of measures of disagreement and percentage of samples below AT_{00} and PT_{00} values for both materials when the interpolation approach is used.

Table 3.5: Statistics of error metrics for the interpolation approach (42 specimens considered for prediction).

Samples	Variable	Mean	SD	$< AT_{00}(\%)$	$< PT_{00}(\%)$
VS-PC (n = 21)	**RMSE**	0.0123	0.0065		
	GFC	0.9999	0.0002		
	ΔL*	0.77	0.43		
	Δa*	0.13	0.12		
	Δb*	0.73	0.67		
	ΔE_{00}	0.91	0.42	100	47.61
VD (n = 21)	**RMSE**	0.0104	0.0064		
	GFC	1.0000	0.00001		
	ΔL*	0.81	0.43		
	Δa*	0.11	0.12		
	Δb*	0.29	0.67		
	ΔE_{00}	0.72	0.39	100	57.14
VS-PC and VD (n = 42)	**RMSE**	0.0114	0.0064		
	GFC	0.9999	0.0001		
	ΔL*	0.79	0.48		
	Δa*	0.12	0.11		
	Δb*	0.52	0.54		
	ΔE_{00}	0.81	0.41	100	52.38

All performance metrics predictors of quality of fit exhibit considerable better values ($RMSE = 0.01$; $GFC > 0.999$) when interpolation approach is considered to evaluate the results, since, without exception, color differences between predicted and measured values decreased when extreme test theoretical thicknesses of 0.5 mm and 2.5 mm are excluded for the computation of the error metrics. In this scenario, the overall total color difference was equal to the corresponding perceptibility threshold for dentistry ($\Delta E_{00} = 0.81$). Slightly higher values were found for VS-PC ceramic material ($\Delta E_{00} = 0.91$) while color was predicted more efficiently in case of the VD resin composite ($\Delta E_{00} = 0.72$). These results suggest that the PCA-based algorithm is able to predict the final color of a sample within the limits of perceptibility, when only reflectance spectra of intermediate thicknesses are predicted (interpolation approach). Furthermore, the difference between the predicted and measured color of the samples was always lower than the acceptability threshold, while in roughly 5 out of 10 cases (52.38%) the color difference was not noticeable to an average human observer. When comparing the 2 studied materials, there was a slight increase in $PT_{00}\%$ and $AT_{00}\%$ for VD compared to VS-PC samples (57.14% vs 47.61%), suggesting again that this type of prediction algorithm performed slightly better for the DRC material.

Figure 3.6 shows the measured and estimated spectral reflectances for both studied materials and all shades for the samples with intermediate thicknesses (0.9mm, 1.2mm, 1.5mm for VS-PC and 1.0mm, 1.5mm, 2.0mm for VD), and the bivariate plots of measured against estimated spectral reflectance. High correlation values of $R^2 = 0.987$ and $R^2 = 0.993$ were globally obtained for VS-PC and VD, respectively.

Based on the results of this study, the first research hypothesis was accepted, since satisfactory spectral estimation was achieved using the predictive method proposed. As reported by other authors [168], a RMSE of around 2% and a $GFC \geq 0.9999$ result in a very good spectral reconstruction, which is the case for both RMSE and GFC

values found in this study (Tables 3.3 and 3.5). According to our results, differences between predicted and measured reflectance spectra are mostly in intensity (scale) rather than in the shape of the curve, as can be seen in Figure 3.6.

(a) Suprinity Translucent

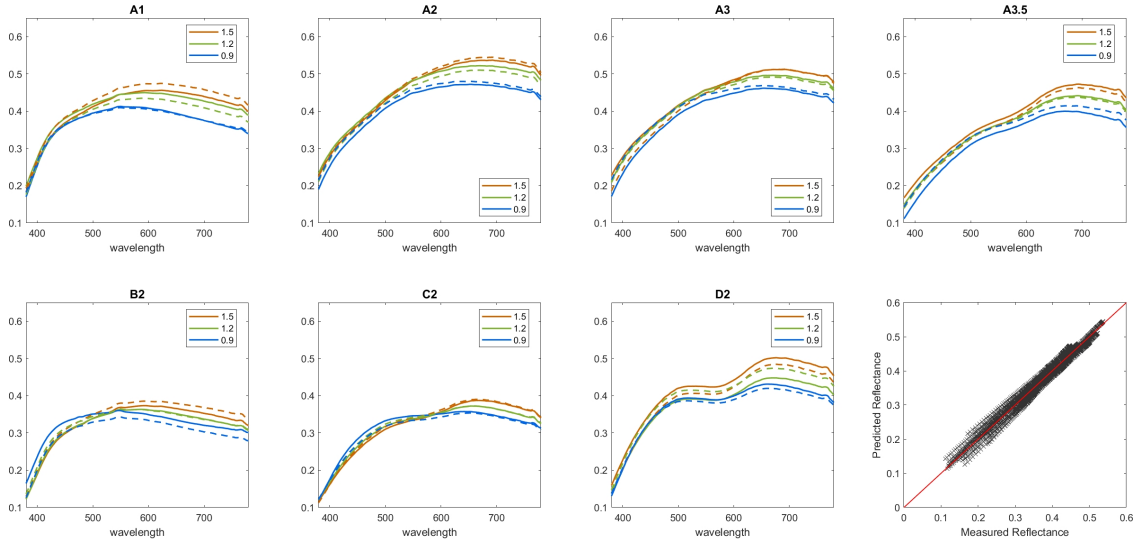

(b) VITAPAN dentine

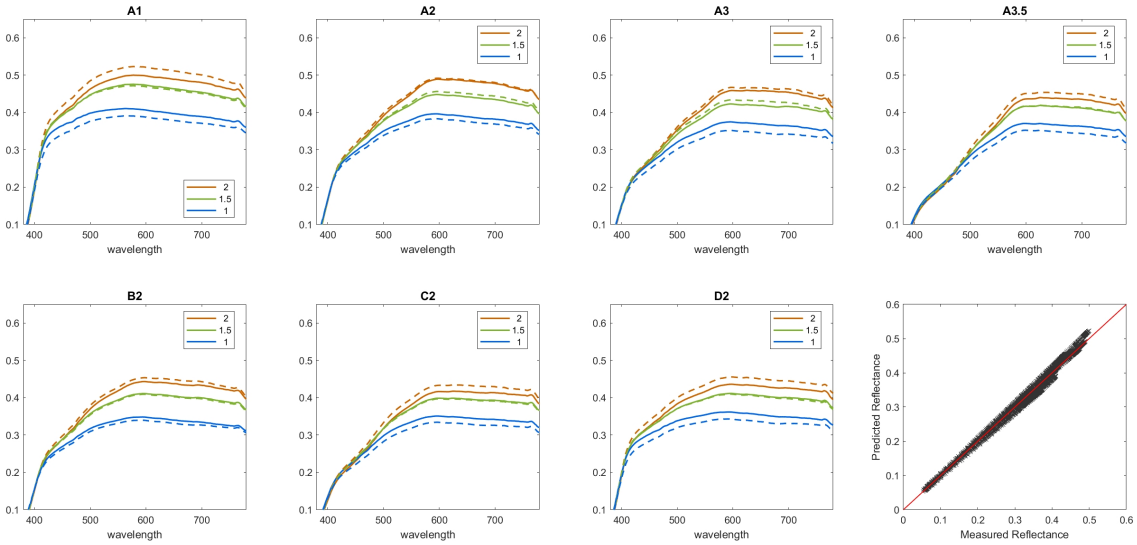

Figure 3.6: Measured (solid line) and estimated (dotted line) reflectances curves and bivariate plots, showing the perfect match (red line) and the measured versus estimated reflectances for all the specimens and shades.

The GFC index is independent of scale factors. In consequence, two samples differing only in scale but not in shape would result in a GFC of 1 (perfect match). These results are in agreement with the absolute differences found for L*a*b* chromatic differences, since a variation in the spectral reflectance value of the specimen (scale) leads to a variation in lightness (L*), while a change in its spectral reflectance behavior (shape) would result in a variation in its chromaticity (a* and b* coordinates) [12,169] (Table 3.5).

As it can be observed in Tables 3.3 and 3.4, ΔE_{00} values corresponding to extrapolation approach (that is, when minimum and maximum thicknesses available are also predicted) are higher, compared to those corresponding to predictive models which do not perform color prediction of data outside the training data set (interpolation approach). These results were somehow expected, as the predictive power of any model diminishes when marginal data points are being predicted. Nevertheless, for a training set that includes both thicker and thinner samples, the excellent correlation (Figure 3.6) between the predicted and measured reflectances ensures that, overall and independently of the dental material analyzed (ceramic or resin composite), the PCA-based algorithm will always provide predicted reflectance curves that exhibit a color difference lower than the acceptability threshold (Tables 3.5) [92]. Under these conditions, we can state that the second research hypothesis of this study was also accepted.

Finally, the results of this study indicate that PCA-based prediction algorithms perform better for DRC specimens (VD) than for ceramic samples (VS-PC) (Tables 3.4 and 3.5). Therefore, the third research hypothesis was also accepted, as performance of the PCA-based algorithm for reflectance estimation is material-dependent. However, it has to be considered that VD samples were prepared under laboratory conditions and following rigorous manufacturing procedures, while the ceramic samples were

prepared under clinical laboratory conditions in a dental technician office, and that for the later ones, mean values of three different samples, instead of only one sample were used for the computation. This differences in manufacturing procedures and number of tested specimens might have had an impact on the robustness and reproducibility of the individual features of the prepared specimens, which could partially explain the differences found.

It is noteworthy that the samples were prepared using different procedures and with different clinically relevant thicknesses, which proves that the performance of the method does not depend on the preparation of the samples or thicknesses used. Thus, it can be considered that the performance of the algorithm proposed is likewise independent of the thickness and the samples preparation procedure.

In addition, it should be considered that there were still some sources of non-modelable errors, such as those derived from the measuring device itself or the reproducibility of the experimental method, that were not completely known and that probably affected the performance of the proposed algorithm to some extent. One would expect that using more PCs as well as a higher degree polynomials would lead to improved results (less "noise" in the data), but this did not happen. This suggests that, the previously mentioned errors (linked to the experimental device and the measuring instrument) limited the predictive capacity of the mathematical models and made it very difficult to further improve the obtained results. Nevertheless, the low variability in the obtained results confirms that the method proposed for the reconstruction of the reflectance spectra can be used to find an optimum color match of samples with varying thicknesses.

In future studies, a broader range of single and multi-layered materials (as the ones proposed in the following Chapters of this PhD Thesis) and shades should be analyzed in order to better understand the extent of the predictive capacity of the

proposed PCA-based models.

CHAPTER

4

REFLECTANCE AND COLOR PREDICTION OF LAYERED DENTAL RESIN COMPOSITES WITH VARYING THICKNESS

In this Chapter a new PCA-based prediction algorithm is proposed for reflectance and color prediction of stacked layered dental resin composite of different materials and shades with varying clinically relevant thickness.

It extends the study published as:

M. Tejada-Casado, R. Ghinea, M. Pérez, J. Cardona, A. Ionescu, H. Lübbe, and L. Herrera, "Color prediction of layered dental resin composites with varying thickness," *Dental Materials*, vol. 38, no. 8, pp. 1261–1270, 2022.

4.1 Introduction

Natural teeth consist of at least three layers of different materials —the translucent enamel on the outer surface, the yellowish dentine below the enamel and the reddish pulp at heart of the teeth. This is the reason why, in a clinical scenario, when performing direct restorations with resin composites, the optical properties and appearance of the natural teeth are reproduced through layering of appropriate enamel and dentine composite shades [2]. Due to the higher translucency of enamel layer, dentine shade will strongly affect the overall chromatic appearance of the restoration. However, this effect can be modulated by enamel layer thickness, which will play a significant role in the final appearance of the restoration [47,48]. The relationship between thickness, color and the optical properties of a dental material was already highlighted in several studies [45,46,50–53]. Parallel to this, it has to be considered that the thicknesses of the different layers are not uniform across the dental structure, but vary with respect to the location in the tooth. Therefore, to adequately mimic the natural color and appearance of a tooth, a highly esthetic direct dental restoration usually is a merge

of the layering of several restorative materials with different optical properties and thicknesses [170].

An object's color depends largely on its reflectance spectrum. Therefore, being able to estimate reflectance and final color of layered samples of dental restorative materials would be of great interest not only for manufacturers of dental materials, but also for dentists and dental technicians.

Color prediction in dentistry is a growing research area [134] and many methods have been implemented for spectral estimation of dental materials [101, 138–141]. However, predicting color of layered dental restorative materials has not been fully investigated yet.

Among all the mathematical techniques that have been implemented to reconstruct spectral reflectance data in different color research areas [142–146], PCA is worth to be highlighted for its simplicity and versatility [145, 149]. To the best of our knowledge, PCA has never been used for spectral estimation of layered dental materials. Therefore, the main objective of this study is to develop and assess the accuracy of a PCA-based predictive algorithm for reflectance reconstruction and color estimation of layered dental resin-based composites with varying thicknesses.

The following research hypotheses were tested in this study:

1. The reflectance spectrum of layered dental samples can be predicted with satisfactory results using a PCA-based algorithm.

2. PCA-based models performance depends on the number of samples that constitute the training set.

3. The use of different types or shades of DRC do not affect the performance of the predictive algorithm.

4.2 Materials and method

4.2.1 Specimen preparation

Disk-shaped DRC samples of 15 mm diameter corresponding to three different dentine types —VITAPAN Excell (VE), VITAPAN Dentine (VD) and VITA Physiodens (VP) (Vita Zahnfabrik, Bad Säckingen, Germany)— and one enamel —VITA Enamel (EN) (Vita Zahnfabrik, Bad Säckingen, Germany)—, with different shades and thicknesses, were used in this study (Table 4.1).

In order to evaluate the performance of the predictive model as a function of DRC type, VE, VD and VP samples of the same shade (A2) were prepared. Whereas to test the performance of the predictive model as a function of dentine shade, VE samples corresponding to two light shades (which for presentation purposes will be named S1 and S2), two intermediate shades (named S3 and S4) and one dark shade (named S5), were prepared. According to manufacturer recommendations, for each dentine composite a specific enamel shade should be used, therefore, samples of three different enamel (EN) shades were fabricated - EN1, EN2 and EN3 (Table 4.1).

Table 4.1: Used dental resin-based composites with corresponding selected shades, composition and thickness.

Composite	Shades	Chemical composition	Thicknesses (mm)
VITAPAN Excell (VE)	A2, S1, S2, S3, S4, S5	PMMA (84-86%) , SiO_2 (14-15%) and Pigments ($< 1\%$)	0.7 ± 0.1; 1.0 ± 0.1; 1.5 ± 0.1; 2.0 ± 0.1 and 2.5 ± 0.1
VITAPAN Dentine (VD)	A2		
VITA Physiodens (VP)	A2		
VITA Enamel (EN)	EN1, EN2, EN3		

Monolithic dentine and enamel pellets were produced by polymerization of dental masses under combined heat-and-pressure treatment according to manufacturer's specifications, as was previously described in Chapter 3 Section 3.2.1 (Figure 4.1).

All monolithic specimens were ground to the following specific thicknesses 0.7 mm, 1.0 mm, 1.5 mm, 2.0 mm and 2.5 mm, with a tolerance of ± 0.1 mm. All samples were polished with $9\mu m$ diamond paste by the same trained operator, and cleaned from debris in an ultrasonic bath.

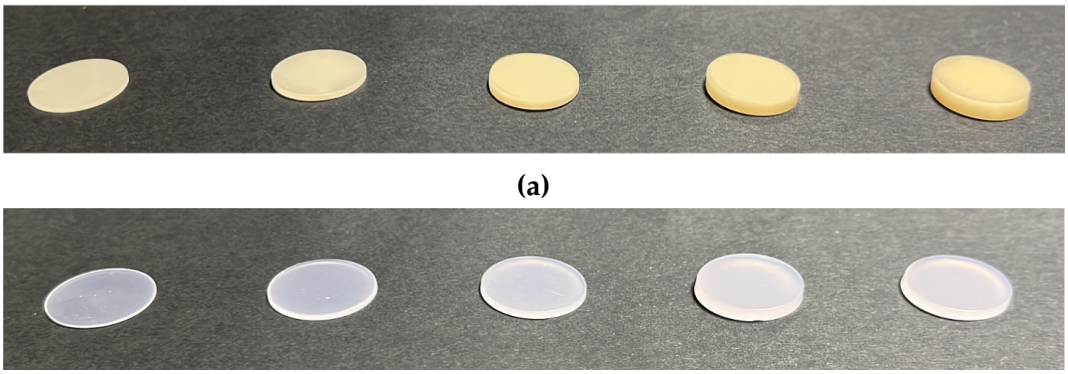

(a)

(b)

Figure 4.1: Monolithic specimens used for the fabrication of the layered samples. **a)** Denine samples of 5 different thicknesses. **b)** Enamel samples of 5 different thicknesses.

The stacked bilayer specimens were obtained by pressure bonding each dentine layer with its corresponding enamel. This was possible due to the quality of the samples used in the study. These were fabricated under very precise manufacturing processes and, therefore, resulted in samples with a completely flat surface that allowed for a perfect coupling between the two layers (Figure 4.2) . By combining all thicknesses (n=5) of the first layer (dentine) with all thicknesses (n=5) of the second layer (enamel), a total of 25 possible stacked layered samples of different enamel-dentine combinations for each DRC system were obtained. In total, 8 different DRC systems have been used in this study, each with 25 enamel-dentine combinations as specified before : VE-A2+EN1, VD-A2+EN3, VP-A2+EN3, VE-S1+EN1, VE-S2+EN1, VE-S3+EN2, VE-S4+EN2 and VE-S5+EN2.

For performance assessment of the predictive model as a function of DRC type,

the following systems were considered: VE-A2+EN1, VD-A2+EN3 and VP-A2+EN3. Lastly, to assess the performance of the predictive model as a function of dentine shade, 5 DRC systems were considered: VE-S1+EN1, VE-S2+EN1, VE-S3+EN2, VE-S4+EN2 and VE-S5+EN2 (VE samples corresponding to different shades were combined with their corresponding enamel shade).

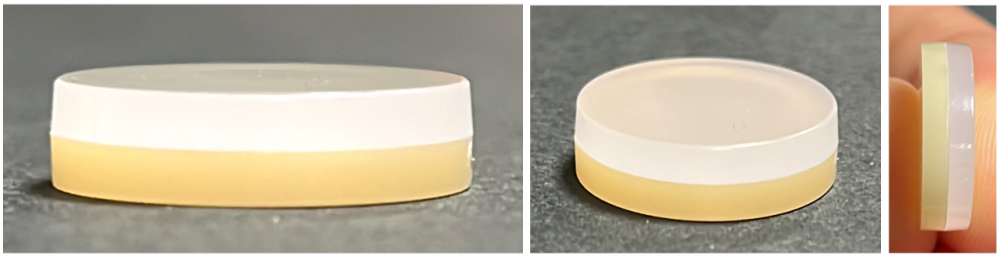

(a) **(b)** **(c)**

Figure 4.2: Dentine and enamel monolithic pellets coupling for the fabrication of DRC stacked layered system, viewed from different perspectives.

The 25 dentine-enamel combinations corresponding to each DRC system were subsequently divided into a training and a testing set of samples. Thus, for each combination, two different approaches were tested: 1. a 5-samples training set and 2. a 9-samples training set. For each approach, reflectances corresponding to samples included in the training set were used to build the PCA-based predictive models, while the reflectances of the samples included in the testing set were used for performance evaluation of the proposed predictive models.

In order to fully encompass the sampling space, and as recommended by dental material manufacturing experts, the layered samples included in each training set were heuristically selected. Different arrangements of training and testing sets were tested for each approach. Figures 4.3 and 4.4 show the different configurations for the 5-samples and 9-samples training sets, respectively. For each configuration, all stacked layered samples not included in the training set were automatically assigned to the corresponding testing set.

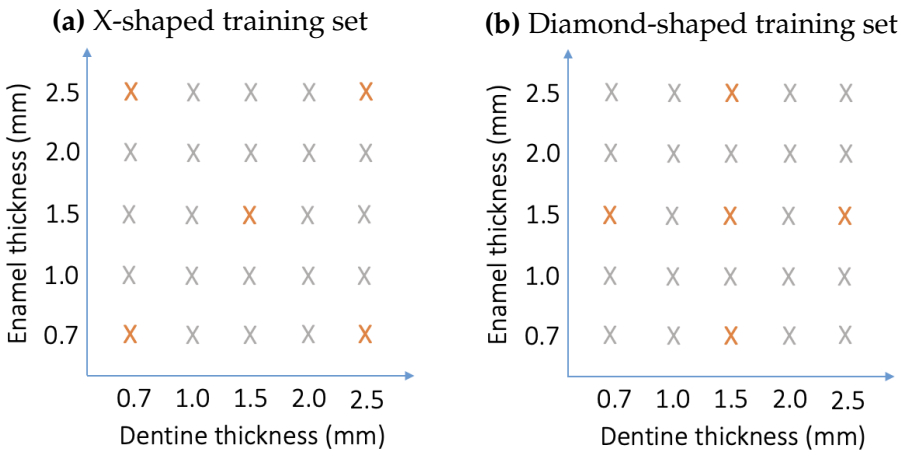

Figure 4.3: Different arrangements of samples being included in the training (orange) and testing (gray) sets for the 5-samples approach.

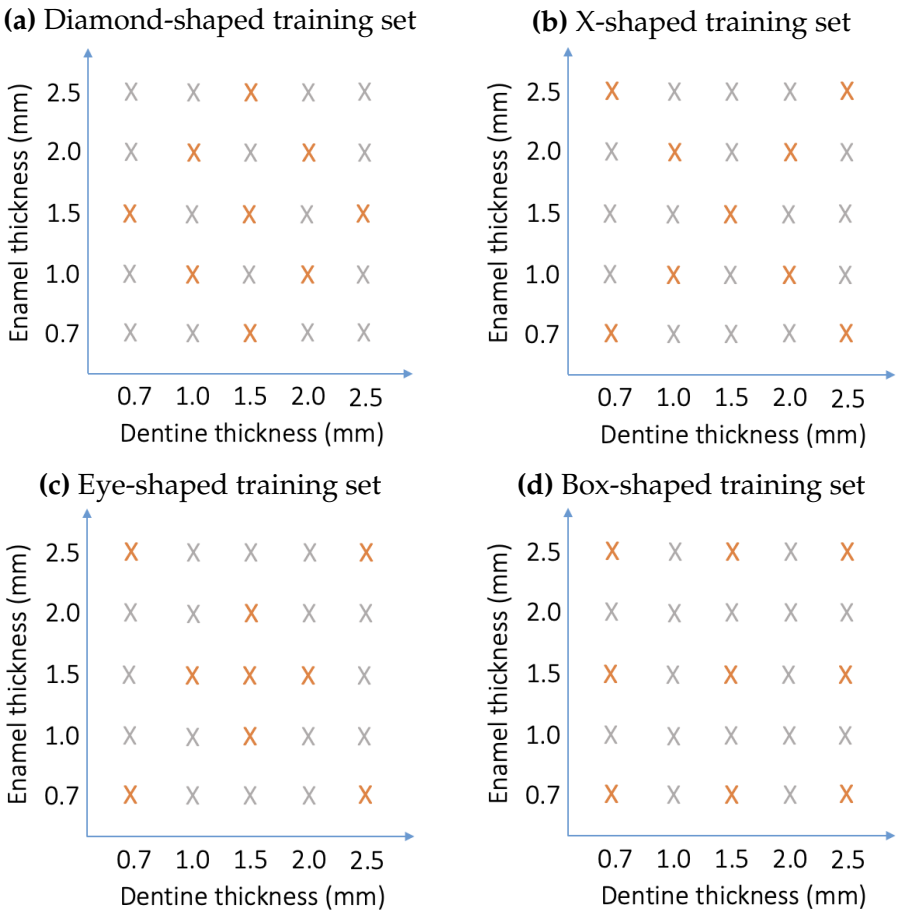

Figure 4.4: Different arrangements of samples being included in the training (orange) and testing (gray) sets for the 9-samples approach.

4.2.2 Spectral reflectance and color coordinates

The spectral reflectance spectrum of all layered samples was measured as previously described in section 3.2.2. Three repeated reflectance measurements without replacement were performed for each specimen, and the results were averaged. Spectral reflectance values were converted into CIELAB color coordinates using the CIE 2° Standard Observer and the CIE D65 Standard Illuminant.

4.2.3 Computational method

The prediction of the spectral reflectance, $R(\lambda)$, for unknown samples was performed using a set of known stacked layered samples reflectances and a PCA-based algorithm [149], similar to the one described in Chapter 3 Section 3.2.3, but adapted to stacked layered samples.

Again, for a given reflectance dataset with n samples (noted as X), any known spectrum $R(\lambda)$ can be represented as the linear combination of the eigenvectors of the correlation matrix XX^T, as shown in equations 3.2.1 and 3.2.2:

Thus, having a training-set of n-samples and using M-PCs that cover more data for the model, the weights that correspond to each sample in X are generated as shown in equation 3.2.2, obtaining the weighting coefficient matrix, W (3.2.3).

As described in the previous chapter, these weights will be used to estimate the weights of the unknown layered samples. Since the current samples are layered, the weights will be now represented in a 3D space as a function of thickness of the first layer (dentine), thickness of the second layer (enamel) and their value, as shown in figure 4.5. Then, for each principal component, the coefficient of a layered sample of defined dentine and enamel thicknesses is estimated by finding its position in the best-fit-surface.

(a) 5-samples training set (X-shaped)

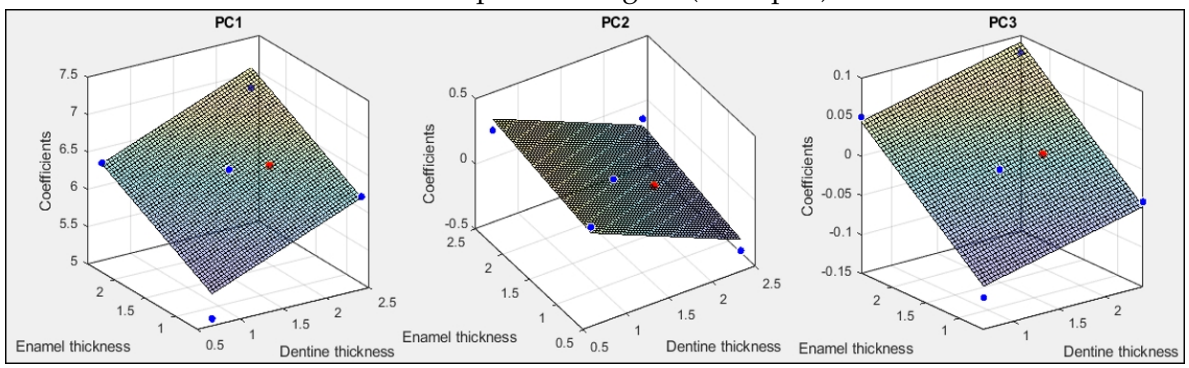

(b) 9-samples training set (diamond-shaped)

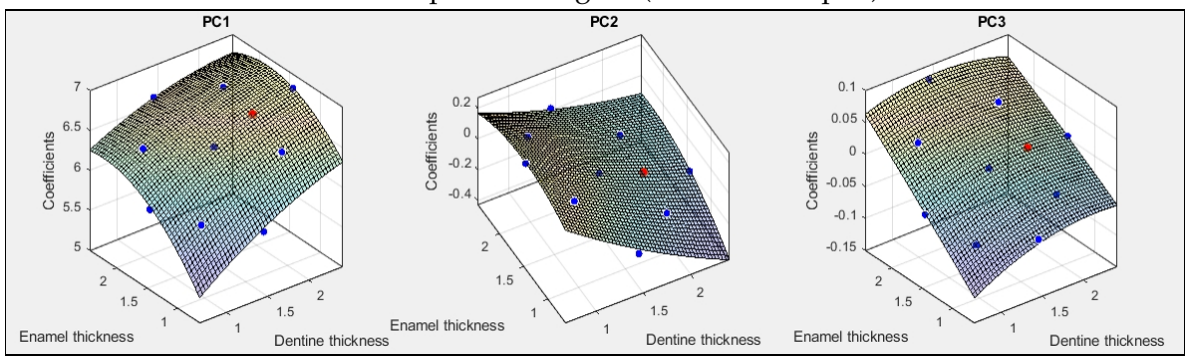

Figure 4.5: Best-fit-surfaces for the weighting coefficients (blue) obtained with a training set of 5-samples (a) and a training set of 9-samples (b), and the estimated coefficient (red) for each principal component.

According to best performance achieved in preliminary tests, X-shaped arrangement, first degree polynomial surface fit and 3 principal components were used for the 5-samples training set approach. Similarly, diamond-shaped arrangement, second degree polynomial surface fit and 3 principal components were used for the 9-samples training set approach. More details are discussed in the next section. Therefore, the reflectance of the new sample can be estimated by multiplying those coefficients (red points in Figure 4.5) with their corresponding eigenvectors, as shown in equation 3.2.1.

4.2.4 Performance metrics

As previously described in Chapter 3 Section 3.2.4, the performance metrics used to evaluate the matching quality between predicted and measured reflectances have been divided into two analysis groups: spectral curve similarity analysis and color difference analysis.

4.2.4.1 Evaluation of Spectral Curves Similarity

Two spectral metrics have been used to evaluate the degree of similarity between the predicted and measured spectral reflectances: the Root Mean Square Error (RMSE) and the Goodness-of-fit coefficient (GFC) [162,168], computed as shown in Equations 3.2.4 and 3.2.5, respectively.

RMSE evaluates the absolute differences between two spectral signals. This metric is not independent of scale factors. For a perfect match, $RMSE = 0$, while higher values of RMSE correspond to increasing disagreement between the two analyzed spectral curves.

GFC is independent of scale factors, thus, it focuses on the shape of the curves being compared. A perfect match is described by $GFC = 1$. Values of $GFC \geq 0.9999$ and $GFC \geq 0.999$ correspond to excellent and very good spectral matches, respectively [162].

4.2.4.2 Evaluation of color differences

Total color differences between the CIE-L*a*b* values corresponding to measured and predicted spectral reflectance curves were computed using the CIEDE2000(1:1:1) [95] total color difference formula (Eq. 3.2.6),

ΔE_{00} values were evaluated according to the corresponding 50:50% perceptibility

(PT_{00}) and acceptability (AT_{00}) thresholds for color difference in dentistry, as described in available literature [27,92] and recommended by the ISO/TR 28642:2016 [94] (PT_{00}: $\Delta E_{00} = 0.8$; AT_{00}: $\Delta E_{00} = 1.8$).

4.3 Results and discussion

Two different configurations —5-samples and 9-samples training sets— were used to build the PCA-based predictive models proposed in this study. Different arrangements and polynomial degrees have been tested for each training set configuration. The general statistics of ΔE_{00} color differences between measured and predicted CIE-L*a*b* values (including the 8 DRC dentine-enamel systems used in the study) for the different polynomial degrees and for the different training set arrangements presented in Figures 4.3 and 4.4, are included in tables 4.2 and 4.3, respectively.

Table 4.2: Statistics of total ΔE_{00} color differences between measured and predicted CIE-L*a*b* values for the different 5-samples training set arrangements and polynomial degrees tested in the predictive methods, including the 8 DRC dentine-enamel systems used in the study.

Train Set Arrangement	**X**		**Diamond**	
Polynomial Degree	1^{st}	2^{nd}	1^{st}	2^{nd}
Max	**3.16**	114.86	5.54	135.83
Mean	**0.99**	7.62	1.14	19.79
SD	0.37	6.74	0.65	17.21
$< AT_{00}\%$	**96.25**	37.50	90.00	23.75
$< PT_{00}\%$	**32.50**	11.25	29.63	17.50

Table 4.3: Statistics of total ΔE_{00} color differences between measured and predicted CIE-L*a*b* values for the different 9-samples training set arrangements and polynomial degrees tested in the predictive methods, including the 8 DRC dentine-enamel systems used in the study.

Train Set Arrangement	**Diamond**		**X**		**Eye**		**Box**	
Polynomial Degree	1^{st}	2^{nd}	1^{st}	2^{nd}	1^{st}	2^{nd}	1^{st}	2^{nd}
Max	4.49	**2.06**	3.33	3.54	2.94	3.24	2.64	2.31
Mean	1.06	**0.50**	0.97	1.04	0.93	0.75	0.93	0.52
SD	0.64	0.30	0.40	0.41	0.41	0.36	0.36	0.26
$< AT_{00}\%$	89.84	**99.22**	95.31	89.06	95.31	93.75	96.88	**99.22**
$< PT_{00}\%$	40.63	**84.38**	41.41	38.28	48.44	66.41	37.50	83.44

As can be seen from the results presented above, although satisfactory results were obtained for most of the configurations, slightly better values were obtained for the X-shaped and diamond-shaped arrangements for the 5-samples and 9-samples training sets, respectively. Therefore, these were the configurations used for the spectral reconstruction of the stacked layered samples used in this study. In addition, given the number of samples included in each training set, optimal results were found when first degree polynomial surface fit was used for the 5-samples training set and second degree polynomial surface fit was used for the 9-samples training set. For both approaches, 3 principal components were used in the model.

For each dentine-enamel system, 25 layered samples have been obtained by combining all monolithic specimens, of 5 different thicknesses (ranging from 0.7 mm - to 2.5 mm) of both layers. In order to simulate clinical situations, all the shades used in the experiment were translucent at clinically relevant thickness values [171] and a standard black background was used in order to simulate the oral cavity.

A spectroradiometer was used to measure the reflectance spectrum of all the specimens, since it is considered the gold standard device for reflectance measurements and, hence, the evaluation of the optical and colorimetric properties of dental materials [4, 163–167].

As mentioned before, many studies confirmed that the spectral reflectance of different dental materials can be reconstructed based on different approaches [101, 138–141]. However, these usually do not consider a wide variety of thicknesses. To the best of our knowledge, there are no studies that adapted PCA-based algorithms for their use in spectral reconstruction of layered samples in dentistry. Another advantage of our study is that a very wide range of dentine-enamel combinations of clinically relevant thicknesses were used to create the layered samples, which helped us understand how the method would perform in a real scenario. Additionally, in

order to more precisely analyze the performance of the proposed algorithm, and following a similar procedure to the study presented in the previous chapter, not only color difference metrics (ΔE_{00}) but also spectral metrics (RMSE and GFC) [162] were implemented for the evaluation of the proposed spectral reconstruction method.

When assessing the performance of the predictive model as a function of DRC type, measured and predicted reflectances of VE-A2+EN1, VD-A2+EN3 and VP-A2+EN3 systems have been compared. Tables 4.4, 4.5, 4.6 and 4.7 show the ΔE_{00} color differences and spectral metrics between measured and predicted spectral reflectance curves, for both training set arrangements used in this study. The means and standard deviations, as well as the percentage of samples below AT_{00} and PT_{00}, are presented in Table 4.8.

For the 5-samples training set, the spectral error metrics values ($RMSE < 0.015$; $GFC > 0.999$) denote a very good fit between predicted and measured spectral reflectances for all DRC. Slightly better values were obtained for the 9-samples training set ($RMSE < 0.0098$; $GFC > 0.9999$), which denotes an excellent fit.

Regarding color matching between measured and predicted reflectances, for the 5-samples training set approach, mean color differences of $\Delta E_{00} = 0.93$, $\Delta E_{00} = 1.05$ and $\Delta E_{00} = 1.38$, were obtained for the three types of DRC (VE, VD and VP, respectively). Again, as was the case for the spectral metrics, better values were obtained for the 9-samples training set approach. For VE and VD, the mean color differences were $\Delta E_{00} = 0.49$ and $\Delta E_{00} = 0.46$, for VE and VD, respectively. Prediction metrics for VP, resulted in slightly higher values for color matching, with a mean color difference of $\Delta E_{00} = 0.85$ (Table 4.8).

Table 4.4: ΔE_{00} color differences between measured and predicted CIE-L*a*b* values for the test stacked layered samples of different materials when a training set of 5-samples is used in the model.

Test Thickness	**DRC Dentine-Enamel Systems**		
D(mm)+E(mm)	**VE A2-EN1**	**VD A2-EN3**	**VP A2-EN3**
2.5 + 2.0	1.15	1.54	2.20
2.5 + 1.5	1.50	1.56	1.89
2.5 + 1.0	0.83	0.39	0.50
2.0 + 2.5	0.18	0.40	0.73
2.0 + 2.0	0.65	0.42	0.82
2.0 + 1.5	1.41	0.82	0.97
2.0 + 1.0	0.83	1.02	1.27
2.0 + 0.7	1.54	1.92	1.78
1.5 + 2.5	0.72	1.05	1.20
1.5 + 2.0	0.41	0.53	1.12
1.5 + 1.0	0.77	1.00	2.29
1.5 + 0.7	1.34	1.77	3.16
1.0 + 2.5	1.01	1.43	0.71
1.0 + 2.0	0.65	0.86	0.61
1.0 + 1.5	1.08	0.94	1.32
1.0 + 1.0	0.70	1.19	1.55
1.0 + 0.7	0.55	1.01	1.48
0.7 + 2.0	1.11	0.54	0.38
0.7 + 1.5	1.06	1.11	1.27
0.7 + 1.0	1.20	1.54	2.31

Table 4.5: RMSE and GFC metrics between measured and predicted spectral reflectance curves for test stacked layered samples of different materials when a training set of 5-samples is used in the model.

	DRC Dentine-Enamel Systems					
Test Thickness	**VE A2-EN3**		**VD A2-EN1**		**VP A2-EN3**	
D(mm)+E(mm)	**RMSE**	**GFC**	**RMSE**	**GFC**	**RMSE**	**GFC**
2.5 + 2.0	0.00800	0.99992	0.01104	0.99984	0.02318	0.99974
2.5 + 1.5	0.01279	0.99982	0.00860	0.99981	0.01240	0.99975
2.5 + 1.0	0.01183	0.99995	0.00558	0.99997	0.00553	0.99995
2.0 + 2.5	0.00194	0.99999	0.00492	0.99998	0.01337	1.00000
2.0 + 2.0	0.01285	0.99999	0.00465	0.99999	0.00496	0.99994
2.0 + 1.5	0.02640	0.99995	0.01310	0.99997	0.01070	0.99994
2.0 + 1.0	0.01713	0.99999	0.01603	0.99998	0.02130	0.99999
2.0 + 0.7	0.01301	0.99974	0.01587	0.99967	0.01488	0.99977
1.5 + 2.5	0.00532	0.99994	0.01375	0.99993	0.01195	0.99975
1.5 + 2.0	0.00733	0.99999	0.00992	1.00000	0.01875	0.99992
1.5 + 1.0	0.01485	1.00000	0.01564	1.00000	0.03203	0.99986
1.5 + 0.7	0.00862	0.99981	0.01546	0.99976	0.03487	0.99940
1.0 + 2.5	0.00797	0.99988	0.01469	0.99977	0.00509	0.99993
1.0 + 2.0	0.00972	0.99998	0.01411	0.99998	0.00638	0.99995
1.0 + 1.5	0.01897	0.99998	0.01604	0.99999	0.01055	0.99970
1.0 + 1.0	0.01032	0.99998	0.01945	1.00000	0.00918	0.99963
1.0 + 0.7	0.00446	0.99998	0.00607	0.99989	0.01287	0.99981
0.7 + 2.0	0.02154	0.99999	0.00861	0.99998	0.00493	0.99996
0.7 + 1.5	0.01213	0.99988	0.00750	0.99980	0.00974	0.99956
0.7 + 1.0	0.00742	0.99983	0.01148	0.99971	0.01958	0.99908

Table 4.6: ΔE_{00} color differences between measured and predicted CIE-L*a*b* values for the test stacked layered samples of different materials when a training set of 9-samples is used in the model.

Test Thickness	DRC Dentine-Enamel Systems		
D(mm)+E(mm)	VE A2-EN1	VD A2-EN3	VP A2-EN3
2.5 + 2.5	0.80	0.57	1.26
2.5 + 2.0	0.85	0.37	0.69
2.5 + 1.0	0.46	0.37	0.78
2.5 + 0.7	0.23	0.24	0.98
2.0 + 2.5	0.21	0.41	0.41
2.0 + 1.5	0.46	0.23	0.44
2.0 + 0.7	0.45	0.40	1.02
1.5 + 2.0	0.48	0.31	0.55
1.5 + 1.0	0.19	0.35	0.76
1.0 + 2.5	0.58	0.27	0.99
1.0 + 1.5	0.18	0.15	0.66
1.0 + 0.7	0.34	0.59	2.06
0.7 + 2.5	0.53	0.16	0.37
0.7 + 2.0	0.83	0.26	0.71
0.7 + 1.0	0.45	1.03	0.46
0.7 + 0.7	0.85	1.69	1.46

Table 4.7: RMSE and GFC metrics between measured and predicted spectral reflectance curves for the test stacked layered samples of different materials when a training set of 9-samples is used in the model.

	DRC Dentine-Enamel Systems					
Test Thickness	VE A2-EN3		VD A2-EN1		VP A2-EN3	
D(mm)+E(mm)	RMSE	GFC	RMSE	GFC	RMSE	GFC
2.5 + 2.5	0.00657	0.99991	0.00528	0.99996	0.01794	0.99996
2.5 + 2.0	0.01009	0.99994	0.00243	0.99999	0.00571	0.99996
2.5 + 1.0	0.00586	0.99997	0.00375	0.99999	0.00674	0.99997
2.5 + 0.7	0.00219	0.99999	0.00243	0.99999	0.01629	0.99999
2.0 + 2.5	0.00432	1.00000	0.00759	0.99998	0.00284	0.99999
2.0 + 1.5	0.00701	0.99999	0.00213	0.99999	0.00461	0.99999
2.0 + 0.7	0.00342	0.99999	0.00474	0.99996	0.01932	0.99998
1.5 + 2.0	0.00978	0.99999	0.00492	1.00000	0.00582	0.99995
1.5 + 1.0	0.00125	1.00000	0.00292	0.99999	0.00784	0.99996
1.0 + 2.5	0.00792	0.99999	0.00322	0.99997	0.00991	0.99981
1.0 + 1.5	0.00347	1.00000	0.00254	1.00000	0.00660	0.99993
1.0 + 0.7	0.00252	0.99999	0.00929	0.99996	0.02102	0.99975
0.7 + 2.5	0.00639	0.99999	0.00448	0.99997	0.00438	0.99997
0.7 + 2.0	0.01525	0.99998	0.00226	0.99999	0.00715	0.99992
0.7 + 1.0	0.00388	0.99999	0.01251	0.99996	0.00378	0.99995
0.7 + 0.7	0.01328	0.99999	0.02225	0.99998	0.01543	0.99994

Table 4.8: Statistics of error metrics for the test stacked layered samples of shade A2 of different materials.

		5-samples training set				9-samples training set			
Layers	**Variable**	**Mean**	**SD**	$< AT_{00}(\%)$	**<PT(%)**	**Mean**	**SD**	$< AT_{00}(\%)$	$< PT_{00}(\%)$
VE A2 - EN1	**RMSE**	0.01163	0.00597			0.00645	0.00401		
	GFC	0.99993	0.00008			0.99998	0.00002		
	ΔL*	0.66	0.44			0.42	0.31		
	Δa*	0.06	0.06			0.14	0.09		
	Δb*	0.74	0.54			0.26	0.21		
	ΔE_{00}	0.93	0.37	100	40.00	0.49	0.24	100	75.00
VD A2 - EN3	**RMSE**	0.01162	0.00442			0.00580	0.00525		
	GFC	0.99990	0.00011			0.99998	0.00001		
	ΔL*	0.76	0.41			0.37	0.50		
	Δa*	0.13	0.09			0.11	0.06		
	Δb*	0.85	0.66			0.27	0.18		
	ΔE_{00}	1.05	0.46	95	25.00	0.46	0.39	100	87.5
VP A2 - EN3	**RMSE**	0.01411	0.00858			0.00971	0.00611		
	GFC	0.99978	0.00023			0.99994	0.00007		
	ΔL*	0.91	0.75			0.69	0.52		
	Δa*	0.16	0.14			0.20	0.12		
	Δb*	1.20	0.73			0.53	0.38		
	ΔE_{00}	1.38	0.72	75	25.00	0.85	0.45	93.75	62.5

When assessing the performance of the predictive model as a function of dentine shade, measured and predicted reflectances of VE-S1+EN1, VE-S2+EN1, VE-S3+EN2, VE-S4+EN2 and VE-S5+EN2 DRC systems were compared. Tables 4.9, 4.10, 4.11 and 4.12 show the ΔE_{00} color differences and spectral metrics between measured and predicted spectral reflectance curves, for both training set arrangements used in this study. The means and standard deviations of the performance metrics as well as the percentage of samples below AT_{00} and PT_{00}, are presented in Table 4.13. As expected, better performance metrics were obtained for the 9-samples training set. Nevertheless, it is worth noting that even for the 5-samples arrangements, all the color differences found between predicted and measured values are below AT_{00}. In the case of 5-samples training set approach, the quality of the reconstruction decreases with darker shades, as it is reflected by the higher mean ΔE_{00} values $\Delta E_{00} = 0.94$, $\Delta E_{00} = 1.10$ and $\Delta E_{00} = 1.17$ registered for S3, S4 and S5 shades, respectively. Whereas for lighter shades, the mean ΔE_{00} values are below PT_{00},

exhibiting $\Delta E_{00} = 0.71$ and $\Delta E_{00} = 0.65$ for S1 and S2 shades, respectively. However, for the 9-samples training set, it seems that performance of the PCA-based predictive models does not depend on shade type, although slightly better values were obtained for S2, S3 and S4 shades: $\Delta E_{00} = 0.43$, $\Delta E_{00} = 0.36$ and $\Delta E_{00} = 0.43$, respectively. For the lightest and darkest shades tested (S1 and S5), the mean color differences are slightly higher, but still below PT_{00}: $\Delta E_{00} = 0.47$ and $\Delta E_{00} = 0.54$, respectively.

Table 4.9: ΔE_{00} color differences between measured and predicted CIE-L*a*b* values for the test stacked layered samples of different shades of VE when a training set of 5-samples is used in the model.

Test Thickness	DRC Dentine-Enamel Systems				
D(mm)+E(mm)	VE S1-EN1	VE S2-EN1	VE S3-EN2	VE S4-EN2	VE S5-EN2
2.5 + 2.0	0.98	1.16	0.91	1.14	1.31
2.5 + 1.5	0.96	1.05	1.19	1.53	1.65
2.5 + 1.0	0.41	0.45	1.01	0.90	1.01
2.0 + 2.5	0.41	0.77	0.45	0.52	0.48
2.0 + 2.0	0.17	0.20	0.77	0.85	0.94
2.0 + 1.5	0.74	0.80	1.00	1.15	1.30
2.0 + 1.0	0.77	0.49	1.18	1.14	0.95
2.0 + 0.7	1.26	1.04	0.98	1.39	1.33
1.5 + 2.5	0.40	0.55	0.62	0.87	0.90
1.5 + 2.0	0.40	0.21	0.89	0.90	1.06
1.5 + 1.0	0.89	0.72	1.55	1.22	1.07
1.5 + 0.7	1.02	0.96	0.81	1.40	1.72
1.0 + 2.5	1.01	0.73	0.89	1.12	1.21
1.0 + 2.0	0.77	0.35	0.90	1.04	1.08
1.0 + 1.5	1.43	0.72	1.07	1.13	1.12
1.0 + 1.0	0.48	0.42	1.18	1.29	0.92
1.0 + 0.7	0.35	0.59	0.52	0.97	1.55
0.7 + 2.0	0.26	0.22	0.78	0.84	0.95
0.7 + 1.5	0.70	0.60	1.04	1.26	1.49
0.7 + 1.0	0.82	0.87	1.17	1.36	1.45

Table 4.10: RMSE and GFC metrics between measured and predicted spectral reflectance curves for the test stacked layered samples of different shades of VE when a training set of 5-samples is used in the model.

	DRC Dentine-Enamel Systems									
Test Thickness	VE S1-EN1		VE S2-EN1		VE S3-EN2		VE S4-EN2		VE S5-EN2	
D(mm)+E(mm)	RMSE	GFC	RMSE	GFC	RMSE	GFC	RMSE	GFC	RMSE	GFC
2.5 + 2.0	0.01888	0.99997	0.02144	0.99997	0.00790	0.99990	0.01024	0.99985	0.01272	0.99979
2.5 + 1.5	0.00783	0.99992	0.00935	0.99991	0.01572	0.99990	0.02111	0.99984	0.01704	0.99973
2.5 + 1.0	0.00970	0.99999	0.00459	0.99998	0.01828	0.99995	0.01327	0.99993	0.01233	0.99989
2.0 + 2.5	0.00967	1.00000	0.01735	1.00000	0.00977	1.00000	0.00900	0.99999	0.00770	0.99999
2.0 + 2.0	0.00310	1.00000	0.00172	1.00000	0.01249	0.99996	0.01530	0.99998	0.01545	0.99996
2.0 + 1.5	0.01508	0.99999	0.01216	0.99997	0.01598	0.99995	0.02032	0.99997	0.01900	0.99992
2.0 + 1.0	0.01818	1.00000	0.01037	1.00000	0.02151	0.99996	0.02027	1.00000	0.01532	0.99998
2.0 + 0.7	0.01620	0.99991	0.00806	0.99989	0.00716	0.99989	0.01030	0.99974	0.00946	0.99972
1.5 + 2.5	0.00353	0.99998	0.00797	0.99995	0.00552	0.99997	0.00690	0.99993	0.00694	0.99991
1.5 + 2.0	0.00718	0.99999	0.00276	0.99998	0.01729	0.99999	0.01726	1.00000	0.01983	1.00000
1.5 + 1.0	0.02006	1.00000	0.01488	1.00000	0.02805	0.99995	0.02081	0.99999	0.01692	0.99999
1.5 + 0.7	0.01434	0.99993	0.00749	0.99989	0.00535	0.99994	0.00889	0.99975	0.01106	0.99955
1.0 + 2.5	0.01588	0.99993	0.00658	0.99990	0.00567	0.99992	0.00699	0.99988	0.00813	0.99984
1.0 + 2.0	0.01483	0.99998	0.00428	0.99998	0.01709	0.99999	0.01904	0.99999	0.01929	0.99999
1.0 + 1.5	0.03135	0.99996	0.01240	0.99998	0.01802	0.99997	0.02037	0.99999	0.02018	0.99999
1.0 + 1.0	0.00964	1.00000	0.00524	0.99999	0.01723	0.99990	0.02138	0.99997	0.01410	0.99999
1.0 + 0.7	0.00531	0.99998	0.01051	0.99998	0.00905	1.00000	0.00607	0.99990	0.00958	0.99969
0.7 + 2.0	0.00291	0.99999	0.00200	0.99999	0.01434	0.99999	0.01501	0.99999	0.01467	0.99996
0.7 + 1.5	0.00975	0.99994	0.00638	0.99994	0.01386	0.99994	0.01229	0.99987	0.01485	0.99980
0.7 + 1.0	0.00766	0.99986	0.00912	0.99988	0.01028	0.99977	0.01059	0.99972	0.01071	0.99967

Table 4.11: ΔE_{00} color differences between measured and predicted CIE-L*a*b* values for the test stacked layered samples of different shades of VE when a training set of 9-samples is used in the model.

Test Thickness	DRC Dentine-Enamel Systems				
D(mm)+E(mm)	VE S1-EN1	VE S2-EN1	VE S3-EN2	VE S4-EN2	VE S5-EN2
2.5 + 2.5	0.96	0.57	0.20	0.21	0.37
2.5 + 2.0	0.55	0.77	0.23	0.37	0.39
2.5 + 1.0	0.42	0.14	0.36	0.51	0.53
2.5 + 0.7	0.70	0.48	0.34	0.39	0.11
2.0 + 2.5	0.44	0.15	0.14	0.19	0.37
2.0 + 1.5	0.23	0.37	0.41	0.49	0.65
2.0 + 0.7	0.44	0.41	0.52	0.30	0.32
1.5 + 2.0	0.29	0.54	0.19	0.12	0.17
1.5 + 1.0	0.19	0.09	0.60	0.27	0.19
1.0 + 2.5	0.23	0.67	0.27	0.61	0.67
1.0 + 1.5	0.74	0.12	0.22	0.17	0.34
1.0 + 0.7	0.37	0.28	0.53	0.69	1.10
0.7 + 2.5	0.40	0.92	0.35	0.56	0.63
0.7 + 2.0	0.61	0.35	0.12	0.34	0.28
0.7 + 1.0	0.18	0.30	0.29	0.56	1.09
0.7 + 0.7	0.82	0.65	0.97	1.10	1.52

Table 4.12: RMSE and GFC metrics between measured and predicted spectral reflectance curves for the test stacked layered samples of different shades of VE when a training set of 9-samples is used in the model.

	DRC Dentine-Enamel Systems									
Test Thickness	VE S1-EN1		VE S2-EN1		VE S3-EN2		VE S4-EN2		VE S5-EN2	
D(mm)+E(mm)	RMSE	GFC	RMSE	GFC	RMSE	GFC	RMSE	GFC	RMSE	GFC
2.5 + 2.5	0.02010	0.99997	0.01271	0.99999	0.00379	0.99999	0.00354	0.99998	0.0060	1.0000
2.5 + 2.0	0.00479	0.99997	0.01435	0.99997	0.00255	0.99999	0.00431	0.99998	0.0041	1.0000
2.5 + 1.0	0.00610	0.99999	0.00212	0.99999	0.00449	0.99998	0.00377	0.99997	0.0036	1.0000
2.5 + 0.7	0.01592	0.99999	0.00407	0.99999	0.00579	0.99999	0.00655	1.00000	0.0018	1.0000
2.0 + 2.5	0.00899	1.00000	0.00158	1.00000	0.00126	1.00000	0.00243	1.00000	0.0019	1.0000
2.0 + 1.5	0.00241	1.00000	0.00462	1.00000	0.00608	1.00000	0.00440	0.99999	0.0042	1.0000
2.0 + 0.7	0.00701	0.99999	0.00178	0.99999	0.00613	0.99998	0.00282	0.99999	0.0042	1.0000
1.5 + 2.0	0.00518	1.00000	0.01155	0.99999	0.00130	1.00000	0.00097	1.00000	0.0017	1.0000
1.5 + 1.0	0.00306	1.00000	0.00122	1.00000	0.01060	0.99998	0.00316	0.99999	0.0026	1.0000
1.0 + 2.5	0.00442	1.00000	0.01163	0.99999	0.00263	0.99999	0.00584	0.99999	0.0029	1.0000
1.0 + 1.5	0.01667	0.99998	0.00085	1.00000	0.00237	1.00000	0.00164	0.99999	0.0025	1.0000
1.0 + 0.7	0.00520	0.99999	0.00395	1.00000	0.00772	0.99998	0.00491	0.99996	0.0042	1.0000
0.7 + 2.5	0.00893	1.00000	0.01612	0.99998	0.00448	0.99999	0.00596	0.99999	0.0020	1.0000
0.7 + 2.0	0.01265	0.99999	0.00203	0.99999	0.00158	1.00000	0.00449	1.00000	0.0019	1.0000
0.7 + 1.0	0.00338	0.99997	0.00354	0.99998	0.00255	0.99998	0.00472	0.99995	0.0069	0.9998
0.7 + 0.7	0.01504	0.99999	0.01042	0.99999	0.01567	0.99999	0.01568	0.99998	0.0092	0.9998

Table 4.13: Statistics of error metrics for test stacked layered samples of different shades of VE.

		5-samples training set				9-samples training set			
Layers	**Variable**	**Mean**	**SD**	$< AT_{00}(\%)$	$< PT_{00}(\%)$	**Mean**	**SD**	$< AT_{00}(\%)$	$< PT_{00}(\%)$
VE S1 - EN1	**RMSE**	0.01205	0.00703			0.00874	0.00559		
	GFC	0.99997	0.00004			0.99999	0.00001		
	ΔL*	0.69	0.47			0.50	0.37		
	Δa*	0.05	0.04			0.08	0.05		
	Δb*	0.49	0.33			0.23	0.17		
	ΔE_{00}	0.71	0.34	100	60.00	0.47	0.24	100	87.50
VE S2 - EN1	**RMSE**	0.00873	0.00512			0.00641	0.00535		
	GFC	0.99996	0.00004			0.99999	0.00001		
	ΔL*	0.47	0.37			0.42	0.37		
	Δa*	0.04	0.03			0.10	0.07		
	Δb*	0.51	0.35			0.20	0.12		
	ΔE_{00}	0.65	0.29	100	75.00	0.43	0.25	100	93.75
VE S3 - EN2	**RMSE**	0.01353	0.00598			0.00494	0.00384		
	GFC	0.99994	0.00005			0.99999	0.00001		
	ΔL*	0.86	0.51			0.33	0.31		
	Δa*	0.07	0.05			0.09	0.05		
	Δb*	0.59	0.40			0.17	0.14		
	ΔE_{00}	0.94	0.25	100	25.00	0.36	0.22	100	93.75
VE S4 - EN2	**RMSE**	0.01427	0.00545			0.00470	0.00330		
	GFC	0.99991	0.00009			0.99999	0.00001		
	ΔL*	0.89	0.52			0.31	0.28		
	Δa*	0.08	0.08			0.15	0.11		
	Δb*	0.76	0.55			0.25	0.18		
	ΔE_{00}	1.10	0.24	100	5.00	0.43	0.25	100	93.75
VE S5 - EN2	**RMSE**	0.01376	0.00420			0.00375	0.00212		
	GFC	0.99987	0.00014			0.99997	0.00006		
	ΔL*	0.87	0.41			0.21	0.10		
	Δa*	0.23	0.15			0.26	0.25		
	Δb*	0.87	0.60			0.34	0.28		
	ΔE_{00}	1.17	0.30	100	5.00	0.54	0.39	100	81.25

As an example of the output of the developed predicitive algorithms, Figure 4.6 shows all the measured spectra of the stacked layered samples of the DRC system VE-S3+EN2 that belong both to the 5-samples and 9-samples test-sets, together with their corresponding predicted (reconstructed) spectra.

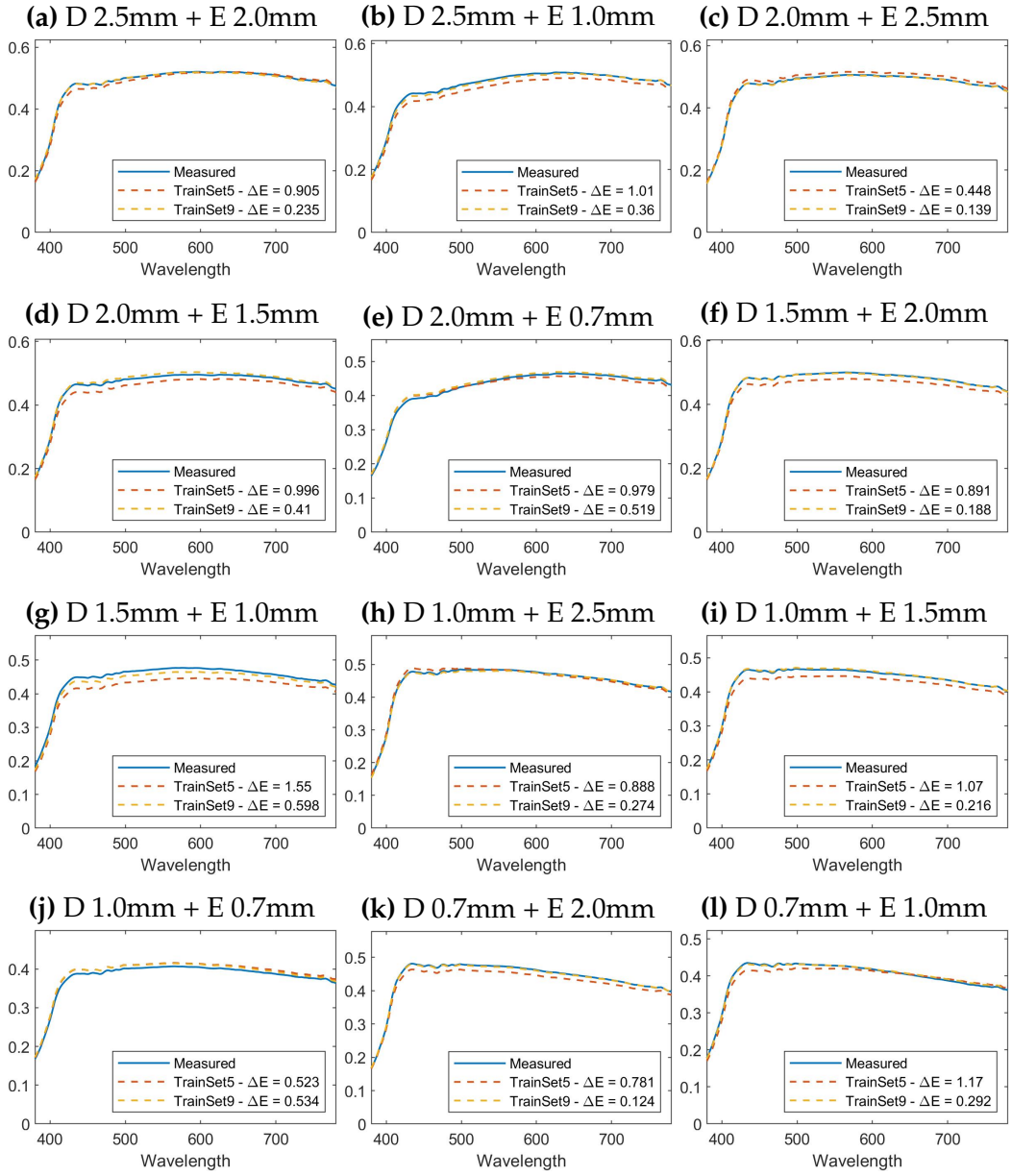

Figure 4.6: Reflectance reconstruction of the stacked layered samples of VE-S3+EN2 of different thicknesses, using the 5-samples and 9-samples training sets.

Therefore, based on the results of this study, the first research hypothesis was accepted, since the reflectance spectrum of layered dental samples was predicted with satisfactory results using a PCA-based algorithm. According to other studies [168], a RMSE of around 2% and a $GFC \geq 0.9999$ result in an very good reconstruction, which is the case of our RMSE and GFC values obtained when comparing the directly measured and the predicted reflectance curves (Table 4.8 and Table 4.13). When analyzing the color differences between predicted and measured values, the values obtained can be classified as very good in most cases, since the vast majority of them are below the acceptability threshold for color differences in dentistry. Furthermore, it can be observed that these color differences are mainly introduced by the L* and b* coordinates. This is somehow expected, since the tooth color range is roughly L* = 51.5 - 85.5, a* = -1.5 - 12.6 and b* = 12.0 - 43.3 [63], therefore the differences in CIE a* coordinate values are much smaller than those of CIE L* and b* coordinates.

Moreover, if we compare the performance of the predictive algorithm when using 5-samples or 9-samples configuration of training set, it can be observed that the number of samples introduced in the training set clearly affects the accuracy of the method. Just by looking at Figure 4.6, it is clear that there is a notable difference in performance between the two configurations. While a training set of 5 samples (X-shaped arrangement) already gives promising results, with very good $RMSE$ and GFC values [168], the use of a training set of 9 samples (diamond-shaped arrangement) results in an considerably improvement of the quality of the predictive model, especially regarding the percentage of samples below AT_{00} (Table 4.8). This becomes even more evident when analyzing the percentage of samples below PT_{00}, which exceeds 80% in most cases for the 9-samples training set, while is considerably lower for the 5-samples one (between 5% and 75%). One might think that this error partly derives from the fact that using 5-samples in the training set implies using 20 samples

in the testing set, while when using the extended 9-samples training set, the testing set only uses 16 samples. However, if we pay attention to the standard deviation values it can be observed that they are similar in both configurations. Therefore, we can assume that the additional measurements in the 9-samples training set are necessary to achieve a considerable increase in performance. Furthermore, it has to be considered that the diamond-shaped configuration for the training set implies that there is no input for extreme thickness combinations (for example: 0.7 mm dentine + 0.7 mm enamel; 2.5 mm dentine + 0.7 mm enamel, 2.5 mm dentine + 2.5 mm enamel, etc.). This requires the algorithm to forecast reflectance values for an area for which it does not have input values (extrapolation), which could, beforehand, diminish its predictive capability and result in a lower performance. However, this is not the case, as the 9-samples training set consistently provides better performance metrics than the 5-samples configuration. Thus, the second research hypothesis of this study was also accepted.

Lastly, the third hypothesis was partially rejected. According to the results presented in Table 4.8, it is observed that the errors obtained for VE or VD are clearly lower than those obtained for VP. This occurs independently of the number of samples introduced in the training set. Therefore, it is clear that the performance of the PCA-based predictive algorithm depends, to some extent, on the type of DRC used. In the case when different shades for dentine samples were used, the method performs differently for each training set configuration. So, while there are more significant errors when dark shades are used in the case of the 5-samples training set, there is no clear tendency observed for the 9-sample configuration, as results obtained for all shades are all within the same error range (Table 4.13). Furthermore, according to the ΔE_{00} values presented in Tables 4.8 and 4.13, the percentage of reconstructed samples below AT_{00} and PT_{00} varies according to the DRC system, as well as, in some cases,

according to dentine shade.

Bearing the limitations in mind, given the current experimental setup, the thickness of the monolithic samples must be precisely controlled in order to produce homogeneously spread training and test sets. Also, it is important to consider that the layered samples were obtained by stacking two monolithic pellets. This implies an abrupt material change at the interface between the two layers, which is not usually the case when materials are coupled by polymerization processes, that generally result in fuzzier transitions between the layers. Moreover, only composite materials have been used, therefore future research should include a wider range of multi-layer materials and shades. Another limitation of the present study might be related to the use of a combination of only two layers (dentine and enamel) when preparing samples, which might not always be the case in a clinical scenario. However, the use of only two composites (dentine + enamel) for direct restorations are usually considered enough to achieve a proper color match with the surrounding natural tooth structures [172].

Nevertheless, the high accuracy obtained with the shades and materials already tested confirms that the proposed method for reconstructing reflectance spectra of stacked layered samples can be used to find an optimal color match for dental materials. Nonetheless, future studies testing the proposed algorithm in polymerized (stratified) layered samples are still needed.

CHAPTER

5

DEVELOPMENT OF THICKNESS-DEPENDENT PREDICTIVE METHOD FOR THE ESTIMATION OF THE CIE L*a*b* COLOR COORDINATES OF MONOLITHIC AND LAYERED DENTAL RESIN COMPOSITES

In this Chapter a new regression algorithm is developed for color prediction of monolithic and layered dental resin composites of different materials and shades with varying clinically relevant thickness.

It extends the study submitted as:

M. Tejada-Casado, R. Ghinea, M. Pérez, J. Ruiz-López, H. Lübbe and L. Herrera, "Development of thickness-dependent predictive methods for the estimation of the CIEL*a*b* color coordinates of monolithic and layered dental resin composites". (Submitted to *Materials*, 2022)

5.1 Introduction

The goal of any dental restoration is to create a natural appearance that is highly esthetic while remaining functional [173]. It has already been highlighted that the final color of a direct dental restoration results from the merge of the layering of several restorative materials of different shades and thicknesses [170].

Finding the best dentine and enamel shades combination is not an easy task for the dental clinician. In most clinical settings, shade matching of natural tooth color to dental restorations is carried out by visual comparisons with shade guides. However there are many parameters that might influence the final shade selection, such as variability among different shade guides, the background or the lighting conditions [13,70,71,73].

For this reason, the reflectance spectrum of an object is known as the best way to describe its color. Nonetheless, devices that are able to properly measure reflectance spectrum are usually very expensive and thus they are mostly used for research

purposes only [53,137]. To approach objective color measurements to the dental field and make the shade matching process more accurate and not so highly subjective, simpler measuring devices, such as spectrophotometers or colorimeters [65,67,68], have been introduced within the clinical practice. These clinically commercial devices usually provide measurements of the CIE-L*a*b* color coordinates. Therefore, if these parameters could be predicted with a certain accuracy, the trial-and-error in the shade matching process and the esthetic outcome of dental restorations could be considerably enhanced.

The fundamentals of most studies that have attempted color prediction in dentistry are usually based on spectral measurements [134,138,139,141], although, as mentioned before, spectral measurement devices are barely available in the clinical practice. Few studies [59,60] proposed color estimations of CIE-L*a*b* color coordinates of natural dental structures using color readings obtained with clinical dental color measuring devices. These studies used both linear and non-linear regressions methods, but the performance of the proposed predictive algorithms is prone to improvement. To the best of our knowledge, there are no studies that using only color data measurements (CIE-L*a*b* color coordinates), aimed for predictions of CIE-L*a*b* values of dental materials.

Therefore, the main objective of this study is to develop and assess the accuracy of a prediction method for the CIE-L*a*b* chromaticity coordinates of both monolithic and layered dental resin-based composites with varying shades and thicknesses and under different illuminants.

The following research hypotheses were tested in this study:

1. Linear regression-based prediction algorithms can be used to estimate the CIE-L*a*b* chromaticity coordinates of monolithic and layered dental samples under different illuminants with satisfactory results.

2. There are differences in estimation accuracy for monolithic and layered DRC samples.

3. The performance of the proposed method will be affected by the use of different types or shades of DRC.

5.2 Materials and method

5.2.1 Specimen preparation

Monolithic DRC samples of different materials, shades and thicknesses were used in this study (Table 5.1). As for the previous study (Ch.4), the monolithic dentine and enamel pellets were produced by polymerization of dental masses under combined heat-and-pressure treatment according to manufacturer's specifications, as was described in detail in Chapter 3 Section 3.2.1. All monolithic specimens were ground to specific thicknesses 0.7 mm, 1.0 mm, 1.5 mm, 2.0 mm and 2.5 mm with a tolerance of $\pm$0.1 mm, polished with 9μm diamond paste by the same trained operator and cleaned from debris in an ultrasonic bath.

The performance of the proposed method was tested for both monolithic and layered samples:

- Monolithic samples:
  VITAPAN Dentine pellets corresponding to 7 VITA Classical shades -A1, A2, A3, A3.5, B2, C2 and D2-, were used.

- Layered samples:
  The layered samples were obtained by stacking monolithic specimens, following the procedure described in Chapter 4. This is by pressure bonding each dentine

sample with each enamel sample of the 5 different thicknesses. Again, as described in the previous Chapter (Ch. 4), the algorithm was evaluated as a function of DRC type and as a function of dentine shade. To this end, monolithic samples of VE, VD and VP of the same shade (A2); monolithic samples VE of two light shades (named S1 and S2), two intermediate shades (named S3 and S4) and one dark shade (named S5); and three different enamel shades (EN1, EN2 and EN3) were prepared (Table 5.1) and combined according to manufacturer's indications, in order to create 8 different DRC systems (dentine-enamel combination) as follows:

- Testing according to DRC type:

  VE-A2+EN1, VD-A2+EN3 and VP-A2+EN3.

- Testing according to DRC shade:

  VE-S1+EN1, VE-S2+EN1, VE-S3+EN2, VE-S4+EN2 and VE-S5+EN2.

Table 5.1: Used dental resin-based composites with corresponding selected shades, composition and thickness.

Composite	Shades	Chemical composition	Thickness (mm)
VITAPAN Excell (VE)	A2, S1, S2, S3, S4, S5	PMMA (84-86%) , SiO_2 (14-15%) and Pigments ($< 1\%$)	0.7 ± 0.1; 1.0 ± 0.1; 1.5 ± 0.1; 2.0 ± 0.1 and 2.5 ± 0.1
VITAPAN Dentine (VD)	A1, A2, A3, A3.5, B2, C2, D2		
VITA Physiodens (VP)	A2		
VITA Enamel (EN)	EN1, EN2, EN3		

Examples of the specimens used in this study are presented in Figures 4.1 and 4.2.

5.2.2 Color measurements

The spectral reflectance spectrum (380 nm – 780 nm) of both monolithic and stacked layered samples was measured as previously described in Section 3.2.2. Three repeated reflectance measurements without replacement were performed for each specimen, and the results were averaged. To test the performance of the predictive algorithm for different illuminants, the spectral reflectance measurements were converted into CIELAB color coordinates using the CIE 2° Standard Observer and three different CIE illuminants: CIE D65 Standard Illuminant, for being the current recommendation of the CIE [12]; CIE D55 illuminant, since it is the most used within dental color measuring clinical devices [174]; and CIE LED-B1, since, among all the newly proposed LED illuminants by the CIE is the closest one (in terms of CCT and xy-chromaticity coordinates) to CIE D65 and CIE D55 [11, 12].

5.2.3 Computational method

In order to develop and evaluate a predictive method, and similar to previous studies presented in this PhD Thesis, the samples were divided into training and testing sets. Computed CIE-L*a*b* coordinates corresponding to the samples included in the training set were used to build the regression models, while those of the samples included in the testing set were used exclusively for testing the appropriate functioning of the model as well as its accuracy. The procedure used to allocate samples in the training and testing sets was different for monolithic and layered samples.

As was explained in Chapter 3, for monolithic samples, given a total of 5 different samples (i.e. 5 different thicknesses) for each VD shade, our set was divided in such a way that, if the CIE-L*a*b* coordinates of one of the dental samples was

predicted, only the samples corresponding to the same shade but with different thickness were used for the development of the predictive model (training set). As previously described, this separation into training and testing groups is repeated for all thicknesses of each shade. A diagram of this division is shown in Figure 5.1a.

As was explained in Chapter 4, in the case of stacked layered samples, combining all 5 different samples of the first layer (dentine) with all 5 samples of the second layer (enamel), resulted in a total of 25 enamel-dentine layered combinations for each DRC system. These 25 layered specimens were subsequently divided into a training and a testing set of samples. According to the findings of the previous study (Ch. 4), a training set of 9 samples arranged in a diamond-shaped configuration is optimal to achieve very good color estimations, therefore the same configuration was used, resulting in a training set of 9 samples and a testing set of 16 samples for each DRC system. The arrangement of training and testing sets for layered samples is shown in figure 5.1b.

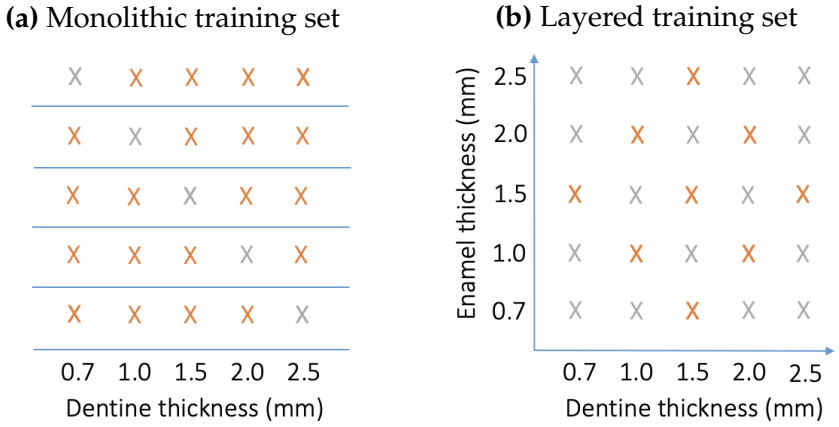

Figure 5.1: Samples being included in the training set (orange) and testing set (gray). (**a**) For monolithic samples, each thickness is used as a test sample while the other four thicknesses are included in the training set. (**b**) For stacked layered samples, 25 dentine + enamel combinations are obtained and divided into 9-samples training set and 16-samples testing set.

Linear Regression Models were used to predict each CIE-L*, CIE-a* and CIE-b* coordinates of all monolithic and layered samples of different thicknesses included in the testing sets. Since the coordinates were predicted individually, three different models were computed for each test sample. According to best performance achieved in preliminary tests, 2^{nd} degree polynomial was used to find the best-fit-curve and best-fit-surface for monolithic and layered samples, respectively.

For single layer samples, the equation describing the models is:

$$f(x) = p_1x^2 + p_2x + p_3 \tag{5.2.1}$$

where, f is the predicted CIE-L*, CIE-a* or CIE-b* values, x corresponds to the sample thickness, and p_1 to p_3 are the parameters of the model.

For layered samples, the surface is defined as:

$$s(x, y) = p_1x^2 + p_2y^2 + p_3xy + p_4x + p_5y + p_6 \tag{5.2.2}$$

where s is the predicted CIE-L*, CIE-a* or CIE-b* coordinate value, x and y correspond to the dentine and enamel thicknesses respectively and p_1 to p_6 are the parameters of the models.

In order to solve both problems, specific functions were implemented in MATLAB (MathWorks, Natick, MA) to compute the Linear Least Squares for monolithic and layered test samples, respectively. Once these curves and surfaces are determined, the CIE-L*, CIE-a* or CIE-b* values corresponding to any different desired thickness can be extracted. An example of this procedure is shown in figure 5.2.

(a) Dentine A3.5: Test Thickness = 2 mm

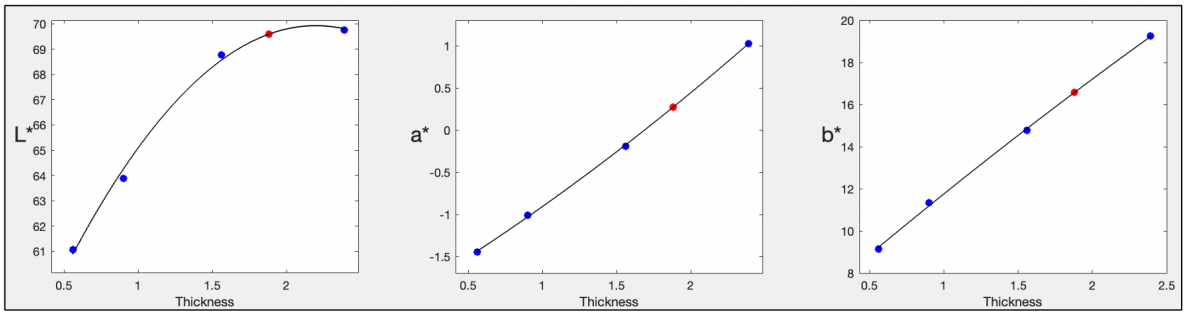

(b) VE A2-EN1: Test Thickness = D(2 mm)+E(1.5 mm)

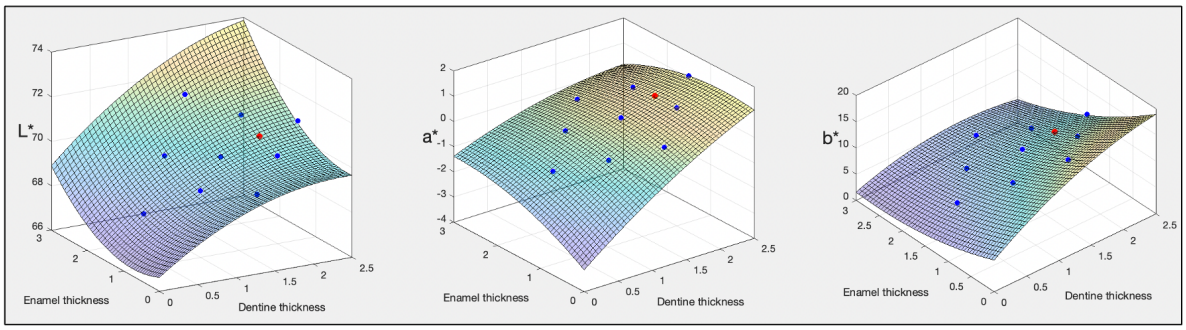

Figure 5.2: Examples of best-fit-curve (**top**) and best-fit-surface (**bottom**) for the CIE-L*, CIE-a* and CIE-b* color coordinates for a given monolithic and layered sample. Blue dots represent the values corresponding to the training set samples and red dots the values predicted by the model for a specific thickness.

5.2.4 Evaluation of color differences

Total color differences between measured and predicted values for each sample in the testing group were computed using the CIEDE2000 (ΔE_{00}) total color difference formula [95] as shown in Equation 3.2.6. Similarly as described in previous chapters of this PhD Thesis, ΔE_{00} values were comparatively evaluated to their corresponding 50:50% perceptibility (PT_{00}) and acceptability (AT_{00}) thresholds for dentistry, as recommended by the ISO/TR 28642:2016 [94]: $PT_{00} = 0.8$ and $AT_{00} = 1.8$ [27, 92].

5.3 Results and discussion

In this study, linear regression models were used to predict the CIE-L*, CIE-a* and CIE-b* color coordinates for different sets of monolithic and layered samples of different thicknesses, shades and materials. As described in previous chapters, a spectroradiometer was used to measure the reflectance spectrum of all monolithic and layered specimens over a standard black background, in order to simulate the darkness in the oral cavity. This type of devices have been already recognized as first option when performing highly accurate color measurements in dental research [26, 81].

It is well known that the color of a sample is strongly dependant on the illumination under which it is observed. In order to evaluate the performance of the proposed predictive methods under different illumination conditions, the spectral reflectance measurements were converted into CIELAB color coordinates using the CIE 2° Standard Observer and a set of three different illuminants: CIE D65 Standard Illuminant, CIE D55 illuminant and CIE LED-B5.

Some studies have estimated CIE-L*a*b* values of dental natural structures based on data obtained with clinical color measurements devices [59, 60]. However, their predictive models focused on color of natural teeth with respect to age and gender but not on dental materials, which is also of interest in dental restorations. Many existing studies confirmed that color of different dental materials can be estimated based on different predictive approaches [138, 139, 141, 154, 175, 176]. Noteworthy, all the proposed predictive models are based on acquired spectral data, which is not provided by most of the clinically available color measurement devices. In this sense, an advantage of the predictive method proposed in this study is that it is based exclusively on CIE-L*a*b* coordinates, making it easier to implement and deploy

in a real clinical scenario. Additionally, a wide variety of shades (including light, intermediate and dark colors) and clinically relevant thicknesses [171] were used in this study, which allowed us to analyze the performance of the proposed algorithm with respect to different parameters.

As the standard metric for color evaluation in dental research [13, 65, 71, 72, 82, 102, 177], color differences between real measured values and estimated ones were calculated with the CIEDE2000 color difference formula, since it has proven to fit more accurately with visual perception [95]. The results have been evaluated according to the 50:50% perceptibility and acceptability thresholds established for dentistry and dental applications ($PT_{00} = 0.8$ and $AT_{00} = 1.8$) [27, 92].

According to our results, the performance of the predictive methods was almost identical for all three illuminants tested, being the total mean color differences between measured and predicted CIE-L*a*b* values for the whole data set (including monolithic and layered) of $\Delta E_{00} = 0.74$, $\Delta E_{00} = 0.75$ and $\Delta E_{00} = 0.74$, for CIE D65, CIE D55 and CIE LED-B5, respectively. When analyzing the percentage of color estimations that returned a color difference lower than the acceptability threshold, it was found that, for the three illuminants tested, in 91.4 (%) of the cases the color differences between real and predicted values were lower than AT_{00}. In the case of PT_{00}, the percentage of color differences between real and predicted values that were imperceptible to an average observer varied slightly for the different illuminants tested, being 72.4%, 73.0% and 71.8%, for CIE D65, CIE D55 and CIE LED-B5, respectively.

Although there are differences among the different illuminants tested, these are very subtle and there is not a clear outperformance of any of the illuminants used. In this regard, for presentation purposes and simplicity, only the results corresponding to the CIE-L*a*b* values computed for the Standard Illuminant D65 are further

presented for a deeper analysis, as it is the recommended illuminant by the CIE [12].

Tables 5.2, 5.3 and 5.4 show the ΔE_{00} color differences between measured and predicted CIE-L*a*b* values, for monolithic and stacked layered samples, respectively. For the single layers, the values presented in the table correspond to those of a certain test thickness when the other four samples of the same shade are being used to build the model. For the stacked layered samples, the presented values correspond to the samples included in the testing set, as previously described in section 5.2.3.

Table 5.2: ΔE_{00} color differences between measured and predicted CIE-L*a*b* values for all monolithic samples tested in our study.

Text Thickness	**Shade**						
Dentine (mm)	**A1**	**A2**	**A3**	**A3.5**	**B2**	**C2**	**D2**
2.5	3.83	1.57	2.80	3.31	2.21	3.62	3.66
2.0	1.31	0.48	0.80	1.01	0.73	1.13	1.23
1.5	0.39	0.57	0.68	0.15	0.12	0.09	0.26
1.0	1.49	0.98	1.65	1.41	0.83	1.36	1.45
0.7	3.91	1.99	3.38	3.01	1.91	3.11	3.49

Table 5.3: ΔE_{00} color differences between measured and predicted CIE-L*a*b* values for stacked layered samples of different materials tested in this study.

Test Thickness	**DRC Dentine-Enamel Systems**		
D(mm)+E(mm)	**VE A2-EN1**	**VD A2-EN3**	**VP A2-EN3**
2.5 + 2.5	0.89	0.67	1.58
2.5 + 2.0	0.90	0.49	0.89
2.5 + 1.0	0.42	0.25	0.61
2.5 + 0.7	0.20	0.12	1.06
2.0 + 2.5	0.26	0.46	0.17
2.0 + 1.5	0.38	0.13	0.41
2.0 + 0.7	0.35	0.42	1.16
1.5 + 2.0	0.49	0.27	0.60
1.5 + 1.0	0.22	0.36	0.75
1.0 + 2.5	0.43	0.15	0.87
1.0 + 1.5	0.19	0.18	0.58
1.0 + 0.7	0.19	0.59	1.86
0.7 + 2.5	0.40	0.14	0.26
0.7 + 2.0	0.79	0.26	0.69
0.7 + 1.0	0.51	1.02	0.50
0.7 + 0.7	0.99	1.71	1.74

Table 5.4: ΔE_{00} color differences between measured and predicted CIE-L*a*b* values for stacked layered samples of different shade lightness tested in this study.

Test Thickness	DRC Dentine-Enamel Systems				
D(mm)+E(mm)	VE D1-EN1	VE D2-EN1	VE D3-EN2	VE D4-EN2	VE D5-EN2
2.5 + 2.5	1.09	0.80	0.55	0.51	0.54
2.5 + 2.0	0.65	0.77	0.44	0.48	0.59
2.5 + 1.0	0.26	0.19	0.31	0.30	0.27
2.5 + 0.7	0.67	0.30	0.36	0.33	0.31
2.0 + 2.5	0.42	0.10	0.10	0.14	0.25
2.0 + 1.5	0.22	0.31	0.35	0.29	0.32
2.0 + 0.7	0.36	0.17	0.41	0.27	0.29
1.5 + 2.0	0.26	0.56	0.15	0.11	0.21
1.5 + 1.0	0.15	0.12	0.60	0.29	0.28
1.0 + 2.5	0.20	0.54	0.30	0.30	0.13
1.0 + 1.5	0.75	0.09	0.16	0.16	0.33
1.0 + 0.7	0.35	0.27	0.54	0.40	0.34
0.7 + 2.5	0.38	0.73	0.34	0.35	0.11
0.7 + 2.0	0.60	0.29	0.21	0.40	0.18
0.7 + 1.0	0.14	0.33	0.27	0.62	1.17
0.7 + 0.7	0.89	0.77	1.10	1.21	1.36

In a recent study [13], it was stated that color gamuts of a set of teeth, tested under several illuminants (including D65 and LED-B5, among others), showed similar volume and shape in CIELAB color space, but their centers of gravity changed in different directions. Considering that the sensitivity of the human visual system also changes with illumination and that the CIEDE2000 has been designed to fit more accurately with visual perception [95], a change of illumination could lead to higher ΔE_{00} between measured and estimated CIE-L*a*b* values. However, in the present study, very similar results were obtained independently of the illuminant considered (CIE D65, D55 or LED-B5), which proves the robustness of the proposed predictive method, and ensures satisfactory outcomes for its implementation in different settings. Therefore, the first research hypothesis was accepted, since satisfactory color coordinates estimations can be achieved for monolithic and layered samples using the proposed methods, independently of the illuminant used, as shown by the ΔE_{00}

values presented in Tables 5.2, 5.3 and 5.4.

As was already mentioned in the study presented in Chapter 3 of this PhD Thesis, when dealing with predicted data, different modelling behaviours can be expected for the estimation of the CIE-L*a*b* values of a test sample whose thickness falls outside (extrapolation) or within the range of available training samples (interpolation). Thus, in order to assess the prediction capability of our method when out-of-the-range predictions are avoided, two different methods of analysis have been performed for the monolithic pellets. Following a similar procedure to that of the previous study, for the extrapolation approach, all samples presented in the testing set are used in the evaluation while for the interpolation approach, the analysis is limited to only those samples that fall within the cloud of available data (samples of 2.0 mm, 1.5 mm and 1.0 mm). The means and standard deviations of the performance metrics (ΔL*, Δa*, Δb* and ΔE_{00}), as well as the percentage of samples lower than AT_{00} and PT_{00} for all shades and thicknesses, are presented in Table 5.5, for both extrapolation and interpolation approaches.

Table 5.5: Statistics of error metrics for the extrapolation (35 specimens considered for prediction) and interpolation approach (21 specimens considered for prediction).

Method of analysis	Variable	Mean	SD	$< AT_{00}(\%)$	$<PT_{00}$**(%)**
Extrapolation (n = 35)	**ΔL***	2.00	1.50		
	Δa*	0.14	0.13		
	Δb*	0.62	0.58		
	ΔE_{00}	1.71	1.22	62.86	28.57
Interpolation (n = 21)	**ΔL***	0.99	0.67		
	Δa*	0.09	0.07		
	Δb*	0.39	0.26		
	ΔE_{00}	0.86	0.49	100	47.62

Similarly to the study previously presented in Chapter 4 for layered samples, the performance of the method have been assessed both as a function of DRC type and shade lightness. As for the monolithic samples, the measured and predicted CIE-L*a*b* values were compared using different color metrics (ΔL*, Δa*, Δb* and

ΔE_{00}). The means and standard deviations, as well as the percentage of samples with color differences between measured and predicted values lower than AT_{00} and PT_{00}, are presented in Tables 5.6 and 5.7, respectively.

Table 5.6: Statistics of error metrics for the test stacked layered samples of shade A2 of different DRC types.

Layers	Variable	Mean	SD	$< AT_{00}(\%)$	$< PT_{00}(\%)$
VE A2 - EN1	**ΔL***	0.39	0.33		
	Δa*	0.05	0.04		
	Δb*	0.34	0.25		
	ΔE_{00}	0.48	0.27	100	81.25
VD A2 - EN3	**ΔL***	0.38	0.51		
	Δa*	0.06	0.04		
	Δb*	0.29	0.21		
	ΔE_{00}	0.45	0.41	100	87.5
VP A2 - EN3	**ΔL***	0.78	0.60		
	Δa*	0.09	0.05		
	Δb*	0.60	0.34		
	ΔE_{00}	0.86	0.51	93.75	56.25

Table 5.7: Statistics of error metrics for the test stacked layered samples of different shades of VITA Excell.

Layers	Variable	Mean	SD	$< AT_{00}(\%)$	$< PT_{00}(\%)$
VE S1 - EN1	**ΔL***	0.51	0.41		
	Δa*	0.04	0.03		
	Δb*	0.24	0.20		
	ΔE_{00}	0.46	0.28	100	87.50
VE S2 - EN1	**ΔL***	0.40	0.37		
	Δa*	0.03	0.02		
	Δb*	0.23	0.14		
	ΔE_{00}	0.40	0.26	100	100
VE S3 - EN2	**ΔL***	0.36	0.35		
	Δa*	0.04	0.02		
	Δb*	0.23	0.15		
	ΔE_{00}	0.39	0.24	100	93.75
VE S4 - EN2	**ΔL***	0.29	0.32		
	Δa*	0.05	0.03		
	Δb*	0.27	0.20		
	ΔE_{00}	0.39	0.26	100	93.75
VE S5 - EN2	**ΔL***	0.20	0.16		
	Δa*	0.10	0.13		
	Δb*	0.36	0.35		
	ΔE_{00}	0.42	0.35	100	87.5

When comparing the performance metrics of the predictive algorithms developed for monolithic and stacked layered samples, it was found that slightly better values were obtained for the later ones. At first sight, this might seem surprising, as predicting color data of monolithic samples should be an easier task and therefore lead to better results (in terms of predictive accuracy). Monolithic samples are easier to fabricate and the respective predictive method is designed for 2 dimensional data versus the 3 dimensions needed for the layered samples. However, the differences in performance between the monolithic and layered samples can be partially explained by the size of the training sets. In the study presented in Chapter 4 of this Thesis, where reflectance data and color of a set of DRC materials was estimated with PCA-based predictive algorithms, it was proved that the sample size of the training set strongly affected the performance of the proposed predictive models. In this regard, in the present study, the training set consisted of only 4 samples for each monolithic shade group, while for the layered specimens the training set consisted of a total of 9 samples (Figure 5.1).

In terms of color differences between predicted and real measured data, in the present study 62.86% and 28.57% of the forecasted data exhibited color differences lower than AT_{00} and PT_{00}, respectively, when training sets of 4 samples, as the ones uses for the monolithic pellets (Table 5.5), were used. These results are in accordance with the ones presented in Chapter 4, that predicted reflectance data and color of a set of layered DRC materials for training sets of 5 samples (Tables 4.8 and 4.13), where values within $75\% - 100\%$ of the color differences between predicted and real measured data below AT_{00}, and $5\% - 75\%$ below PT_{00}, were found.

When a predicted data point falls outside the cloud defined by the set of available data points (i.e. extrapolation approach), the accuracy of the predictive models is expected to decrease. This is the case of monolithic samples of 0.7 mm and 2.5

mm (Table 5.2), which are the extreme thicknesses of our sample data sets. For this reason, the predictive capability of the proposed models was also assessed when samples corresponding to these extreme thicknesses were left out of the testing sets, as suggested in the study presented in Chapter 3 of this Thesis, where significant differences were found for extrapolation and interpolation approaches (Table 5.5). Indeed, more accurate estimations were found when only samples that fall within the cloud of data points defined by the training set (i.e. interpolation approach) were included in the analysis, with 100% and 47.42% of the color differences between predicted and measured data lower than AT_{00} and PT_{00}, were obtained respectively.

However, in the case of the stacked layered specimens, there are also test samples outside the cloud of data points (Tables 5.3 and 5.4), as for example DRC systems conformed of dentine of 2.5 mm - enamel of 0.7 mm, among others, and color values predictions tend to be considerably better than extrapolations of the monolithic samples.

For these reasons, the second research hypothesis was partially accepted, since, in some cases, differences in estimation accuracy were found between monolithic and layered samples, probably due to the size of the training sets and the geometry of the predictive models used -2 dimensions versus 3 dimensions-, for monolithic and layered samples, respectively.

Lastly, when comparing the performance of the predictive methods for different materials and shades (Tables 5.5, 5.6 and 5.7), a clear difference in performance, when different shades of the same material were considered, was not found. However, an important difference in predictive performance was registered when different materials were considered for analysis. For both monolithic and stacked layered samples, the estimations performed for VD and VE materials were considerably better than those obtained for VP material (Table 5.6). In the study presented in Chapter 3 it

was also highlighted that the performance of a predictive method for color estimation of dental materials varied between dental ceramics and DRC materials, being better for the later ones. It was suggested that the differences in performance might come from different sample preparation procedures. However, this is not the case of the current study, as all the specimens were prepared under the exact same conditions and by the same trained operator, which ensured the repeatability of the samples quality. In this sense, it is clear that the performance of the predictive algorithm depends, to great extent, on the type of DRC used. Therefore, the third research hypothesis of this study was also partially accepted, as the performance of the proposed predictive methods is affected by the use of different types of DRC but not by the use of different shades of the same DRC.

Bearing the limitations in mind, only composite materials have been used in this study. Also, as stated in the previous chapter, it is important to consider that the layered samples were obtained by stacking two monolithic pellets and they were not coupled by polymerization processes, which for sure affects the interface between the two layers. Therefore, further studies including polymerized layered pellets are required in order to analyze the effect of these materials transitions within the interface of the two layers and to fully understand the behaviour of the proposed predictive models for DRC samples.

Nevertheless, the low variability in the obtained results and the high accuracy obtained with the shades and materials already tested, confirms that the proposed method for reconstructing the CIE-L*a*b* chromaticity coordinates of single-layer and bi-layered samples can be used to find an optimal color match for dental materials. The predictive methods presented in this study have the potential to provide essential information of the final appearance of both monolithic and layered dental restorations. Lastly, it is worth highlighting that the predictive models developed in the present

study are using as input solely CIE-L*a*b* values, which are ease to obtain with affordable clinical color measurement commercial devices for dentistry.

CHAPTER

6

PERFORMANCE EVALUATION OF COLOR PREDICTION ALGORITHMS IN STRATIFIED LAYERED SAMPLES

In this Chapter, the PCA-based and the linear regression-based algorithms developed for stacked layered samples in Chapters 4 and 5, respectively, are applied for the reflectance and color prediction of polymerized layered (stratified) samples. Also, a general overview on the advantages and disadvantages of the different algorithms proposed is provided.

6.1 Introduction

In this PhD Thesis, different reflectance and color predictive algorithms have been proposed and tested for the color prediction of monolithic and layered dental materials with varying thickness. These layered samples have been produced by staking two monolithic pellets, and were not actually obtained through polymerization processes (stratified samples). In a first stage, working with stacked layered samples has many benefits, since multiple samples with controlled layer thicknesses could be produced consistently and very easily. However, the disadvantage of preparing stacked layered samples relies on the abrupt transition between the different layers, different from the smooth transition usually found in natural dental tissues (dentine-enamel junction) or when two materials are coupled by polymerization processes when manufactured (stratified materials).

Although the algorithms proposed in the previous chapters of this PhD Thesis have proven to be valid for stacked layered samples, further studies including stratified layered pellets are required in order to analyze the effect of these material transitions within the interface of the two layers and to fully understand the behaviour and robustness of the proposed predictive models for DRC samples. Therefore, the

main objective of the study proposed in this chapter is to evaluate and validate the use of the previously proposed PCA-based as well as linear regression-based CIE-L*a*b* prediction algorithms for manufactured stratified layered dental resin composites with different thicknesses and shades.

The following research hypotheses were tested in this study:

1. The reflectance spectrum of stratified layered dental samples can be predicted with satisfactory results using a PCA-based algorithm.

2. Linear regression-based CIE-L*a*b* prediction algorithms can be used to estimate the CIE-L*a*b* color coordinates of stratified layered dental samples with satisfactory results.

6.2 Materials and method

6.2.1 Specimen preparation

Stratified layered samples were produced at VITA Zahnfabrik facilities by a trained materials expert. As was the case for the monolithic pellets fabrication, described in Chapter 3 Section 3.2.1, the fabrication of polymerized stratified layered samples was based on the same organic dentine and enamel masses that are used for the production of prosthesis teeth. As previously explained, these masses were prepared and stored in conventional deep-freezers and just before being used they were taken out and exposed to ambient temperatures.

For the fabrication of the stratified pellets, slices of the produced masses were calendered to sheets of specific thicknesses (Th_{cal}), calculated according to the polymerization shrinkage ratio. First, disc-shaped pieces of 1.5 cm diameter of the calendered enamel masses were die-cut and inserted into the nests of the metallic mold (Figure

6.1a). The masses were then compacted by a combined treatment of uniaxial pressure and vibration in a blender (Figure 6.1b). The thickness of the compacted disc-shaped parts (Th_{press}) was defined by the height of the pressing punch. Compaction ratios were defined as $(Th_{cal} - Th_{press})/Th_{cal}$ and were critical to the success of the fabrication. Afterwards, the dentine material was added, again as a 1.5 cm diameter disc of another calendered sheet. This layer was pressed to slightly overfill the nests of the mold, as can be seen in Figure 6.1c, in order to maintain pressure during the whole process. The pressing was done with a mechanical hand press (Figure 6.1d), which was equipped with a dial gauge that allows to control the height of the punch with sub-millimeter precision.

Controlling these parameters was key, since, for example, insufficient pressure would lead to opaque and blurry polymerized pellets. After the dentine layer was added and adjusted in height, the metallic mould was closed and the two-layer polymerized pellets were produced by the same heat-and-pressure treatment in a conventional transfer press as for the monolithic pellets.

Regarding the thickness of the layers, the enamel layer was directly obtained right after the polymerization, so the pellets were only ground on the dentine side to set up the right thickness of this layer. The dentine thickness was then controlled by measuring the total stratified pellet thickness and subtracting the enamel thickness.

Finally, the produced pellets were polished with a $9\mu m$ diamond paste on the enamel face to achieve a pre-defined surface roughness. The polishing procedure was performed by the same trained operator, as described in previous Chapters. Examples of the specimens used in this study are presented in Figure 6.2.

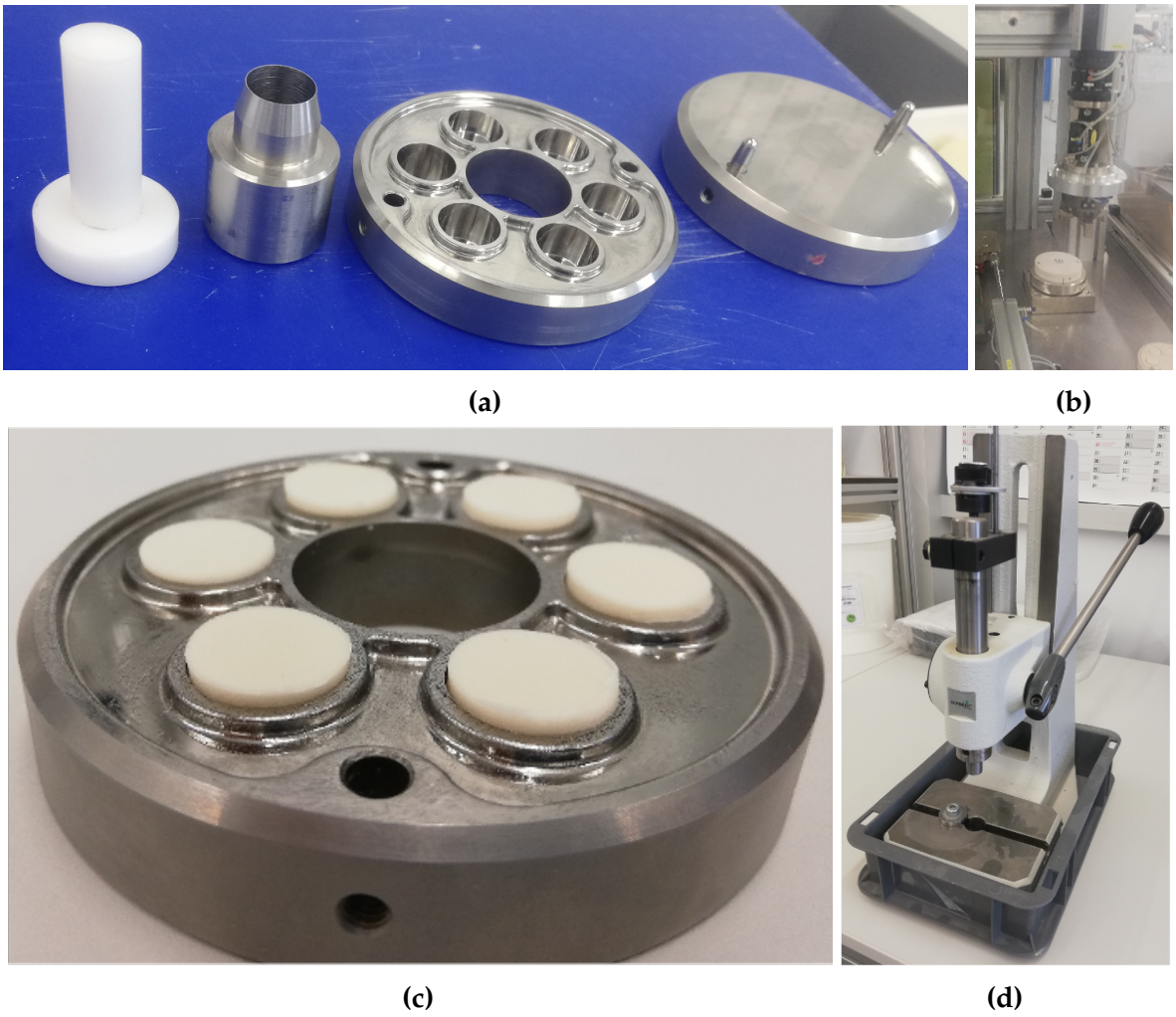

(a) **(b)**

(c) **(d)**

Figure 6.1: Fabrication process of the polymerized layered specimens. **a)** Molds used for the fabrication of the samples. **b)** Vibration blender. **c)** Over filled mold after the dentine layer is added. **d)** Hand press.

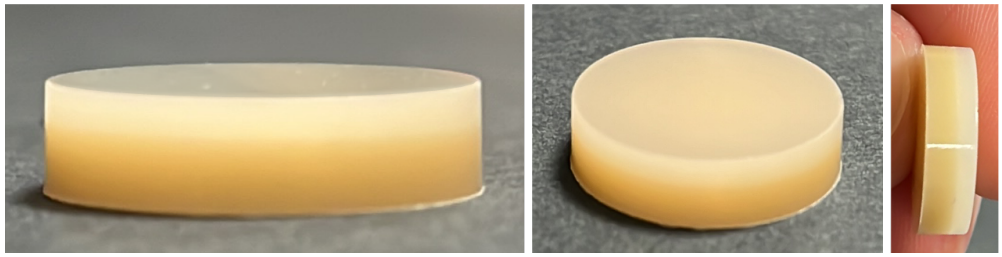

(a) **(b)** **(c)**

Figure 6.2: Example a stratified DRC layered system, viewed from different perspectives.

In order to obtain comparable results to those of the studies included in Chapters 4 and 5, the same dentine and enamel materials which were used for the production of the monolithic pellets were used for the fabrication of the stratified layered samples. Therefore, a total of 5 DRC stratified systems of VE, with increasing dentine lightness, were produced: VE-S1+EN1, VE-S2+EN1, VE-S3+EN2, VE-S4+EN2 and VE-S5+EN2, where S1 and S2 correspond to light shades, S3 and S4 correspond to intermediate shades and S5 correspond to a dark shade. Each system was composed of a total of 16 samples -divided into training and testing sets, as further discussed- with varying dentine and enamel thicknesses ranging from 0.5 mm to 2.5 mm.

6.2.2 Color measurements and evaluation of color differences

Similar to the other studies included in the present PhD Thesis, the spectral reflectance spectrum of the layered samples was measured with a spectroradiometer and the experimental set-up described in section 3.2.2. Consequently, the CIE-L*a*b* color coordinates were computed using the CIE 2° Standard Observer and D65 Standard Illuminant.

6.2.3 Computational method

Stratified samples were divided into training and testing groups to develop and evaluate the predictive methods, respectively. Measured reflectance curves and computed CIE-L*a*b* coordinates, corresponding to the samples included in the training set, were used to build the models, while those corresponding to samples of the testing set, were used exclusively for testing their accuracy.

According to the findings of the study presented in Chapter 4 and similarly to the study in Chapter 5, a training set of 9 samples arranged in a diamond-shaped

configuration was used, since it proved to be the optimal arrangement to achieve very good color estimations. Therefore, for the training set, 9 stratified layered samples with specific thicknesses according to that configuration, were used. However, due to manufacturing constraints, for the testing set only 7 samples, homogeneously distributed within testing set pre-defined limits, were used. The arrangement of stratified samples included in the training and testing sets is shown in figure 6.3.

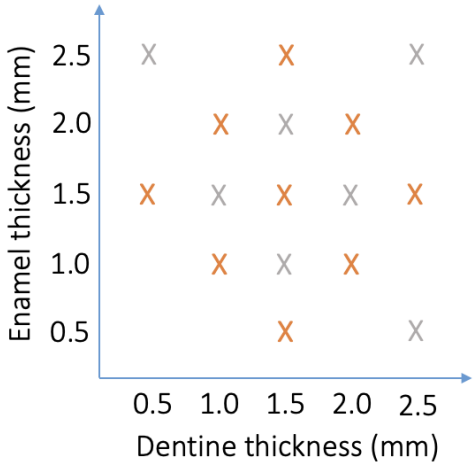

Figure 6.3: Arrangement of training (9-samples) and testing (7-samples) sets. Samples being included in the training set (orange) and testing set (gray).

As previously mentioned, the purpose of this study was to evaluate the performance of the predictive algorithms described in previous chapters of this Thesis, in a more realistic scenario, when stratified layered samples were used instead of stacked layered samples. Therefore, the previously developed PCA-based predictive algorithm described in Chapter 4 and the linear regression-based predictive algorithm described in Chapter 5 were used to estimate the spectral reflectance and CIE-L*a*b* chromaticity coordinates of the layered samples belonging to the testing set.

6.2.4 Evaluation of color differences

Similar to the studies presented in previous Chapters of this Thesis, RMSE (Eq. 3.2.4) and GFC (Eq. 3.2.5) spectral metrics were used to evaluate the performance of the PCA-based algorithms. Additionally, for both predictive models, color differences between measured and predicted values were computed using the CIEDE2000 (ΔE_{00}) total color difference formula [95], as shown in Equation 3.2.6. Consequently, ΔE_{00} values were comparatively evaluated with their corresponding 50:50% perceptibility (PT_{00}) and acceptability (AT_{00}) thresholds for dentistry: $PT_{00} = 0.8$ and $AT_{00} = 1.8$ [27,92,94].

6.3 Results and discussion

In this study, stratified layered samples were employed to test the performance of the prediction algorithms described in former chapters of this PhD Thesis.

The same dentine and enamel shades of VE DRC used for the production of the monolithic pellets in Chapters 4 and 5 were used for the fabrication of the stratified layered samples. A total of 5 DRC stratified layered systems, with different dentine lightness, were obtained: VE-S1+EN1, VE-S2+EN1, VE-S3+EN2, VE-S4+EN2 and VE-S5+EN2. For each DRC system, 9 samples, with specific thicknesses according to the diamond-shaped arrangement were fabricated in order to train the predictive models and 7 samples were fabricated in order to test the performance of the algorithms.

The PCA-based algorithm used to predict reflectance curves of stratified samples is the same as described in Chapter 4, which means that the reflectance spectral curves of the 7 samples belonging to the testing set were predicted using 3 Principal Components and second degree polynomial regression (as it was suggested in Section

4.2.3). From those estimated curves, CIE-L*a*b* color coordinates were computed as described above, and ΔE_{00} color differences between measured and computed values were calculated (Table 6.1). To evaluate the matching quality between measured and estimated reflectances, RMSE and GFC spectral performance metrics were computed and the results are presented in Table 6.2. The means and standard deviations of these performance metrics, as well as the percentage of samples that exhibit total color differences below the 50:50% AT_{00} and PT_{00} thresholds for the 5 DRC systems, are presented in Table 6.3.

Table 6.1: ΔE_{00} color differences between measured and predicted reflectance curves computed with the PCA-based algorithm, for the stratified layered samples tested in this study.

Test Thickness	**DRC Dentine-Enamel Systems**				
D(mm)+E(mm)	**VE S1-EN1**	**VE S2-EN1**	**VE S3-EN2**	**VE S4-EN2**	**VE S5-EN2**
2.5 + 2.5	0.45	0.26	1.15	0.74	0.96
0.5 + 2.5	0.97	0.78	0.59	1.41	0.75
1.5 + 2.0	1.50	0.54	0.43	0.61	0.97
2.0 + 1.5	0.83	0.34	0.43	0.54	0.39
1.0 + 1.5	0.73	0.12	1.37	0.90	0.22
1.5 + 1.0	1.00	0.30	0.44	0.91	1.02
2.5 + 0.5	0.49	0.21	1.19	1.25	1.39

Table 6.2: RMSE and GFC metrics between measured and predicted reflectance curves computed with the PCA-based algorithm, for the stratified layered samples tested in this study.

	DRC Dentine-Enamel Systems									
Test Thickness	**VE S1-EN1**		**VE S2-EN1**		**VE S3-EN2**		**VE S4-EN2**		**VE S5-EN2**	
D(mm)+E(mm)	**RMSE**	**GFC**	**RMSE**	**GFC**	**RMSE**	**GFC**	**RMSE**	**GFC**	**RMSE**	**GFC**
2.5 + 2.5	0.00896	0.99998	0.00239	0.99999	0.01759	0.99986	0.0118	0.9999	0.0101	0.9999
0.5 + 2.5	0.01684	0.99995	0.01025	0.99995	0.00300	0.99997	0.0211	0.9999	0.0079	1.0000
1.5 + 2.0	0.01120	0.99969	0.00443	0.99996	0.00290	0.99998	0.0060	0.9999	0.0118	0.9999
2.0 + 1.5	0.01208	0.99984	0.00485	0.99999	0.00646	0.99999	0.0046	1.0000	0.0053	1.0000
1.0 + 1.5	0.00536	0.99994	0.00202	1.00000	0.02261	0.99999	0.0117	1.0000	0.0024	1.0000
1.5 + 1.0	0.00747	0.99987	0.00489	1.00000	0.00508	0.99998	0.0110	1.0000	0.0110	0.9998
2.5 + 0.5	0.01338	0.99998	0.00289	0.99999	0.01075	0.99976	0.0174	1.0000	0.0138	0.9998

Table 6.3: Statistics of error metrics for the results obtained when the PCA-based algorithm is used for stratified layered samples.

Layers	Variable	Mean	SD	$< AT_{00}(\%)$	$< PT_{00}(\%)$
VE S1 - EN1	**RMSE**	0.01076	0.00385		
	GFC	0.99989	0.00010		
	ΔL*	0.47	0.36		
	Δa*	0.14	0.13		
	Δb*	0.72	0.63		
	ΔE_{00}	0.85	0.36	100	42.85
VE S2 - EN1	**RMSE**	0.00453	0.00278		
	GFC	0.99998	0.00002		
	ΔL*	0.29	0.18		
	Δa*	0.12	0.11		
	Δb*	0.22	0.19		
	ΔE_{00}	0.36	0.22	100	100
VE S3 - EN2	**RMSE**	0.00977	0.00767		
	GFC	0.99993	0.00009		
	ΔL*	0.62	0.61		
	Δa*	0.11	0.09		
	Δb*	0.71	0.55		
	ΔE_{00}	0.80	0.42	100	57.14
VE S4 - EN2	**RMSE**	0.01194	0.00583		
	GFC	0.99995	0.00003		
	ΔL*	0.80	0.59		
	Δa*	0.29	0.11		
	Δb*	0.46	0.34		
	ΔE_{00}	0.91	0.32	100	42.85
VE S5 - EN2	**RMSE**	0.00888	0.00398		
	GFC	0.99991	0.00009		
	ΔL*	0.70	0.34		
	Δa*	0.12	0.09		
	Δb*	0.71	0.48		
	ΔE_{00}	0.82	0.40	100	42.85

For performance evaluation of the linear regression-based prediction algorithm presented in Chapter 5, the CIE-L*, CIE-a* and CIE-b* color coordinates of the test samples of each stratified DRC system were predicted according to the methodology described in section 5.2.3. Besides, ΔE_{00} color differences between measured and estimated values were calculated (Table 6.4). The means and standard deviations, as well as the percentage of samples with color differences between measured and predicted values lower than 50:50% AT_{00} and PT_{00}, are presented in Table 6.5.

Table 6.4: ΔE_{00} color differences between measured and predicted CIE-L*a*b* values computed with the linear regression-based algorithm, for the stratified layered samples tested in this study.

Test Thickness	DRC Dentine-Enamel Systems				
D(mm)+E(mm)	VE S1-EN1	VE S2-EN1	VE S3-EN2	VE S4-EN2	VE S5-EN2
2.5 + 2.5	0.53	0.40	1.32	0.94	1.20
0.5 + 2.5	0.92	0.92	0.42	1.55	0.61
1.5 + 2.0	1.47	0.54	0.44	0.63	0.97
2.0 + 1.5	0.83	0.38	0.48	0.51	0.37
1.0 + 1.5	0.68	0.10	1.34	0.82	0.19
1.5 + 1.0	0.97	0.27	0.49	0.85	1.04
2.5 + 0.5	0.67	0.16	1.06	1.18	1.17

Table 6.5: Statistics of error metrics for the results obtained when the linear regression-based algorithm is used for stratified layered samples.

Layers	Variable	Mean	SD	$< AT_{00}(\%)$	$< PT_{00}(\%)$
VE S1 - EN1	**ΔL***	0.49	0.36		
	Δa*	0.14	0.14		
	Δb*	0.75	0.60		
	ΔE_{00}	0.87	0.31	100	42.85
VE S2 - EN1	**ΔL***	0.28	0.22		
	Δa*	0.07	0.11		
	Δb*	0.32	0.26		
	ΔE_{00}	0.40	0.27	100	85.71
VE S3 - EN2	**ΔL***	0.63	0.59		
	Δa*	0.12	0.12		
	Δb*	0.69	0.50		
	ΔE_{00}	0.79	0.43	100	57.14
VE S4 - EN2	**ΔL***	0.80	0.58		
	Δa*	0.26	0.14		
	Δb*	0.57	0.29		
	ΔE_{00}	0.93	0.35	100	28.57
VE S5 - EN2	**ΔL***	0.70	0.34		
	Δa*	0.16	0.14		
	Δb*	0.61	0.41		
	ΔE_{00}	0.79	0.40	100	42.85

As it can be observed in Table 6.2, very good spectral matches were found between measured and predicted reflectance curves, with very low RMSE values (around 2%) and a $GFC \geq 0.9999$ in all cases. RMSE and GFC values at this range have previously been reported as indicators of a high-quality fit [168]. When analyzing the color differences between measured and predicted values (Table 6.3), all ΔE_{00}

values were below the AT_{00}, which highlights once again the very good results obtained for reflectance and color estimation of stratified layered samples with the proposed method. Similar to the case of stacked layered samples (Table 4.13), the color differences were mostly introduced by variations of the CIE-L* and CIE-b* color coordinates, rather than the CIE-a* coordinate, what can be justified due to the shape of the dental color space, with a narrower range for the a* coordinate (a* = -1.5 - 12.6) as compared to the other two coordinates (L* = 51.5 - 85.5 and b* = 12.0 - 43.3) [63]. Therefore, based on the findings of the present study, the first research hypothesis was accepted since the reflectance spectrum of stratified layered samples can be successfully predicted using the PCA-based proposed algorithm.

Regarding the results obtained for stratified layered samples when the linear regression-based algorithm proposed in Chapter 5 was used to predict the color data, the color differences obtained between measured and predicted values were low in almost all cases (Table 6.4). These very good outcomes are also confirmed by the fact that 100% of the color differences between measured and predicted CIE-L*a*b* color coordinates were below the 50:50% AT_{00} and, in some cases (as for VE-S2+EN1), as much as 85% of the color differences were lower than the 50:50% PT_{00} (Table 6.5). Therefore, the second research hypothesis of this study was also accepted, as it seems clear that linear regression-based prediction algorithms can be used to estimate the CIE-L*a*b* color coordinates of stratified layered dental samples with satisfactory results.

It is true that both algorithms tested in this study perform in a satisfactory manner, since color differences below the acceptability threshold were always obtained for both stacked and stratified layered samples. However, comparing the results obtained for stacked layered samples presented in Tables 4.13 and 5.7 with the ones obtained for stratified layered samples presented in Tables 6.3 and 6.5, a slight decrease in

performance can be observed, especially when analyzing the mean ΔE_{00} color differences and the percentage of color differences below the PT_{00}. For example, for stacked layered samples, mean ΔE_{00} values of roughly 0.5 and 0.4 color units were found for the PCA-based and the linear regression-based algorithms, respectively. However, when polymerized layered samples were used, these values increased to roughly 0.85 color difference units for both algorithms. Also, while, for stacked layered samples, the lowest found percentages of color differences below the PT_{00} were 81.25% and 87.5%, for the PCA-based and the linear regression-based algorithms, respectively, these percentages dropped to 42.82% and 28.57% for the case of stratified layered samples.

By looking at the percentages it seems that the algorithms perform slightly better for stacked samples. However, it is important to consider that, except for very few isolated cases where ΔE_{00} values of roughly 1.5 color difference units were found, the majority of the ΔE_{00} color difference values presented in Tables 6.3 and 6.5 were around the limit of PT_{00} with ΔE_{00} values of roughly 1.0 color difference units. Besides, even very small ΔE_{00} values were obtained for some dentine-enamel combinations, such as $\Delta E_{00} = 0.12$ and $\Delta E_{00} = 0.10$, obtained for the stratified layered sample of D(1.0 mm)+E(1.5 mm) of the VE S2-EN1 system, as can be observed in Tables 6.1 and 6.4, respectively. Therefore, from the results presented above, it can be stated that the fuzzy transition present at the interface between dentine and enamel layers, which was the main concern of the present study, does not seem to negatively affect the predictive capability of the proposed algorithms, since very good color difference values between measured and predicted data were obtained in several cases.

Overall, both algorithms perform in a very similar way with both stacked and stratified layered samples. The differences found between the different studies pre-

sented in this PhD Thesis are not probably attributable to the algorithms themselves, which have proven to be valid for most of the samples tested in the study, and also outperform the results obtained in other studies related to color prediction in dentistry [59, 60, 101, 135, 138, 139, 141, 178–180]. It is very likely that the differences found between the results obtained with stacked and stratified samples to be introduced by other factors that cannot be controlled (non-modelable factors) which are affecting the performance to some extent. For example, it can be mentioned the difficulty to precisely control or measure the thickness of the dentine and enamel layers for stratified layered samples, different to the case of the stacked layered samples, whose monolithic pellets thicknesses were directly measured with a precision caliper. Also, errors derived from the measuring device itself or the reproducibility of the experimental method might impact the outcomes of the predictive methods.

It is clear that each of the proposed algorithms have pros and cons, and therefore, one or the other could be used for color prediction according to the purpose for which the color needs to be predicted. Initially, an algorithm that is able to estimate the reflectance curve of any object is more versatile than other which can only estimate color coordinates. In this sense, complete spectral data can provide information on the consistency of the material and therefore can detect potential problems of metamerism. Knowing the reflectance spectrum of an object also allows the calculation of colorimetric data for each lightning source expected to illuminate the specimen. Another advantage of dealing with complete reflectance spectra is that the Kubelka-Munk theory can be applied for the study of the optical properties of the materials, as has been already used in many research studies in the dental field [53, 84, 161, 164, 167] and therefore, light-material interactions could be also studied. These aspects of a prediction algorithm could be of great interest to dental materials experts and companies. However, there are many other applications, and

especially in clinical settings, where complex data such as reflectance spectra is not easily obtained and, therefore, the prediction of CIE-L*a*b* values could be more convenient and more straightforward for dentists and dental technicians to apply and interpret.

We have seen many different approaches attempting to solve the problem of color prediction in dentistry and it is clear that there is still a long way to go. However, the studies presented in this PhD Thesis open the door to future lines of research that could include the development of new predictive algorithms for more than two-layers dental materials and also the prediction of reflectance and color of complete prosthetic teeth.

CHAPTER

7

CONCLUSIONS

1. The PCA-based algorithm proposed in this PhD Thesis can be used for reflectance estimation of flat monolithic samples of dental ceramics and dental resin composites, of different thicknesses and shades without compromising its performance. The final color of monolithic samples can be estimated at color differences below the acceptability threshold, and in most cases also below the perceptibility threshold.

2. The use of 3 principal components and second degree polynomial was proved to be the best configuration for PCA-based spectral reconstruction. In order to achieve better accuracy in the prediction of the reflectance and color of the monolithic materials, the use of a training set that includes both thicker and thinner samples than those to be predicted (interpolation approach - test samples within the limits of the training set) has to be considered.

3. The PCA-based algorithm can be used for the estimation of the reflectance spectrum and color coordinates of stacked layered samples of dental resin composites of different thicknesses and shades. With a training set of 5-samples in a X-shaped arrangement, color differences between measured and estimated reflectances below the acceptability threshold are generally obtained. However, a training set which includes 9 samples in a diamond-shaped arrangement has proven to be the optimal strategy, since color differences between estimated and measured reflectances are always below the acceptability threshold, and in most cases also below the perceptibility threshold.

4. The performance of the PCA-based predictive algorithm proposed for stacked layered samples is dependent to some extent on the materials used but, within a group of samples manufactured using the same material, it is independent of sample shade.

5. Linear Regression Models can be satisfactorily used for CIE-L*a*b* color coordinates estimation of monolithic and stacked layered dental resin-based composites under different illuminations.

6. The linear regression-based algorithms for CIE-L*a*b* color coordinates estimation are intended for scenarios where spectral measurements are not available. Similar performance metrics to those of more complex algorithms are obtained, with color differences below the acceptability threshold, and generally below the perceptibility threshold.

7. Satisfactory results are also obtained when the PCA-based and linear regression-based algorithms proposed in this PhD Thesis are applied to stratified layered samples of different thicknesses and shades. Although slight differences are observed between the two types of samples evaluated (stacked and stratified), the registered color differences between measured and predicted reflectances were always below the acceptability threshold.

8. Overall, the results in the studies presented in this PhD Thesis demonstrate that the predictive methods proposed can be used to model and predict the reflectance and colorimetric properties of monolithic and layered (stacked and stratified) translucent biomaterials. This could help to custom design dental materials with multiple clinical and industrial applications, such as the fabrication of dental shade guides, the development of new dental materials and, finally, achieving dental restorations that perfectly match the color of the surrounding dental structures. However, future research is needed, where flat samples including more than two layers or tooth shaped samples with different geometries than a flat surface should be included. Also, future studies can be carried out for the development of algorithms capable of identifying optimal combinations of materials and thicknesses in order to achieve a desired color.

CHAPTER

7

CONCLUSIONES

1. El algoritmo basado en ACP propuesto en esta Tesis Doctoral puede utilizarse para la estimación de la reflectancia de muestras monolíticas planas de cerámica y resinas composite, de diferentes espesores y colores sin comprometer su rendimiento. El color final de las muestras monolíticas puede estimarse con diferencias de color por debajo del umbral de aceptabilidad, y en la mayoría de los casos también por debajo del umbral de perceptibilidad.

2. El uso de 3 componentes principales y un polinomio de segundo grado resultó ser la mejor configuración para la reconstrucción espectral basada en ACP. Para lograr una mayor precisión en la predicción de la reflectancia y el color de los materiales monolíticos, hay que considerar el uso de un conjunto de entrenamiento (test) que incluya muestras tanto más gruesas como más finas que las que se van a predecir (estrategia de interpolación - muestras de prueba dentro de los límites del conjunto de entrenamiento).

3. El algoritmo basado en ACP puede utilizarse para la estimación de la reflectancia espectral y las coordenadas de color de muestras de resina de composite superpuestas de diferentes espesores y tonos. Con un conjunto de entrenamiento de 5 muestras en forma de X, generalmente se obtienen diferencias de color entre las reflectancias medidas y estimadas por debajo del umbral de aceptabilidad. Sin embargo, un conjunto de entrenamiento que incluya 9 muestras, en una disposición en forma de diamante, ha demostrado ser la estrategia óptima, ya que las diferencias de color entre las reflectancias estimadas y las medidas están siempre por debajo del umbral de aceptabilidad y, en la mayoría de los casos, también por debajo del umbral de perceptibilidad.

4. El rendimiento del algoritmo de predicción basado en ACP que se propone para las muestras superpuestas depende en cierta medida del material, pero, dentro de un grupo de muestras fabricadas con el mismo material, es independiente del

color de la muestra.

5. Se han utilizado modelos de regresión lineal para estimar con precisión las coordenadas de color CIE-L*a*b* de muestras de resina de composite tanto monolíticas como bicapa superpuestas y bajo diferentes iluminaciones.

6. Los algoritmos basados en regresión lineal diseñados para las estimar las coordenadas de color CIE-L*a*b* están pensados para escenarios en los que no se dispone de medidas de reflectancia espectral. Con estos algoritmos se han obtenido métricas de rendimiento similares a las de algoritmos más complejos, con diferencias de color por debajo del umbral de aceptabilidad, y generalmente por debajo del umbral de perceptibilidad.

7. También se obtienen resultados satisfactorios cuando los algoritmos basados en ACP y en regresión lineal, propuestos en esta Tesis Doctoral, se aplican a muestras bicapa estratificadas de diferentes espesores y tonos. Aunque se observan ligeras diferencias en el rendimiento entre los dos tipos de muestras evaluadas (superpuestas y estratificadas), las diferencias de color encontradas entre las reflectancias medidas y estimadas estuvieron siempre por debajo del umbral de aceptabilidad.

8. En general, los resultados de los estudios presentados en esta Tesis Doctoral demuestran que los métodos predictivos propuestos pueden utilizarse para modelar y predecir la reflectancia espectral y las propiedades colorimétricas de biomateriales translúcidos monolíticos y bicapa (superpuestos y estratificados). Esto podría ayudar a personalizar el diseño de materiales dentales con múltiples aplicaciones clínicas e industriales, como la fabricación de guías de color dentales, el desarrollo de nuevos materiales y, finalmente, conseguir restauraciones que se ajusten perfectamente al color de las estructuras dentales colindantes. Sin embargo, es necesario realizar investigaciones futuras en las que se consideren muestras planas que incluyan más de dos capas o muestras con forma de diente con geometrías diferentes a la de una

superficie plana. Además, se pueden realizar estudios futuros para el desarrollo de algoritmos capaces de identificar combinaciones óptimas de materiales y espesores para conseguir un color deseado.

BIBLIOGRAPHY

[1] A. Della Bona, *Color and appearance in dentistry*. Springer, 2020.

[2] D. Dietschi, S. Ardu, and I. Krejci, "A new shading concept based on natural tooth color applied to direct composite restorations.," *Quintessence. Int.*, vol. 37, no. 2, pp. 91–102, 2006.

[3] A. Baltzer and V. Kaufmann-Jinoian, "The determination of the tooth colors," *Quintessenz Zahntech*, vol. 30, no. 7, pp. 726–740, 2004.

[4] A. Della Bona, O. E. Pecho, R. Ghinea, J. C. Cardona, and M. M. Pérez, "Colour parameters and shade correspondence of cad–cam ceramic systems," *J Dent*, vol. 43, no. 6, pp. 726–734, 2015.

[5] D. Mostafa, M. Taymor, and R. Mohammed, "Effect of resin cement shades & thickness of zirconia reinforced lithium silicate ceramics (vita suprinity) on the

optical properties using dark background compared to lithium disilicate glass ceramics (an in vitro study)," 2019.

[6] D. Sliney, "What is light? the visible spectrum and beyond," *Eye*, vol. 30, no. 2, pp. 222–229, 2016.

[7] R. B. Lotto and D. Purves, "The empirical basis of color perception," *Consciousness and Cognition*, vol. 11, no. 4, pp. 609–629, 2002.

[8] R. Shapley and M. Hawken, "Neural mechanisms for color perception in the primary visual cortex," *Current opinion in neurobiology*, vol. 12, no. 4, pp. 426–432, 2002.

[9] J. Schanda, *Colorimetry: understanding the CIE system*. John Wiley & Sons, 2007.

[10] A. Gilchrist and J. Nobbs, "Colorimetry, theory," *Encyclopedia of spectroscopy and spectrometry*, pp. 328–333, 1999.

[11] S. Jost, M. Ngo, A. Ferrero, T. Poikonen, T. Pulli, A. Thorseth, and P. Blattner, "Determination of illuminants representing typical white light emitting diodes sources," in *CIE Midterm Meeting 2017*, pp. 427–432, CIE-International Commission on Illumination, 2017.

[12] C. I. de l'Eclairage, *CIE Technical Report 015: 2018:* Colorimetry*. Commission Internationale de L'Eclairage, 2018.

[13] M. Melgosa, J. Ruiz-López, C. Li, P. A. García, A. Della Bona, and M. M. Pérez, "Color inconstancy of natural teeth measured under white light-emitting diode illuminants," *Dent Mat*, 2020.

[14] N. Corcodel, S. Helling, P. Rammelsberg, and A. J. Hassel, "Metameric effect between natural teeth and the shade tabs of a shade guide," *Eur J Oral Sci*, vol. 118, no. 3, pp. 311–316, 2010.

[15] F. Pérez-Ocón, E. Hita, L. Jiménez del Barco, and J. Nieves, "Contribution to the experimental review of the colorimetric standard observer," *Color Research & Application*, vol. 24, no. 5, pp. 377–388, 1999.

[16] O. Estévez, "A better colorimetric standard observer for color-vision studies: The stiles and burch 2° color-matching functions," *Color Research & Application*, vol. 7, no. 2, pp. 131–134, 1982.

[17] "CIE Technical Report: colorimetry.," tech. rep., Vienna, Austria: CIE Central Bureau;, 2004. CIE Pub No.15.3.

[18] J. A. Kieser, *Human adult odontometrics: the study of variation in adult tooth size*. No. 4, Cambridge University Press, 1990.

[19] J. M. Doris, B. W. Bernard, and M. M. Kuftinec, "A biometric study of tooth size and dental crowding," *American journal of orthodontics*, vol. 79, no. 3, pp. 326–336, 1981.

[20] M. D. Fairchild, *Color appearance models*. John Wiley & Sons, 2013.

[21] W. M. Johnston, "Color measurement in dentistry," *Journal of dentistry*, vol. 37, pp. e2–e6, 2009.

[22] S. A. Burns, J. B. Cohen, and E. N. Kuznetsov, "The munsell color system in fundamental color space," *Color research & application*, vol. 15, no. 1, pp. 29–51, 1990.

[23] R. A. Crone, *A history of color: the evolution of theories of light and color*. Springer Science & Business Media, 2012.

[24] M. R. Luo and B. Rigg, "Chromaticity-discrimination ellipses for surface colours," *Color Research & Application*, vol. 11, no. 1, pp. 25–42, 1986.

[25] A. Joiner, "Tooth colour: a review of the literature," *Journal of dentistry*, vol. 32, pp. 3–12, 2004.

[26] R. D. Paravina, A. Aleksić, R. N. Tango, A. García-Beltrán, W. M. Johnston, and R. I. Ghinea, "Harmonization of color measurements in dentistry," *Measurement*, vol. 169, p. 108504, 2021.

[27] R. D. Paravina, M. M. Pérez, and R. Ghinea, "Acceptability and perceptibility thresholds in dentistry: a comprehensive review of clinical and research applications," *J Esthet Restor Dent*, vol. 31, no. 2, pp. 103–112, 2019.

[28] R. G. Kuehni, "Color-tolerance data and the tentative cie 1976 l* a* b* formula," *JOSA*, vol. 66, no. 5, pp. 497–500, 1976.

[29] F. J. Clarke, R. McDonald, and B. Rigg, "Modification to the jpc79 colour–difference formula," *Journal of the Society of Dyers and Colourists*, vol. 100, no. 4, pp. 128–132, 1984.

[30] M. R. Luo and B. Rigg, "Bfd (l: c) colour-difference formula part 1ndashdevelopment of the formula," *Journal of the Society of Dyers and Colourists*, vol. 103, no. 2, pp. 86–94, 1987.

[31] R. McDonald and K. J. Smith, "Cie94-a new colour-difference formula," *Journal of the Society of Dyers and Colourists*, vol. 111, no. 12, pp. 376–379, 1995.

[32] M. R. Luo, G. Cui, and B. Rigg, "The development of the cie 2000 colour-difference formula: Ciede2000," *Color Research & Application: Endorsed by Inter-Society Color Council, The Colour Group (Great Britain), Canadian Society for Color, Color Science Association of Japan, Dutch Society for the Study of Color, The Swedish Colour Centre Foundation, Colour Society of Australia, Centre Français de la Couleur*, vol. 26, no. 5, pp. 340–350, 2001.

[33] J. Kristiansen, M. Sakai, J. D. Da Silva, M. Gil, and S. Ishikawa-Nagai, "Assessment of a prototype computer colour matching system to reproduce natural tooth colour on ceramic restorations," *J. Dent.*, vol. 39, pp. e45–e51, 2011.

[34] E. Matalová, V. Lungová, and P. Sharpe, "Development of tooth and associated structures," in *Stem cell biology and tissue engineering in dental sciences*, pp. 335–346, Elsevier, 2015.

[35] A. V. Ritter, *Sturdevant's art & science of operative dentistry-e-book*. Elsevier Health Sciences, 2017.

[36] B.-B. M. F. MJ, "Illustrated dental embryology, histology and anatomy," *St. Louse: Elsevier*, 2010.

[37] R. Llamas Cadaval and A. Villa Vigil, "Biología de la pulpa y de los tejidos periapicales. endodoncia: Técnicas clínicas y bases científicas," 2014.

[38] M. J. Barron, S. T. McDonnell, I. MacKie, and M. J. Dixon, "Hereditary dentine disorders: dentinogenesis imperfecta and dentine dysplasia," *Orphanet journal of rare diseases*, vol. 3, no. 1, pp. 1–10, 2008.

[39] W. Pawlina and M. H. Ross, *Histology: a text and atlas: with correlated cell and molecular biology*. Lippincott Williams & Wilkins, 2018.

[40] B. Touati, P. Miara, D. Nathanson, R. Giordano, and S. L. B. Martins, *Odontología estética y restauraciones cerámicas*. Masson, 2000.

[41] A. Vichi, M. Ferrari, and C. L. Davidson, "Color and opacity variations in three different resin-based composite products after water aging," *Dental Materials*, vol. 20, no. 6, pp. 530–534, 2004.

[42] S. Park, D. H. Wang, D. Zhang, E. Romberg, and D. Arola, "Mechanical properties of human enamel as a function of age and location in the tooth," *Journal of Materials Science: Materials in Medicine*, vol. 19, no. 6, pp. 2317–2324, 2008.

[43] M. Staines, W. Robinson, and J. Hood, "Spherical indentation of tooth enamel," *Journal of materials science*, vol. 16, no. 9, pp. 2551–2556, 1981.

[44] K. R. de Sousa, M. J. Batista, J. R. Gonçalves, and M. d. L. R. de Sousa, "Extrinsic tooth enamel color changes and their relationship with the quality of water consumed," *International Journal of Environmental Research and Public Health*, vol. 9, no. 10, pp. 3530–3539, 2012.

[45] T. Shiraishi and I. Watanabe, "Thickness dependence of light transmittance, translucency and opalescence of a ceria-stabilized zirconia/alumina nanocomposite for dental applications," *Dent Mater*, vol. 32, no. 5, pp. 660–667, 2016.

[46] C. dos Santos, G. O. Rosa, M. N. Quintino, M. F. R. P. Alves, S. Ribeiro, and C. L. Melo-Silva, "Effect of surface finishing and thickness on the translucency of zirconia dental ceramics," *Ceram Int*, vol. 46, no. 6, pp. 7748–7755, 2020.

[47] G. Corciolani, A. Vichi, C. Louca, and M. Ferrari, "Influence of layering thickness on the color parameters of a ceramic system," *Dent. Mater.*, vol. 26, no. 8, pp. 737–742, 2010.

[48] A. Vichi, A. Fraioli, C. L. Davidson, and M. Ferrari, "Influence of thickness on color in multi-layering technique," *Dent. Mater.*, vol. 23, no. 12, pp. 1584–1589, 2007.

[49] Y.-K. Lee, "Translucency of human teeth and dental restorative materials and its clinical relevance," *Journal of Biomedical Optics*, vol. 20, no. 4, p. 045002, 2015.

[50] K. Erdelt, M. L. P. D. Engler, F. Beuer, J.-F. Güth, A. Liebermann, and J. Schweiger, "Computable translucency as a function of thickness in a multi-layered zirconia," *J Prosthet Dent*, vol. 121, no. 4, pp. 683–689, 2019.

[51] H.-K. Kim, S.-H. Kim, J.-B. Lee, J.-S. Han, I.-S. Yeo, and S.-R. Ha, "Effect of the amount of thickness reduction on color and translucency of dental monolithic zirconia ceramics," *J Adv Prosthodont*, vol. 8, no. 1, pp. 37–42, 2016.

[52] Y. Shao and F. G. Shi, "Exploring the critical thickness for maximum reflectance of optical reflectors based on polymer-filler composites," *Opt Mater Express*, vol. 6, no. 4, pp. 1106–1113, 2016.

[53] C. Lucena, J. Ruiz-López, R. Pulgar, A. Della Bona, and M. M. Pérez, "Optical behavior of one-shaded resin-based composites," *Dent Mater*, 2021.

[54] A. Joiner and W. Luo, "Tooth colour and whiteness: A review," *Journal of dentistry*, vol. 67, pp. S3–S10, 2017.

[55] A. R. Tuncdemir, S. Polat, C. Ozturk, M. T. Tuncdemir, and A. Y. Gungor, "Color differences between maxillar and mandibular incisors," *European Journal of General Dentistry*, vol. 1, no. 03, pp. 170–173, 2012.

[56] Y. Zhao and J. Zhu, "In vivo color measurement of 410 maxillary anterior teeth.," *The Chinese journal of dental research: the official journal of the Scientific Section of the Chinese Stomatological Association (CSA)*, vol. 1, no. 3, pp. 49–51, 1998.

[57] L. Odioso, R. Gibb, and R. Gerlach, "Impact of demographic, behavioral, and dental care utilization parameters on tooth color and personal satisfaction.," *Compendium of continuing education in dentistry.(Jamesburg, NJ: 1995). Supplement*, no. 29, pp. S35–41, 2000.

[58] T. A. Esan, A. O. Olusile, P. A. Akeredolu, *et al.*, "Factors influencing tooth shade selection for completely edentulous patients," *J Contemp Dent Pract*, vol. 7, no. 5, pp. 80–7, 2006.

[59] D. Gozalo-Diaz, W. M. Johnston, and A. G. Wee, "Estimating the color of maxillary central incisors based on age and gender," *The Journal of prosthetic dentistry*, vol. 100, no. 2, pp. 93–98, 2008.

[60] C. Gómez-Polo, J. Montero, M. Gómez-Polo, J. A. M. V. de Parga, and A. Celemin-Viñuela, "Natural tooth color estimation based on age and gender," *Journal of Prosthodontics*, vol. 26, no. 2, pp. 107–114, 2015.

[61] C. G. Polo, M. G. Polo, J. Montero, J. A. M. V. De Parga, and A. C. Viñuela, "Correlation of natural tooth colour with aging in the spanish population," *International Dental Journal*, vol. 65, no. 5, pp. 227–234, 2015.

[62] V. Sharma, V. Punia, M. Khandelwal, S. Punia, and R. Lakshmana, "A study of relationship between skin color and tooth shade value in population of udaipur, rajasthan," *International Journal of Dental Clinics*, vol. 2, no. 4, pp. 26–29, 2010.

[63] C. Gómez-Polo, M. P. Muñoz, M. C. L. Luengo, P. Vicente, P. Galindo, and A. M. M. Casado, "Comparison of two color-difference formulas using the bland-altman approach based on natural tooth color space," *The Journal of prosthetic dentistry*, vol. 115, no. 4, pp. 482–488, 2016.

[64] J. C.-C. Yuan, J. D. Brewer, E. A. Monaco Jr, and E. L. Davis, "Defining a natural tooth color space based on a 3-dimensional shade system," *The Journal of prosthetic dentistry*, vol. 98, no. 2, pp. 110–119, 2007.

[65] O. E. Pecho, R. Ghinea, R. Alessandretti, M. M. Pérez, and A. Della Bona, "Visual and instrumental shade matching using cielab and ciede2000 color difference formulas," *Dent Mater*, vol. 32, no. 1, pp. 82–92, 2016.

[66] Z. Velinov, M. Papas, D. Bradley, P. Gotardo, P. Mirdehghan, S. Marschner, J. Novák, and T. Beeler, "Appearance capture and modeling of human teeth," *ACM Transactions on Graphics (ToG)*, vol. 37, no. 6, pp. 1–13, 2018.

[67] J. Brandt, S. Nelson, H.-C. Lauer, U. von Hehn, and S. Brandt, "In vivo study for tooth colour determination—visual versus digital," *Clin Oral Invest*, vol. 21, no. 9, pp. 2863–2871, 2017.

[68] S. J. Chu, R. D. Trushkowsky, and R. D. Paravina, "Dental color matching instruments and systems. Review of clinical and research aspects," *J Dent*, vol. 38, pp. e2–e16, 2010.

[69] A. Della Bona, A. A. Barrett, V. Rosa, and C. Pinzetta, "Visual and instrumental agreement in dental shade selection: three distinct observer populations and shade matching protocols," *dental materials*, vol. 25, no. 2, pp. 276–281, 2009.

[70] C. S. Sampaio, J. Gurrea, M. Gurrea, A. Bruguera, P. J. Atria, M. Janal, E. A. Bonfante, P. G. Coelho, and R. Hirata, "Dental shade guide variability for hues b, c, and d using cross-polarized photography," *Int J Periodontics Restor Dent*, vol. 38, pp. 113–8, 2018.

[71] M. M. Pérez, A. Della Bona, F. Carrillo-Perez, D. Dudea, O. Pecho, and L. Herrera, "Does background color influence visual thresholds?," *J Dent*, vol. 102, 09 2020.

[72] D. Dudea, C. Gasparik, A. Botos, F. Alb, A. Irimie, and R. D. Paravina, "Influence of background/surrounding area on accuracy of visual color matching," *Clin oral Invest*, vol. 20, no. 6, pp. 1167–1173, 2016.

[73] M. Nakhaei, J. Ghanbarzadeh, S. Keyvanloo, S. Alavi, and H. Jafarzadeh, "Shade matching performance of dental students with three various lighting conditions," *J Contemp Dent Pract*, vol. 14, no. 1, p. 100, 2013.

[74] O. E. Pecho, R. Ghinea, M. M. Perez, and A. Della Bona, "Influence of gender on visual shade matching in dentistry," *J Esthet Restor Dent*, vol. 29, no. 2, pp. E15–E23, 2017.

[75] M. Miranda, "Effect of gender, experience, and value on color perception," *Oper Dent*, vol. 37, no. 3, pp. 228–233, 2012.

[76] J. Blaes, "Today's technology improves the shade-matching problems of yesterday.," *Journal (Indiana Dental Association)*, vol. 81, no. 4, pp. 17–19, 2002.

[77] F. Tabatabaian, E. Beyabanaki, P. Alirezaei, and S. Epakchi, "Visual and digital tooth shade selection methods, related effective factors and conditions, and

their accuracy and precision: A literature review," *J. Esthet, Restor. Dent.*, vol. 33, no. 8, pp. 1084–1104, 2021.

[78] S. ISHIKAWA-NAGAI, A. Yoshida, J. D. Da Silva, and L. Miller, "Spectrophotometric analysis of tooth color reproduction on anterior all-ceramic crowns: Part 1: analysis and interpretation of tooth color," *J. Esthet. Restor. Dent.*, vol. 22, no. 1, pp. 42–52, 2010.

[79] A. G. Wee, D. T. Lindsey, S. Kuo, and W. M. Johnston, "Color accuracy of commercial digital cameras for use in dentistry," *Dent. Mater.*, vol. 22, no. 6, pp. 553–559, 2006.

[80] A. Caglar, K. Yamanel, K. Gulsahi, B. Bagis, and M. Özcan, "Could digital imaging be an alternative for digital colorimeters?," *Clin. Oral Investig.*, vol. 14, no. 6, pp. 713–718, 2010.

[81] M. A. Akl, C. P. C. Sim, M. E. Nunn, L. L. Zeng, T. A. Hamza, and A. G. Wee, "Validation of two clinical color measuring instruments for use in dental research," *Journal of Dentistry*, vol. 125, p. 104223, 2022.

[82] M. M. Pérez, C. Benavides-Reyes, M. Tejada-Casado, J. Ruiz-López, and C. Lucena, "Does backgrounds color influence the appearance of gingiva-colored resin-based composites?," *Materials*, vol. 15, no. 10, p. 3712, 2022.

[83] J. Ruiz-López, C. Espinar, C. Lucena, J. de la Cruz Cardona, R. Pulgar, and M. M. Pérez, "Effect of thickness on color and translucency of a multi-color polymer-infiltrated ceramic-network material," *J. Esthet. Restor. Dent.*, 2022.

[84] O. E. Pecho, R. Ghinea, A. M. Ionescu, J. C. Cardona, A. Della Bona, and M. M. Pérez, "Optical behavior of dental zirconia and dentin analyzed by kubelka-munk theory," *Dent. Mater.*, vol. 31, no. 1, pp. 60–67, 2015.

[85] R. I. Ghinea, "Evaluation of the ciede2000 (kl:kc:kh) color difference metrics and development of color prediction algorithms: application to dental materials," 2014.

[86] F. W. Billmeyer, "Comparative performance of color-measuring instruments," *Applied Optics*, vol. 8, no. 4, pp. 775–783, 1969.

[87] D. J. Porter, "Global harmonization of spectrophotometric standards," in *Analytical Spectroscopy Library*, vol. 6, pp. 35–48, Elsevier, 1995.

[88] D. C. Rich, D. Battle, F. Malkin, C. Williamson, and A. Ingleson, "Evaluation of the long-term repeatability of reflectance spectrophotometers," in *Analytical Spectroscopy Library*, vol. 6, pp. 137–153, Elsevier, 1995.

[89] H. Hemmendinger, "Reflectance spectrophotometry: balancing diffuse and specular components," in *Analytical Spectroscopy Library*, vol. 6, pp. 159–172, Elsevier, 1995.

[90] R. S. Berns, *Billmeyer and Saltzman's principles of color technology*. John Wiley & Sons, 2019.

[91] W. Johnston and E. Kao, "Assessment of appearance match by visual observation and clinical colorimetry," *Journal of dental research*, vol. 68, no. 5, pp. 819–822, 1989.

[92] R. D. Paravina, R. Ghinea, L. J. Herrera, A. Della Bona, C. Igiel, M. Linninger, M. Sakai, H. Takahashi, E. Tashkandi, and M. d. Mar Perez, "Color difference thresholds in dentistry," *J Esthet Restor Dent*, vol. 27, pp. S1–S9, 2015.

[93] R. D. Paravina and E. J. Swift Jr, "Color in dentistry: match me, match me not," *Journal of Esthetic and Restorative Dentistry*, vol. 21, no. 2, pp. 133–139, 2009.

[94] "Technical report(E): Dentistry - guidance on color measurements.," tech. rep., Geneva, Switzerland: ISO;, 2016. ISO/TR 28642:2016.

[95] G. Sharma, W. Wu, and E. N. Dalal, "The ciede2000 color-difference formula: Implementation notes, supplementary test data, and mathematical observations," *Color Res App*, vol. 30, no. 1, pp. 21–30, 2005.

[96] A. G. Wee, D. T. Lindsey, K. M. Shroyer, and W. M. Johnston, "Use of a porcelain color discrimination test to evaluate color difference formulas," *The Journal of prosthetic dentistry*, vol. 98, no. 2, pp. 101–109, 2007.

[97] R. Ghinea, M. M. Pérez, L. J. Herrera, M. J. Rivas, A. Yebra, and R. D. Paravina, "Color difference thresholds in dental ceramics," *Journal of dentistry*, vol. 38, pp. e57–e64, 2010.

[98] M. Salas, C. Lucena, L. J. Herrera, A. Yebra, A. Della Bona, and M. M. Pérez, "Translucency thresholds for dental materials," *Dental Materials*, vol. 34, no. 8, pp. 1168–1174, 2018.

[99] T. T. M. SUGENO, "Fuzzy identification of systems and its applications to modeling and control [j]," *Readings in Fuzzy Sets for Intelligent Systems*, vol. 387, 2014.

[100] L. J. Herrera, H. Pomares, I. Rojas, O. Valenzuela, and A. Prieto, "Tase, a taylor series-based fuzzy system model that combines interpretability and accuracy," *Fuzzy sets and systems*, vol. 153, no. 3, pp. 403–427, 2005.

[101] L. J. Herrera, R. Pulgar, J. Santana, J. C. Cardona, A. Guillén, I. Rojas, and M. del Mar Pérez, "Prediction of color change after tooth bleaching using fuzzy logic for vita classical shades identification," *Appl. Optics.*, vol. 49, no. 3, pp. 422–429, 2010.

[102] I.-S. Pop-Ciutrila, R. Ghinea, H. A. Colosi, J. Ruiz-López, M. M. Perez, R. D. Paravina, and D. Dudea, "Color compatibility between dental structures and three different types of ceramic systems," *BMC Oral Health*, vol. 21, no. 1, pp. 1–10, 2021.

[103] N. D. Sarmast, N. Angelov, R. Ghinea, J. M. Powers, and R. D. Paravina, "Color compatibility of gingival shade guides and gingiva-colored dental materials with healthy human gingiva.," *International Journal of Periodontics & Restorative Dentistry*, vol. 38, no. 3, 2018.

[104] A. Seyidaliyeva, S. Rues, Z. Evagorou, A. J. Hassel, P. Rammelsberg, and A. Zenthöfer, "Color stability of polymer-infiltrated-ceramics compared with lithium disilicate ceramics and composite," *Journal of Esthetic and Restorative Dentistry*, vol. 32, no. 1, pp. 43–50, 2020.

[105] J. Ruiz-López, M. M. Perez, C. Lucena, R. Pulgar, A. López-Toruño, M. Tejada-Casado, and R. Ghinea, "Visual and instrumental coverage error of two dental shade guides: an in vivo study," *Clinical Oral Investigations*, pp. 1–8, 2022.

[106] S. Taşın, G. Celik, A. İsmatullaev, and A. Usumez, "The effect of artificial accelerated aging on the color stability, microhardness, and surface roughness

of different dental laminate veneer materials," *Journal of Esthetic and Restorative Dentistry*, vol. 34, no. 2, pp. 405–411, 2022.

[107] M. del Mar Perez, R. Ghinea, L. J. Herrera, A. M. Ionescu, H. Pomares, R. Pulgar, and R. D. Paravina, "Dental ceramics: a ciede2000 acceptability thresholds for lightness, chroma and hue differences," *Journal of Dentistry*, vol. 39, pp. e37–e44, 2011.

[108] J. Biswas and B. Datta, "Biomaterials: an introduction to materials for biomedical applications," in *Nanostructured Materials and their Applications*, pp. 43–53, Springer, 2021.

[109] H. Reza Rezaie, H. Beigi Rizi, M. M. Rezaei Khamseh, and A. Öchsner, "Dental restorative materials," in *A Review on Dental Materials*, pp. 47–171, Springer, 2020.

[110] M. Mhadhbi, F. Khlissa, and C. Bouzidi, "Recent advances in ceramic materials for dentistry," *Advanced Ceramic Materials*, 2021.

[111] C. Shen, H. R. Rawls, and J. F. Esquivel-Upshaw, *Phillips' Science of Dental Materials E-Book*. Elsevier Health Sciences, 2021.

[112] I. Denry and J. Kelly, "Emerging ceramic-based materials for dentistry," *Journal of dental research*, vol. 93, no. 12, pp. 1235–1242, 2014.

[113] I. Denry and J. A. Holloway, "Ceramics for dental applications: a review," *Materials*, vol. 3, no. 1, pp. 351–368, 2010.

[114] W. Höland, M. Schweiger, R. Watzke, A. Peschke, and H. Kappert, "Ceramics as biomaterials for dental restoration," *Expert review of medical devices*, vol. 5, no. 6, pp. 729–745, 2008.

[115] H. J. Conrad, W.-J. Seong, and I. J. Pesun, "Current ceramic materials and systems with clinical recommendations: a systematic review," *The Journal of prosthetic dentistry*, vol. 98, no. 5, pp. 389–404, 2007.

[116] R. Yadav and M. Kumar, "Dental restorative composite materials: A review," *Journal of Oral Biosciences*, vol. 61, no. 2, pp. 78–83, 2019.

[117] X. Zhou, X. Huang, M. Li, X. Peng, S. Wang, X. Zhou, and L. Cheng, "Development and status of resin composite as dental restorative materials," *Journal of Applied Polymer Science*, vol. 136, no. 44, p. 48180, 2019.

[118] J. L. Ferracane, "Resin-based composite performance: are there some things we can't predict?," *Dental materials*, vol. 29, no. 1, pp. 51–58, 2013.

[119] S. C. Bayne, "Dental biomaterials: where are we and where are we going?," *Journal of dental education*, vol. 69, no. 5, pp. 571–585, 2005.

[120] N. Rebholz-Zaribaf and M. Özcan, "Adhesion to zirconia as a function of primers/silane coupling agents, luting cement types, aging and test methods," *Journal of adhesion science and Technology*, vol. 31, no. 13, pp. 1408–1421, 2017.

[121] A. Hervás García, M. Lozano, J. Cabanes Vila, A. Barjau Escribano, and P. Fos Galve, "Composite resins: a review of the materials and clinical indications," 2006.

[122] L. D. Randolph, W. M. Palin, G. Leloup, and J. G. Leprince, "Filler characteristics of modern dental resin composites and their influence on physico-mechanical properties," *Dental Materials*, vol. 32, no. 12, pp. 1586–1599, 2016.

[123] R. Wang, E. Habib, and X. Zhu, "Evaluation of the filler packing structures in dental resin composites: From theory to practice," *Dental Materials*, vol. 34, no. 7, pp. 1014–1023, 2018.

[124] F. Lutz, J. C. Setcos, and R. W. Phillips, "New finishing instruments for composite resins.," *Journal of the American Dental Association (1939)*, vol. 107, no. 4, pp. 575–580, 1983.

[125] J. L. Ferracane, "Resin composite—state of the art," *Dental materials*, vol. 27, no. 1, pp. 29–38, 2011.

[126] N. Ilie and R. Hickel, "Resin composite restorative materials," *Australian dental journal*, vol. 56, pp. 59–66, 2011.

[127] S. D. Heintze, V. Rousson, and R. Hickel, "Clinical effectiveness of direct anterior restorations—a meta-analysis," *Dental materials*, vol. 31, no. 5, pp. 481–495, 2015.

[128] D. Angerame and M. De Biasi, "Do nanofilled/nanohybrid composites allow for better clinical performance of direct restorations than traditional microhybrid composites? a systematic review," *Operative dentistry*, vol. 43, no. 4, pp. E191–E209, 2018.

[129] T.-Y. Kwon, R. Bagheri, Y. K. Kim, K.-H. Kim, and M. F. Burrow, "Cure mechanisms in materials for use in esthetic dentistry," *Journal of investigative and clinical dentistry*, vol. 3, no. 1, pp. 3–16, 2012.

[130] N. Ilie and A. Simon, "Effect of curing mode on the micro-mechanical properties of dual-cured self-adhesive resin cements," *Clinical Oral Investigations*, vol. 16, no. 2, pp. 505–512, 2012.

[131] A. Santini, I. T. Gallegos, and C. M. Felix, "Photoinitiators in dentistry: a review," *Primary dental journal*, vol. 2, no. 4, pp. 30–33, 2013.

[132] M. Blatz, G. Chiche, O. Bahat, R. Roblee, C. Coachman, and H. Heymann, "Evolution of aesthetic dentistry," *Journal of dental research*, vol. 98, no. 12, pp. 1294–1304, 2019.

[133] W. M. Johnston, "Review of translucency determinations and applications to dent mater," *J Esthet Restor Dent*, vol. 26, no. 4, pp. 217–223, 2014.

[134] F. Carrillo-Perez, O. E. Pecho, J. C. Morales, R. D. Paravina, A. Della Bona, R. Ghinea, R. Pulgar, M. d. M. Pérez, and L. J. Herrera, "Applications of artificial intelligence in dentistry: A comprehensive review," *Journal of Esthetic and Restorative Dentistry*, vol. 34, no. 1, pp. 259–280, 2022.

[135] L. J. Herrera, J. Santana, A. Yebra, M. J. Rivas, R. Pulgar, and M. M. Pérez, "A model for prediction of color change after tooth bleaching based on cielab color space," in *Third International Conference on Applications of Optics and Photonics*, vol. 10453, pp. 464–469, SPIE, 2017.

[136] M. M. Perez, C. Hita-Iglesias, R. Ghinea, A. Yebra, O. E. Pecho, A. M. Ionescu, A. Crespo, and E. Hita, "Optical properties of supra-nano spherical filled resin composites compared to nanofilled, nano-hybrid and micro-hybrid composites," *Dent Mater J*, vol. 35, no. 3, pp. 353–359, 2016.

[137] R. Pulgar, C. Lucena, C. Espinar, O. E. Pecho, J. Ruiz-Lopez, A. Della Bona, and M. M. Perez, "Optical and colorimetric evaluation of a multi-color polymer-infiltrated ceramic-network material," *Dent Mater*, vol. 35, no. 7, pp. e131–e139, 2019.

[138] S. S. Mikhail and W. M. Johnston, "Confirmation of theoretical colour predictions for layering dental composite materials," *J Dent*, vol. 42, no. 4, pp. 419–424, 2014.

[139] V. Duveiller, L. Gevaux, R. Clerc, J.-P. Salomon, and M. Hébert, "Reflectance and transmittance of flowable dental resin composite predicted by the two-flux model: on the importance of analyzing the effective measurement geometry," 11 2020.

[140] H. Li, L. Lai, L. Chen, C. Lu, and Q. Cai, "The prediction in computer color matching of dentistry based on ga+ bp neural network," *Comput Math Methods Med*, vol. 2015, 2015.

[141] R. Ghinea, O. Pecho, L. J. Herrera, A. M. Ionescu, J. de la Cruz Cardona, M. P. Sanchez, R. D. Paravina, and M. del Mar Perez, "Predictive algorithms for determination of reflectance data from quantity of pigments within experimental dental resin composites," *Biomed. Eng. Online.*, vol. 14, no. 2, pp. 1–14, 2015.

[142] A. Hajipour and A. Shams-Nateri, "Effect of classification by competitive neural network on reconstruction of reflectance spectra using principal component analysis," *Color Res App*, vol. 42, no. 2, pp. 182–188, 2017.

[143] K. Ansari, J.-B. Thomas, and P. Gouton, "Spectral band selection using a genetic algorithm based wiener filter estimation method for reconstruction of munsell spectral data," *Electron Img*, vol. 2017, no. 18, pp. 190–193, 2017.

[144] N. Attarchi and S. Amirshahi, "Reconstruction of reflectance data by modification of berns' gaussian method," *Color Res App*, vol. 34, pp. 26 – 32, 02 2009.

[145] F. Agahian, S. A. Amirshahi, and S. H. Amirshahi, "Reconstruction of reflectance spectra using weighted principal component analysis," *Color Res Appl*, vol. 33, no. 5, pp. 360–371, 2008.

[146] V. Babaei, S. H. Amirshahi, and F. Agahian, "Using weighted pseudo-inverse method for reconstruction of reflectance spectra and analyzing the dataset in terms of normality," *Color Res Appl*, vol. 36, no. 4, pp. 295–305, 2011.

[147] M. Ringnér, "What is principal component analysis?," *Nature biotechnology*, vol. 26, no. 3, pp. 303–304, 2008.

[148] D.-Y. Tzeng and R. S. Berns, "A review of principal component analysis and its applications to color technology," *Color Research & Application*, vol. 30, no. 2, pp. 84–98, 2005.

[149] I. T. Jolliffe and J. Cadima, "Principal component analysis: a review and recent developments," *Philos T R Soc A*, vol. 374, no. 2065, p. 20150202, 2016.

[150] D. Maulud and A. M. Abdulazeez, "A review on linear regression comprehensive in machine learning," *Journal of Applied Science and Technology Trends*, vol. 1, no. 4, pp. 140–147, 2020.

[151] M. C. Roziqin, A. Basuki, and T. Harsono, "A comparison of montecarlo linear and dynamic polynomial regression in predicting dengue fever case," in *2016 International Conference on Knowledge Creation and Intelligent Computing (KCIC)*, pp. 213–218, IEEE, 2016.

[152] A. K. Prasad, M. Ahadi, B. S. Thakur, and S. Roy, "Accurate polynomial chaos expansion for variability analysis using optimal design of experiments," in

2015 IEEE MTT-S International Conference on Numerical Electromagnetic and Multi-physics Modeling and Optimization (NEMO), pp. 1–4, IEEE, 2015.

[153] R. Oguro, M. Nakajima, N. Seki, A. Sadr, J. Tagami, and Y. Sumi, "The role of enamel thickness and refractive index on human tooth colour," *Journal of dentistry*, vol. 51, pp. 36–44, 2016.

[154] C. Kose, D. Oliveira, J. Roulet, P. Pereira, and M. Rocha, "Algorithm to predict the final color of leucite-reinforced ceramic restorations," *Dental Materials*, vol. 38, p. e65, 2022.

[155] A. G. Wee, W.-Y. Chen, and W. M. Johnston, "Color formulation and reproduction of opaque dental ceramic," *Dental Materials*, vol. 21, no. 7, pp. 665–670, 2005.

[156] T. O. Nielsen, R. B. West, S. C. Linn, O. Alter, M. A. Knowling, J. X. O'Connell, S. Zhu, M. Fero, G. Sherlock, J. R. Pollack, *et al.*, "Molecular characterisation of soft tissue tumours: a gene expression study," *The Lancet*, vol. 359, no. 9314, pp. 1301–1307, 2002.

[157] A. Folch-Fortuny, F. Arteaga, and A. Ferrer, "Pca model building with missing data: New proposals and a comparative study," *Chemometrics and Intelligent Laboratory Systems*, vol. 146, pp. 77–88, 2015.

[158] A. Andersson, T. Olofsson, D. Lindgren, B. Nilsson, C. Ritz, P. Edén, C. Lassen, J. Råde, M. Fontes, H. Mörse, *et al.*, "Molecular signatures in childhood acute leukemia and their correlations to expression patterns in normal hematopoietic subpopulations," *Proceedings of the National Academy of Sciences*, vol. 102, no. 52, pp. 19069–19074, 2005.

[159] S. Yamamoto, Y. Hosoya, N. Tsumura, and K. Ogawa-Ochiai, "Principal component analysis for dental shade color," *Dent Mater*, vol. 28, no. 7, pp. 736–742, 2012.

[160] T. Næs and B.-H. Mevik, "Understanding the collinearity problem in regression and discriminant analysis," *J Chemometr*, vol. 15, no. 4, pp. 413–426, 2001.

[161] C. Lucena, C. Benavides-Reyes, J. Ruiz-López, M. Tejada-Casado, R. Pulgar, and M. M. Pérez, "Relevant optical properties for gingiva-colored resin-based composites," *Journal of Dentistry*, p. 104316, 2022.

[162] J. Hernández-Andrés, J. Romero, and R. L. Lee, "Colorimetric and spectroradiometric characteristics of narrow-field-of-view clear skylight in Granada, Spain," *J Opt Soc Am A*, vol. 18, pp. 412–420, 03 2001.

[163] I.-S. Pop-Ciutrila, D. Dudea, M. Eugenia Badea, M. Moldovan, S. I. Cîmpean, and R. Ghinea, "Shade correspondence, color, and translucency differences between human dentine and a cad/cam hybrid ceramic system," *J Esthet Restor Dent*, vol. 28, pp. S46–S55, 2016.

[164] O. E. Pecho, R. Ghinea, E. A. N. do Amaral, J. C. Cardona, A. Della Bona, and M. M. Pérez, "Relevant optical properties for direct restorative materials," *Dent Mater*, vol. 32, no. 5, pp. e105–e112, 2016.

[165] R. Arif, B. Yilmaz, and W. M. Johnston, "In vitro color stainability and relative translucency of cad-cam restorative materials used for laminate veneers and complete crowns," *J Prosthet Dent*, vol. 122, no. 2, pp. 160–166, 2019.

[166] A. Della Bona, O. Pecho, R. Ghinea, J. Cardona, R. Paravina, and M. Perez, "Influence of bleaching and aging procedures on color and whiteness of dental composites," *Oper Dent*, vol. 44, no. 6, pp. 648–658, 2019.

[167] S. S. Mikhail and W. M. Johnston, "In vitro optical characterization of dental resin composite aged in darkness," *Color Res App*, vol. 45, no. 2, pp. 345–351, 2020.

[168] F. H. Imai, M. R. Rosen, and R. S. Berns, "Comparative study of metrics for spectral match quality," in *Conference on Colour in Graphics, Imaging, and Vision*, no. 1, pp. 492–496, Soc Imaging Sci Technol, 2002.

[169] D. J. Wood, T. Shiraishi, N. Shinozaki, and R. van Noort, "Spectral reflectance and color of dentin ceramics for all-ceramic restorations," *Dent Mater*, vol. 24, no. 12, pp. 1661–1669, 2008.

[170] D. Angerame, L. Fanfoni, M. De Biasi, L. Bevilacqua, and L. Generali, "Influence of thickness and shade on the color of layered novel nanohybrid composite systems.," *Int. J. of Periodont. Rest.*, vol. 41, no. 3, 2021.

[171] S. S. Mikhail, S. R. Schricker, S. S. Azer, W. A. Brantley, and W. M. Johnston, "Optical characteristics of contemporary dental composite resin materials," *J. Dent.*, vol. 41, no. 9, pp. 771–778, 2013.

[172] J. Manauta, A. Salat, A. Putignano, W. Devoto, G. Paolone, and L. Hardan, "Stratification in anterior teeth using one dentine shade and a predefined thickness of enamel: a new concept in composite layering–part i," *Trop. Dent. J.*, vol. 37, 2014.

[173] J. Da Costa, P. Fox, and J. Ferracane, "Comparison of various resin composite shades and layering technique with a shade guide," *Journal of Esthetic and Restorative Dentistry*, vol. 22, no. 2, pp. 114–124, 2010.

[174] S. Westland, "Review of the cie system of colorimetry and its use in dentistry," *Journal of Esthetic and Restorative Dentistry*, vol. 15, pp. S5–S12, 2003.

[175] M. Tejada-Casado, R. Ghinea, M. M. Perez, H. Lübbe, I. Pop-Ciutrila, J. Ruiz-López, and L. Herrera, "Reflectance and color prediction of dental material monolithic samples with varying thickness," *Dental Materials*, vol. 38, no. 4, pp. 622–631, 2022.

[176] M. Tejada-Casado, R. Ghinea, M. Pérez, J. Cardona, A. Ionescu, H. Lübbe, and L. Herrera, "Color prediction of layered dental resin composites with varying thickness," *Dental Materials*, vol. 38, no. 8, pp. 1261–1270, 2022.

[177] J. C. Ragain, "A review of color science in dentistry: Colorimetry and color space," *J. Dent. Oral Disord. Ther*, vol. 4, pp. 1–5, 2016.

[178] E. A. Chavarriaga Miranda, N. A. Correa Rojas, J. F. Montoya Carvajal, and O. J. Restrepo Baena, "Color prediction in ceramic enamels using the kubelka munk model," *Tecciencia*, vol. 10, no. 19, pp. 1–5, 2015.

[179] L. Schabbach, F. Bondioli, and M. Fredel, "Color prediction with simplified kubelka–munk model in glazes containing fe2o3–zrsio4 coral pink pigments," *Dyes and pigments*, vol. 99, no. 3, pp. 1029–1035, 2013.

[180] Y. Miyagawa and J. Powers, "Materials science: Prediction of color of an esthetic restorative material," *Journal of Dental Research*, vol. 62, no. 5, pp. 581–584, 1983.

SCIENTIFIC PRODUCTION

JOURNAL ARTICLES INCLUDED IN THIS PHD THESIS

M. Tejada-Casado, R. Ghinea, M. M. Perez, H. Lübbe, I. Pop-Ciutrila, J. Ruiz-López and L. Herrera, "Reflectance and color prediction of dental material monolithic samples with varying thickness," *Dental Materials*, vol. 38, no. 4, pp. 622–631, 2022.

M. Tejada-Casado, R. Ghinea, M. Pérez, J. Cardona, A. Ionescu, H. Lübbe and L. Herrera, "Color prediction of layered dental resin composites with varying thickness," *Dental Materials*, vol. 38, no. 8, pp. 1261–1270, 2022.

M. Tejada-Casado, R. Ghinea, M. Pérez, J. Ruiz-López, H. Lübbe and L. Herrera, "Development of thickness-dependent predictive methods for the estimation of the CIEL*a*b* color coordinates of monolithic and layered dental resin composites". (Submitted to *Materials*, 2022)

OTHER JOURNAL ARTICLES

J. Ruiz-López, M. M. Perez, C. Lucena, R. Pulgar, A. López-Toruño, **M. Tejada-Casado** and R. Ghinea, "Visual and instrumental coverage error of two dental shade guides: an in vivo study," *Clinical Oral Investigations*, pp. 1–8, 2022.

M. M. Pérez, F. Carrillo-Perez, **M. Tejada-Casado**, J. Ruiz-López, C. Benavides-Reyes and L. J. Herrera, "Ciede2000 lightness, chroma and hue human gingiva thresholds," *Journal of Dentistry*, vol. 124, p. 104213, 2022.

C. Lucena, C. Benavides-Reyes, J. Ruiz-López, **M. Tejada-Casado**, R. Pulgar and M. M. Pérez, "Relevant optical properties for gingiva colored resin-based composites," *Journal of Dentistry*, vol. 126, p. 104316, 2022.

M. M. Pérez, C. Benavides-Reyes, **M. Tejada-Casado**, J. Ruiz-López and C. Lucena, "Does backgrounds color influence the appearance of gingiva-colored resin-based composites?," *Materials*, vol. 15, no. 10, p. 3712, 2022

M. Tejada-Casado, R. Ghinea, M.A. Martínez-Domingo, M.M. Perez, J. Cardona, J. Ruiz-López and L. Herrera, "Validation of a hyperspectral imaging system for color measurement of in-vivo dental structures," *Micromachines*, vol. 13, p.1929, 2022.

CONFERENCE AND SCIENTIFIC MEETINGS COMMUNICATIONS

M. Tejada-Casado, R. Ghinea, M.M. Pérez, J. Ruiz-López, H. Lübbe and L.J. Herrera. "Color prediction of layered dental resin composites." 10^{th} Edition of the International Symposium Napoca-Biodent New Challenges in Dental Research. Cluj-Napoca, Romania. November 5^{th}– 6^{th}, 2021.

J. Ruiz-López, R. Ghinea, M.M. Pérez, **M. Tejada-Casado**, C. Gasparik and D. Dudea. "Color variations in bucco-lingual sections of human extracted teeth." 10^{th} Edition of the International Symposium Napoca-Biodent New Challenges in Dental Research. Cluj-Napoca, Romania. November 5^{th}– 6^{th}, 2021.

J. Ruiz-López, C. Espinar, A. Della Bona, **M. Tejada-Casado**, R. Pulgar and M.M. Perez. "Effect of thickness and printing angle on color of 3D printing dental restorative polymer-based materials." 5^{th} International Conference on Applications of Optics and Photonics (AOP2022). Guimarães, Portugal. July 18-22, 2022. ISBN 978-989-8798-08-4.

M. Tejada-Casado, J. Ruiz-López; J. Cardona, M.A. Martinez-Domingo, A. Ionescu and R. Ghinea. "Hyperspectral Colorimetry of in-vivo dental structures." 5^{th} International Conference on Applications of Optics and Photonics (AOP2022). Guimarães, Portugal. July 18-22, 2022. ISBN 978-989-8798-08-4.

M. Tejada-Casado, R. Ghinea, J. Ruiz-López, H. Lübbe, M. M. Perez and L.J. Herrera. "Color prediction of monolithic and layered dental resin composites of varying thicknesses." 5^{th} International Conference on Applications of Optics and Photonics (AOP2022). Guimarães, Portugal. July 18-22, 2022. ISBN 978-989-8798-08-4.

C. Espinar, **M. Tejada Casado**, J. Ruiz-López, A. Della Bona, R. Pulgar, J. Cardona, A.M. Ionescu and M.M. Pérez. "Color variations among different shades, thickness and printing angle of 3D printing dental restorative polymer based materials." IX International congress of histology and tissue engineering. Granada, España. September 6–9, 2022.

M. Tejada-Casado, L. M. Ragoo, L. Gómez-Robledo and M. Melgosa. "Simulating CIE LED Illuminants With a Low-Cost Six-Channels LED System." Proceedings of the 14^{th} European Lighting Conference LUX EUROPA 2022. Prague, Czech Republic. September 20–22, 2022.

RESEARCH STAY

University of Passo Fundo, Faculty of Dentristy - Postgraduate Program in Dentistry, Brazil. **3 months.** Supervisor: Alvaro Della Bona, Senior Professor and Chair, Postgraduate Program in Dentistry.

PHD SCHOLARSHIPS

- Simulation of multilayer bodies of translucent dental materials. - "Ayudas Predoctorales para la realización de Tesis en colaboración con Instituciones, Empresas o Entidades del Plan Propio de Investigacion de la Universidad de Granada. OTRI Contract 4346. 15/03/2020 - 15/03/2023. Financed by Vita Zahnfabrik H. Rauter GmbH & Co. KG.

- PhD Students Mobility Scholarship: Plan Propio de Internacionalización: Programme 1.2. Academic year 2021/2022.

PARTICIPATION IN RESEARCH PROJECTS

- Desarrollo de métodos basados en técnicas ópticas y de inteligencia computacional para la evaluación y control de biomateriales biogenerados y sintéticos con aplicación en medicina regenerativa y restauradora. Proyect P20-00200. 04/10/2021-30/6/23. Ministry of Economy, Innovation, Science and Technology - Government of Andalusia.

- Measurement, modelling and prediction of optical properties and final appearance of translucent layered biomaterials with application in dentistry. OTRI Contract 4744. 25/02/2021 - 24/02/2024. Financed by Vita Zahnfabrik H. Rauter GmbH & Co. KG.

AWARDS

Third Place Student Presentation: M. Tejada-Casado, J. Ruiz-López; J. Cardona, M.A. Martinez-Domingo, A. Ionescu and R. Ghinea. Hyperspectral Colorimetry of in-vivo dental structures. 5^{th} International Conference on Applications of Optics and Photonics (AOP2022). Guimarães, Portugal, July 18-22, 2022.

OTHER RESEARCH ACTIVITIES

Organizer and jury: "Ciencia en una Foto". Scientific photography contest organized by the Asociación Montilla para la Divulgación y Difusión de la Ciencia (AMDIC). 2021.

Invited talk: "Pursuing the Academic Dream" in an event organized by the Postgraduate Program in Dentistry at The University Federal of Santa Maria (Brazil). October 2022.

Invited talk: "Color in Dentistry" in an event organized by the Postgraduate Program in Dentistry at The University Federal of Santa Maria (Brazil). October 2022.

Invited lecture: "Introduction to Artificial Intelligence in Dentistry and Color Prediction Algorithms" in an event organized by the Postgraduate Program in Dentistry at The University of Passo Fundo (Brazil). November 2022.

TEACHING ACTIVITIES

- Teaching lessons in the Department of Optics and Optometry of the University of Granada. Courses: Contact Lenses II (2021, practical lessons), Ophthalmic Lens Technology II (2021, practical lessons), Physical Optics II (2022- practical lessons and theory) and Optics II (2022, practical lessons).

- Participation in "El equipo docente de mentorización como plataforma multidisciplinarpara la formación en ciencias experimentales y técnicas". XI Convocatoria de Equipos Docentes de Formación Inicial del Profesorado y Equipos Docentes de Formación Continua. Plan FIDO UGR-Plan de Formación e Innovación Docente 2022-2023. Unidad de Calidad, Innovación Docente y Prospectiva. University of Granada.

- Participation in "Desarrollo de Proyectos Interdisciplinares en Ciencias". XI Convocatoria de Equipos Docentes de Formación Inicial del Profesorado y Equipos Docentes de Formación Continua. Plan FIDO UGR-Plan de Formación e Innovación Docente 2022-2023. Unidad de Calidad, Innovación Docente y Prospectiva. University of Granada.